

ADA131750

(1)

SILICIDE FORMATION AND SCHOTTKY BARRIER
OF RARE-EARTH METALS ON SI
FINAL TECHNICAL REPORT

Reporting period: June 1, 1981 - September 30th, 1983
Principal Investigator: S.S. Lau
Telephone: (714) 452-3097
Sponsored by: Defense Advanced Research Projects
Agency DARPA order no. 3011-4276

Contract no. MDA 903-81-C-0348
Effective: June 1, 1981
Expiration: September 30, 1983
Contractor: University of California, San Diego
Office of Contract and Grant
Administration
Q-023
La Jolla, California

APPROVED FOR PUBLIC RELEASE
DISTRIBUTION UNLIMITED

DTIC
SELECTED
AUG 25 1983
A

DTIC FILE COPY

83 08 23 11 6

Table of Contents

	<u>Page</u>
I. Introduction	1
II. Summary of Results	2
III. Conclusions	7
IV. Hardware development	8
V. Further Research	9
VI. List of Publications and Talks	10
VII. Published Articles	(see Appendices 1 - 10)

I. Introduction

The objectives of this program are to investigate the electrical properties and growth characteristics of rare-earth silicides that potentially form low energy barriers on n-type Si. A more general objective is to set up Rutherford backscattering spectrometry at UCSD. For the investigation of rare-earth silicides, we concentrate working on ErSi_2 (all rare-earth silicides are similar in characteristics and properties, Er is slightly less reactive with oxygen). More recently GdSi_2 has also been investigated. We report here the results of our investigation. Generally speaking, we believe that the major problems of rare-earth silicides have been solved. Rutherford backscattering spectrometry is now on-line at UCSD.



Accession For	
NTIS GRA&I	<input checked="checked" type="checkbox"/>
DTIC TAB	<input type="checkbox"/>
Unannounced	<input type="checkbox"/>
Justification	
By	
Distribution/	
Availability Codes	
Avail and/or	
Part	Special
A	

II. Summary of Results

1. The major problem of rare-earth silicides as Schottky diodes is the non-planar (pitted) interface between the silicide layer and the Si substrate, thus causing non-ideal diode performance. We found three ways to reduce or eliminate the surface pitting. The simplest way is to use a sample configuration of Si(a)/Er/Si <xtal>. Laterally uniform (pit-free) ErSi_2 layers are formed at relatively low temperatures ($\sim 380^\circ\text{C}$). The other two ways to reduce surface pitting are (a) ion beam mixing technique, and (b) ultra-high vacuum preparation of the Si surface before deposition. These two techniques are considerably more cumbersome compared to the first technique (see paper #1 in Appendix).
2. The maximum barrier height of ErSi_2 on p-type Si is found to be 0.78 ± 0.02 eV, $n = 1.05$ at room temperature. The barrier height of ErSi_2 on n-type Si is found to be 0.34 ± 0.02 eV, at room temperature. We believe these values are more realistic than those reported previously, since this is the first time planar (pit-free) ErSi_2 layers were made (see paper #2 in Appendix).
3. Systematic study of barrier height on p-Si as a function of annealing temperature has been made. We found that there is an optimum temperature of annealing (to induce silicide formation) for achieving maximum barrier height. We have a simple model to explain this phenomenon and it was reported at the MRS annual meeting at Boston 1982 (see paper #2 in Appendix).
4. We believe that the problem of fabricating pit-free and stable ErSi_2 Schottky diodes is basically solved by our research effort under this sponsorship.
5. We have also engaged in ion-beam mixing experiments, primarily in collaboration with Professor Marc Nicolet and his group at Caltech. We found

that PtSi/n-Si diodes formed by ion beam mixing followed by thermally annealing do not perform electrically as ideal diodes. Radiation damage in the Si substrate is primarily the cause of poor electrical behavior (see paper #3 in Appendix). For this reason, we did not investigate ion-beam induced ErSi₂ diode characteristics. On the other hand, we believe that planar ErSi₂ diodes formed by ion beam mixing can be made with reasonable electrical behavior if ion irradiation is done in a well controlled manner. Since we found a much simpler way to make planar ErSi₂ layers, the ion beam mixing technique was not pursued. Ion-beam mixing in electronics should be much more useful in the area of ohmic contact for small-dimensional devices (self-aligned gate technology in MESFETS).

6. In the area of amorphous phase formation by ion-beam mixing, we assisted the Caltech group in the formulation of the "structural difference rule". We gave an invited and contributed paper at the *International Conference on Ion Beam Modification of Materials* in Grenoble, France in September 1982 (see paper #4 in Appendix).

7. Our General Ionex Tandetron accelerator has been installed and the first backscattering spectrum was obtained on January 11th, 1983. A paper on accelerator energy calibration was presented at the 6th *International Conference on Ion Beam Analysis* (see paper #6 in Appendix).

8. We have interacted with other laboratories under this program on the following projects:

- a. Rare-Earth Silicide Formation and Schottky Diode Study of Co-evaporated Gd-Si Film (with IBM Watson Research Center).

We found that Gd behaves similarly as compared to Er. The co-evaporation scheme is yet another approach to eliminate pits as well as to promote shallow contact. The bilayer approach

(Si(a)/Gd/Si <xtal>) to eliminate pits appears to be a simpler method and easier to control since it does not require simultaneous deposition. The results of this investigation will be reported in the literature at a later date.

b. Interaction of Pd-Er Alloys with Silicon (with IBM Watson Research Center).

In situ resistivity measurements together with MeV $^4\text{He}^+$ backscattering, x-ray diffraction, barrier height measurements and Auger electron spectroscopy combined with Ar sputtering have been used to investigate the interaction of silicon with alloys of rare-earth and near-noble metals. Alloys of Pd-Er with three different compositions have been prepared by dual e-gun coevaporation on both n and p-type silicon and Pd/Er bilayers have been deposited on SiO_2 . The results show that as-deposited these alloys are amorphous and the initial stages of the reaction with silicon is controlled by the metal-metal interaction as well as the metal-silicon interaction. The Er-rich alloy ($\text{Pd}_{15}\text{Er}_{85}$) segregates Er and forms Pd_2Er_5 . The segregated Er reacts with silicon producing ErSi_2 . For the Pd-rich alloy ($\text{Pd}_{65}\text{Er}_{35}$) the excess Pd is segregated at the silicon surface forming Pd_2Si . The near 50-50 alloy forms PdEr and a slightly higher temperature is necessary to promote the reaction with silicon. The barrier heights of these alloy films after interactions with the Si substrate are observed to decrease on n-type Si (ϕ_B^n) from 0.65 eV for $\text{Pd}_{65}\text{Er}_{35}$ to 0.40 eV for $\text{Pd}_{15}\text{Er}_{85}$ (ϕ_B^p increases with Er concentration in the alloy). (See paper #9 in Appendix.)

c. Current Injection Methods for Barrier Height Measurement (with IBM Watson Research Center).

This technique is derived from conventional methods for obtaining

barrier height and series resistance values in photovoltaic devices. The application of this simple technique, not necessarily requiring transparent metallizations, extends the linear region of the $\ln J$ versus V plot, allowing for an accurate determination of the saturation current. The measurement of both open circuit voltage and the short circuit current as a function of illumination intensity allows the junction characteristics to be determined free from series resistance effects. The short circuit, usually not easily measurable, is determined by injecting current from a current source until the photo-voltage approaches zero. The applicability of this technique to Schottky barriers of ErSi_2 and those formed on GaAs is investigated (see paper #10, abstract intended for MRS 1983, in Appendix).

d. Scanning Laser Induced ErSi_2 Formation (with Stanford University) and Scanning Electron Beam Induced ErSi_2 Formation (with Sandia National Lab, Albuquerque).

These transient annealing techniques are applied to Er/Si <xtal> samples to induce the formation of ErSi_2 . It was found that both transient techniques are capable of inducing uniform layers (pit-free) of ErSi_2 by reacting Er directly with Si substrate. The barrier heights of ErSi_2 formed by transient annealing techniques are comparable to those found by thermal annealing of samples with a configuration of $\text{Si(a)}/\text{Er/Si}$ <xtal>. The results of this investigation will be reported in the literature at a later date.

e. Photo-Response Measurement of ErSi_2 Diodes at Low Temperatures (with Hanscom AFB).

For this project, we have sent samples to P. Pelligrini for barrier height measurement of ErSi_2 on n and p-type Si at low temperatures. At

present we are facing two difficulties: (1) the photo-response measurement apparatus at Hanscom AFB is under repair; (2) Schottky diodes of ErSi_2 formed thermally in vacuum on n-type Si shows high n factor ($n \sim 3$) at 77°K . It has been our experience that ErSi_2 diodes formed in vacuum always have a large recombination-generation current as compared to those obtained by annealing in forming gas. The reason for this observation is not clear at present. It is our plan to fabricate a new batch of diodes (with oxide passivation and guard ring structure) formed by thermal annealing in forming gas for further investigation by I-V and photo-response measurements.

III. Conclusions

- (1) The problem of fabricating pit-free and stable ErSi_2 diodes is basically solved by using a sample configuration of $\text{Si(a)}/\text{Er}/\text{Si}$ <xtal>.
- (2) The maximum barrier height of ErSi_2 on p-type Si, ϕ_B^p , is 0.78 ± 0.02 eV ($n = 1.05$) at room temperature. The minimum barrier height on n-type Si, ϕ_B^n , is 0.33 ± 0.02 eV at room temperature (assuming $n = 1$). At 77°K , ϕ_B^n is 0.27 ± 0.02 eV ($n = 1.2$).
- (3) The contribution from the recombination-generation current to the total forward current is much more significant for samples annealed in vacuum as compared to those annealed in forming gas (~ 10 times higher for samples annealed in vacuum). The reason for this is still under investigation.
- (4) The reverse current of pit-free ErSi_2 formed by annealing in forming gas on p-type Si with guard ring structure is about 10 times the theoretical value at 10 volts.
- (5) The formation characteristics and electronic performance of GdSi_2 diodes are similar to those of ErSi_2 .
- (6) We believe that rare-earth silicide Schottky diodes on n-type Si can be potentially useful for infrared detection.

IV. Hardware Development

Backscattering spectrometry is now established at UCSD. The General Ionex accelerator is capable of delivering beams of 3 MeV $^4\text{He}^{++}$ and 2 MeV $^1\text{H}^+$. We are now set up for backscattering and channeling experiments. We intend to develop proton induced x-ray emission capability in the future, using the same accelerator but at a different beam line.

V. Further Research

For future research in rare-earth silicide formation and their Schottky diode characteristics, there are at least three areas that require further attention:

- (1) *The origin of a large recombination-generation current component in the total forward current observed in diodes formed by thermal annealing in vacuum.*
- (2) *The modulation of barrier height of silicides by introducing Ge in the silicide layer. It is known that barrier height of a single metal layer on Si can be modulated by the addition of a second metal component. This scheme does not always work due to phase separation of bilayer or alloy film structure. A homogeneous layer of $\text{Er}(\text{Si}_x\text{Ge}_{1-x})_2$ can be easily formed and phase separation does not seem to occur.*
- (3) *It has recently been established by x-ray photo emission that the core level shift of a silicide correlates with the silicide barrier height on n-type Si. Measurements have been made on Ni_2Si , NiSi , Pd_2Si , Pt_2Si and PtSi .*

The barrier heights, ϕ_B^n , of these silicides are all higher than 0.6 eV. In order to establish the validity of this correlation fully, it would be of interest to measure the bonding-antibonding splitting of ErSi_2 ($\phi_B^n \sim 0.33$ eV) and IrSi ($\phi_B^n \sim 0.9$ eV) and extend the range of correlation from very low ϕ_B^n to very high ϕ_B^n . This type of investigation can provide an insight into the relevance of metal-silicon bond energies on Schottky barrier heights.

List of Publications and Talks Related to this Program:

1. S. S. Lau, C. S. Pai, C. S. Wu, T. F. Kuech and B-X. Liu, "Surface Morphology of Erbium Silicide", Appl. Phys. Lett. 41 (1), 77 (1982).
2. C. S. Wu, S. S. Lau, T. F. Kuech and B-X. Liu, "Surface Morphology and Electronic Properties of Erbium Silicide", presented at the MRS Annual Meeting, Boston 1982, to be published in Thin Solid Films.
3. T. Banwell, M. Finetti, B-X. Liu, M-A. Nicolet, S. S. Lau and D. M. Scott, "Ion Irradiation Effects on Silicide Contacts Formed on Slightly Oxidized Substrates", presented at MRS Annual Meeting, Boston 1982. To be published in the Conference Proceedings.
4. S. S. Lau, B-X. Liu and M-A. Nicolet, "Ion Mixing and Phase Diagrams", presented at the Third International Conference on Ion Beam Modification of Materials, Grenoble, France, September 1982. To be published in Nuclear Instruments and Methods.
5. M-A. Nicolet and S. S. Lau, "Formation and Characterization of Transition Metal Silicides", to be published as a chapter in VLSI Electronics: Microstructure Science, Norman Einspruch, Series Editor, Vol. 6, Materials and Process Characterization, Graydon Larrabee, Guest Editor.
6. D. M. Scott, B. M. Paine, "Accelerator Energy Calibration Using Non-Resonance Nuclear Reactions", presented at the 6th International Conference on Ion Beam Analysis, to be published in Nucl. Inst. & Meth.
7. S. S. Lau, "MeV Ion Backscattering Spectrometry Applied to the Analysis of Beam Processed Semiconductors", invited paper at the 3rd Oxford Conference on Microscopy of Semiconducting Materials", March 1983, to be published in the Institute of Physics "Conference Series".
8. W. F. Tseng, B. Zhang, D. Scott, S. S. Lau, A. Christou and B. R. Wilkins, "Characterization of Tantalum-Silicon Films on GaAs at

Elevated Temperatures", submitted to Electron Device Letters.

9. G. Ottaviani, K. N. Tu, R. D. Thompson, J. W. Mayer and S. S. Lau,
"Interaction of Pd-Er Alloys with Silicon", submitted to J. Appl. Phys.
10. T. F. Kuech, C. S. Wu and S. S. Lau, "The Measurement of Silicide
Schottky Barrier Heights by use of Photovoltaic Techniques", Abstract
intended for MRS 1983.

APPENDIX 1

SURFACE MORPHOLOGY OF ERBIUM SILICIDES

S. S. Lau, C. S. Pai and C. S. Wu
University of California, San Diego
Department of Electrical Engineering & Computer Sciences
La Jolla, California 92093

T. F. Kuech^{a)} and B. X. Liu^{b)}
California Institute of Technology
Pasadena, California 91125

The surface of rare-earth silicides (Er, Tb, etc.), formed by the reaction of thin film metal layers with a silicon substrate, is typically dominated by deep penetrating, regularly shaped pits. These pits may have a detrimental effect on the electronic performance of low Schottky barrier height diodes utilizing such silicides on n-type Si. This study suggests that contamination at the metal-Si or silicide-Si interface is the primary cause of surface pitting. Surface pits may be reduced in density or eliminated entirely through either the use of Si substrate surfaces prepared under ultra high vacuum conditions prior to metal deposition and silicide formation or by means of ion implantation techniques. Silicide layers formed by these techniques possess an almost planar morphology.

The solid state interactions between rare-earth metals (such as Er, Tb) and single-crystal Si exhibits a "critical temperature" phenomenon^[1,2]. Below the critical annealing temperature, interactions are very sluggish and often escape detection. Above the critical annealing temperature, interactions are fast such that within minutes of annealing a layer of rare-earth metal (typically a few thousand Å thick) deposited on a Si substrate is consumed completely to form a rare-earth metal silicide. For example, little or no silicide formation was observed for a Er (~ 1000Å)/<100>Si sample after annealing at 380°C for 60 minutes, however, annealing at 390°C led to a rapid formation of the ErSi₂ phase^[2]. The formation of rare-earth metal silicides is further characterized by the observation that Si is the dominant moving species during interactions^[3]. The surface morphology of the silicide is typically dominated by a heavy pitting. The pitting is often crystallographic in nature exhibiting the symmetry of the underlying Si Substrate. These rare-earth silicides form a low Schottky barrier height, ϕ , to n-type Si with $\phi \approx 0.4$ eV^[4,5]. This suggests the utility of these Schottky barrier diodes in infrared detecting applications. The presence of surface non-uniformities, such as surface pitting, could prove to have a detrimental effect on the electronic performance of Schottky barrier devices. The present study examines the origin of this surface pitting and presents several means by which a smooth planar morphology can be achieved. It will be shown that the nature and cleanliness of the original metal-silicon interface plays a determining role in the development of these surface pits.

Two types of structures were initially investigated in order to determine the role of the crystalline Si substrate in surface pitting. In the first structure, ErSi₂ was formed by the reaction of a layer of Er deposited onto a single crystal Si substrate while in the second structure the silicide was formed by the reaction of Er with an amorphous Si layer. Specifically,

substrates of $\langle 100 \rangle$ Si used in both structures were first cleaned by organic solvents and then etched in a dilute HF solution, prior to loading into an ion-pumped vacuum chamber. The base pressure of the chamber was $\sim 5 \times 10^{-8}$ torr and the pressure during E-gun evaporation ($\sim 10^{-8}$ Å/sec) was $\sim 1 \times 10^{-7}$ torr. In the first structure the deposited layer of Er (~ 1700 Å) was reacted with the Si substrate by annealing at 450°C in vacuum ($\sim 10^{-6}$ torr) to form ErSi_2 . The resulting surface morphology can be seen in the cross-sectional micrograph of Figure 1. The pits are generally a few μm in size and penetrate deep into the Si substrate with a depth generally 2 to 3 times the total silicide thickness. The pits possess a square or rectangular shape on $\langle 100 \rangle$ Si (and triangular on $\langle 111 \rangle$ Si, not shown in Figure 1), thus suggesting that the pits are related to the crystalline nature and orientation of the Si substrate.

The second structure was formed by the sequential deposition of first Si (~ 5000 Å) then Er (~ 1700 Å) onto a $\langle 100 \rangle$ Si substrate without breaking vacuum between depositions. Tsaur and Hung^[6] have shown that the metal/amorphous Si interface in samples prepared by sequential deposition without breaking vacuum is relatively free of contamination compared to that of metal/crystalline Si samples cleaned chemically. The amorphous Si thickness used here was more than enough to react completely with the Er layer to form ErSi_2 . Annealing of the Er/Si(a) samples results in layer-by-layer formation of silicides at low temperatures (300°C to 350°C); the thickness of the silicide increases as (annealing time)^{1/2}. These silicide formation characteristics are in marked contrast to those observed on Er/ $\langle 100 \rangle$ Si samples. After annealing at 450°C , the silicide surface appeared undulated (typical of most silicides) but free of pits. This can be seen in Figure 2.

The absence of deep surface pitting in the Er/Si(a) structure may be due to either unique interfacial reactions present in the Er/Si(a) system

or the relative cleanliness of the Er/Si(a) interface. The presence of a clean Er-Si interface would promote a uniform silicide reaction over the Si surface.

Three experiments were performed to further ascertain the origins of the silicide surface pitting. The first experiment consisted of preparing Er/<100>Si samples in ultra-high vacuum (UHV) to obtain a clean Er/crystalline Si interface. A thin thermal oxide ($\sim 2000\text{\AA}$) was first grown on the <100> Si substrate, the oxide layer was then etched off with a 10% HF-H₂O solution, followed by immediate loading into an ion pumped vacuum chamber. Once a vacuum of $\sim 5 \times 10^{-10}$ torr was obtained, the Si substrate was backside heated to 500-600°C. This heating resulted in the desorption of mainly Fluorine atoms (originating from HF used on the Si surface) from the substrate surface as determined by a residual gas analyzer. After cooling to room temperature, the substrate Er ($\sim 1300\text{\AA}$) was deposited onto the Si surface at a rate of 10-20Å/sec. The chamber pressure was 10^{-9} torr during deposition. We believe the Er/<100> Si interface thus prepared is much cleaner than that for the sample shown in Figure 1, although no chemical analysis was done on the samples^[7,8]. After silicide formation, the surface possessed a low density of very shallow pits (see Figure 3). This experimental result indicates that relatively clean Er/crystalline Si interface leads to little or no surface pitting.

Ion-beam mixing technique was used to modify the silicide surface morphology in a second experiment. It has been shown that interfacial contaminants such as thin oxide layers interlaced between a metal layer and Si substrate can be "broken-up" and dispersed, thus allowing silicide formation to proceed as if the oxide layer was absent^[9]. In our case, Si ions were used to irradiate a sample of Er (1700Å)/<100> Si (similar to the sample shown in Figure 1). Ion

implantation was done at 300 keV with a dose of $5 \times 10^{15} \text{ Si}^+/\text{cm}^2$ at room temperature. Under these implantation conditions, the Si substrate near the Er/Si interface would be damaged by implantation, however, the silicide reaction after annealing would consume more than the implantation damaged region in the Si substrate [the damaged thickness in Si is estimated to be R_p (projected range) + ΔR_p (standard deviation)]. The silicide layer would then contact relatively damage-free Si after the silicide formation. The surface of such a sample (after implantation and annealing) is again relatively free of pits as illustrated in Figure 4. This experiment again points to the role of surface impurities or contamination in the development of a rough and pitted morphology.

A third experiment was performed in an attempt to develop a simple means by which a smooth silicide layer may be formed without the use of UHV or ion-implantation techniques. Samples of Er ($\sim 1700\text{\AA}$)/Si(a), $\sim 1300\text{\AA}/\langle 100 \rangle$ Si were prepared by sequential deposition in moderate vacuum ($\sim 1 \times 10^{-7}$ torr) onto a $\langle 100 \rangle$ Si substrate. The substrate cleaning procedure was identical to that used in the structures of Figures 1 and 2. It is to be noted that the amorphous Si thickness was less than necessary to consume all Er to form ErSi_2 , additional Si from the substrate was needed to react the Er layer completely. After silicide formation the silicide layer would be in contact with crystalline Si, similar to the situation described in the previous experiment (ion irradiation). In this case, surface pits were again observed. Although here the density of pits is decreased from the case of Figure 1, and the shape of the pits was not regular (see Figure 5). This indicates that while a smooth silicide layer may be initially formed through the reaction of Er and a-Si, the progression of the silicide reaction through a contaminated a-Si/Si interface nucleates the pit structures.

Differences in the physical structures of the silicide formed under the varying experimental conditions were also investigated in this study. X-ray diffraction experiments (Read Camera) showed that ErSi_2 layers formed by various processing steps have hexagonal structure, as reported before^[1]. However, strong texture $[(100)\text{ErSi}_2// (100)\text{Si}]$ was observed for ErSi_2 formed on clean $\langle 100 \rangle$ Si substrate (sample shown in Figure 3). The texture was so strong that modest channeling effect could be observed by MeV He^+ beam aligned with the $\langle 100 \rangle$ direction of Si. Clean Si surface, therefore, not only promotes pit free silicide formation but also provides a certain degree of epitaxial alignment of the silicide. Silicide layers formed on contaminated $\langle 100 \rangle$ Si (Figure 1), amorphous Si (Figures 2 & 5) and on $\langle 100 \rangle$ Si with ion irradiation (Figure 4) were randomly oriented.

All these experimental results are consistent with the idea that interfacial contamination is the cause of surface pits in the silicide layer. We recognize that no chemical analysis (SIMS or Auger) was performed to determine interfacial cleanliness, however, we believe that the experimental evidence is strong enough to draw such a conclusion. We speculate that silicide nucleates initially through "weak" spots at the contaminated interface. Once silicide formation is initiated, reaction kinetics are so rapid that columns of silicide are formed. Silicon atoms from the substrate migrate through the silicide columns and then spread laterally to react with the remaining Er. The silicide between the columns are formed by a lateral growth of the columns and not by a spatially uniform reaction between the remaining Er layer and the Si substrate underneath. In such a manner, the initially formed columns are observed as pits. This concept is consistent with the observation that Si is the moving species during silicide formation. On clean surfaces (either by high-vacuum processing or by ion beam dispersion of interfacial contamination), silicide formation proceeds in a uniform manner across the entire sample surface, resulting in a silicide layer which is relatively flat and free of pits.

In summary, we believe the deep surface pits formed on rare-earth silicides are caused by interfacial contamination at the silicon-silicide interface. It has been shown that by use of in-situ cleaning in a UHV vacuum environment or by use of ion-implantation techniques the surface pitting can be reduced or eliminated. Work is currently underway to determine the effects of varying surface morphology on the electronic performance of silicide Schottky barrier devices.

Acknowledgments

The authors are indebted to Rouel Fernandez for technical assistance. This work is supported by DARPA (MAA 903-81-C-0348, S. Roosild) at University of California, San Diego. The implantation part of this study at Caltech was financially supported by the U.S. Department of Energy through an agreement with the National Aeronautics and Space Administration and monitored by the Jet Propulsion Laboratory, California Institute of Technology, (D. Bickler). We would like to acknowledge Dr. Martti Mäenpää for his participation in the initial stage of this work.

References

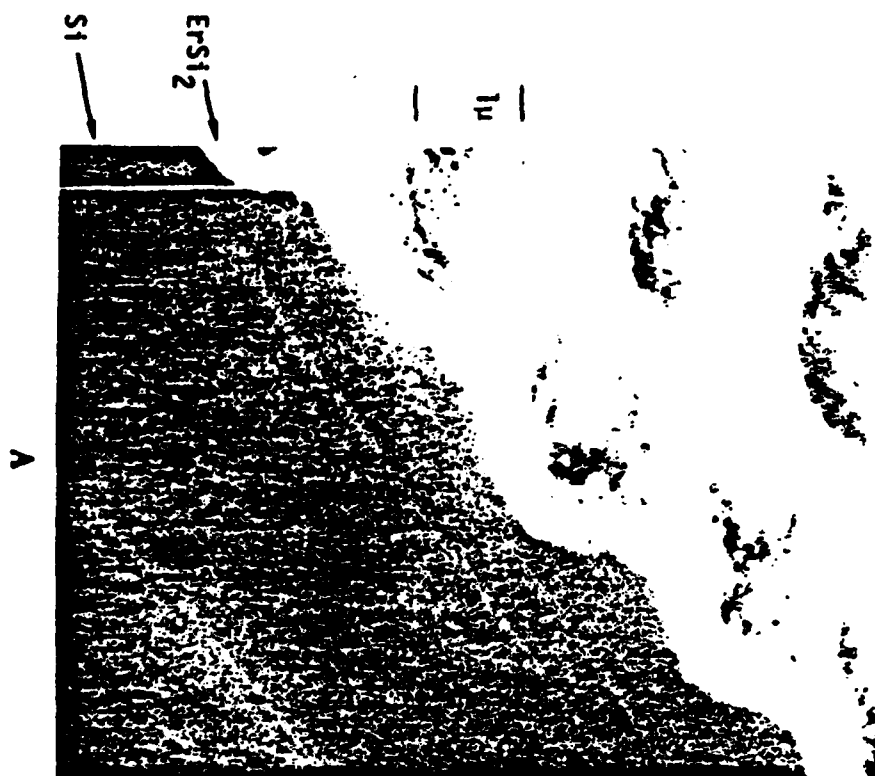
a) Present Address: IBM Research Center, Yorktown Heights, NY 10598

b) Permanent Address: Qinghua University, Beijing, The People's Republic of China

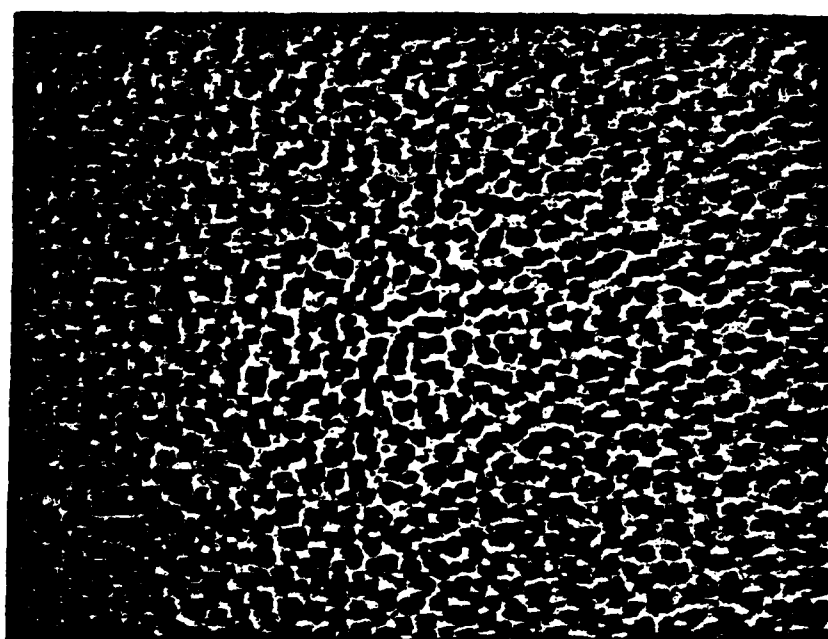
1. J. E. E. Bagliu, F. M. d'Heurle and C. S. Petersson, Appl. Phys. Lett. 36, 594 (1980).
2. R. D. Thompson, B. Y. Tsaur and K. N. Tu, Appl. Phys. Lett. 38, 535 (1981).
3. J. E. E. Bagliu, F. M. d'Heurle and C. S. Petersson, J. Appl. Phys. 52, 2841 (1981).
4. K. N. Tu, R. D. Thompson and B. Y. Tsaur, Appl. Phys. Lett. 38, 626 (1981).
5. H. Norde, J. de Sousa Pires, F. d'Heurle, F. Pesavento, S. Petersson and P. A. Tove, Appl. Phys. Lett. 38, 865 (1981).
6. B. Y. Tsaur and L. S. Hung, Appl. Phys. Lett. 37, 922 (1980).
7. L. S. Hung, S. S. Lau, M. von Allmen, J. W. Mayer, B. M. Ullrich, J. E. Baker, P. Williams and W. F. Tseng, Appl. Phys. Lett. 37, 909 (1980).
8. S. I. Raider, R. Flitsch and M. J. Palmer, J. Electrochem. Soc. 122, 413 (1975)
9. L. S. Wielunski, C. D. Lien, B. X. Liu and M.-A. Nicolet, J. Vac. Sci. Technol., to be published (1982).

Figure Captions

- Figure 1 Surface morphology of ErSi_2 on $\langle 100 \rangle$ Si, formed by vacuum annealing (450°C , 30 min) a sample of $\text{Er} (\sim 1700\text{\AA})/\langle 100 \rangle$ Si. (a) scanning electron micrograph of cross-sectional view, (b) optical micrograph taken with Normaski interference.
- Figure 2 Surface morphology of ErSi_2 on amorphous Si, formed by vacuum annealing (450°C , 30 min) a sample of $\text{Er} (\sim 1700\text{\AA})/\text{Si(a, } \sim 5000\text{\AA})/\langle 100 \rangle$ Si. (a) scanning electron micrograph of cross-sectional view, (b) optical micrograph taken with Normaski interference.
- Figure 3 Surface morphology of ErSi_2 on $\langle 100 \rangle$ Si, formed as before. A clean substrate surface was prepared in situ under a vacuum of $\sim 5 \times 10^{-10}$ torr. (a) scanning electron micrograph of cross-sectional view, (b) optical micrograph taken with Normaski interference.
- Figure 4 Surface morphology of ErSi_2 on $\langle 100 \rangle$ Si. This sample [$\text{Er}(\sim 1700\text{\AA})/\langle 100 \rangle \text{Si}$] has been implanted with Si ions and then vacuum annealed to form ErSi_2 . (a) scanning electron micrograph of cross-sectional view, (b) optical micrograph taken with Normaski interference.
- Figure 5 Surface morphology of ErSi_2 formed on a sample with initial configuration of $\text{Er} (\sim 1700\text{\AA})/\text{Si (a, } \sim 1300\text{\AA})/\langle 100 \rangle$ Si. The thickness of a-Si is less than necessary to consume the Er layer. Additional Si from the substrate is needed to react the Er layer completely. (a) Scanning electron micrograph of cross-sectional view, (b) optical micrograph taken with Normaski interference.

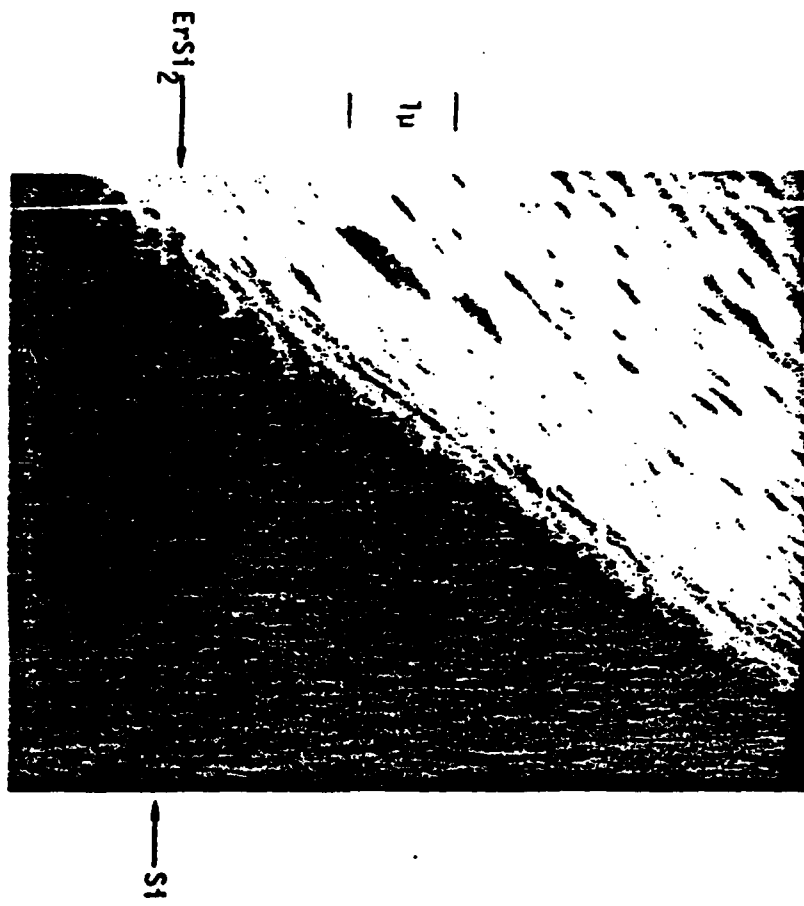


A

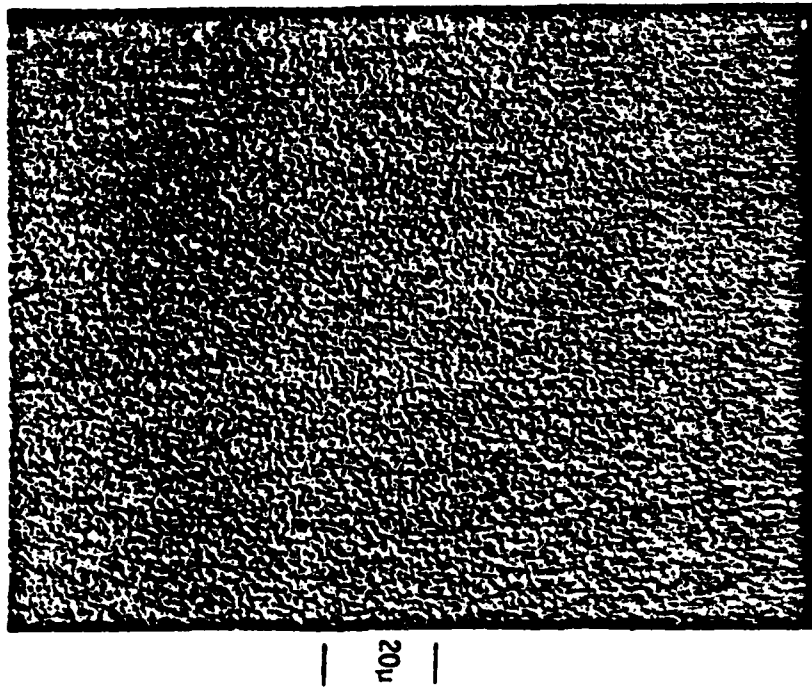


B

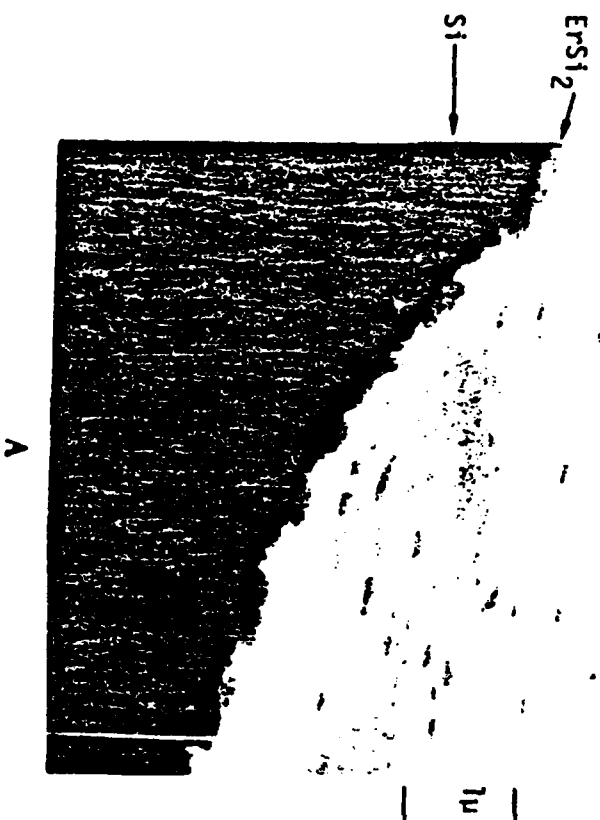
20μ



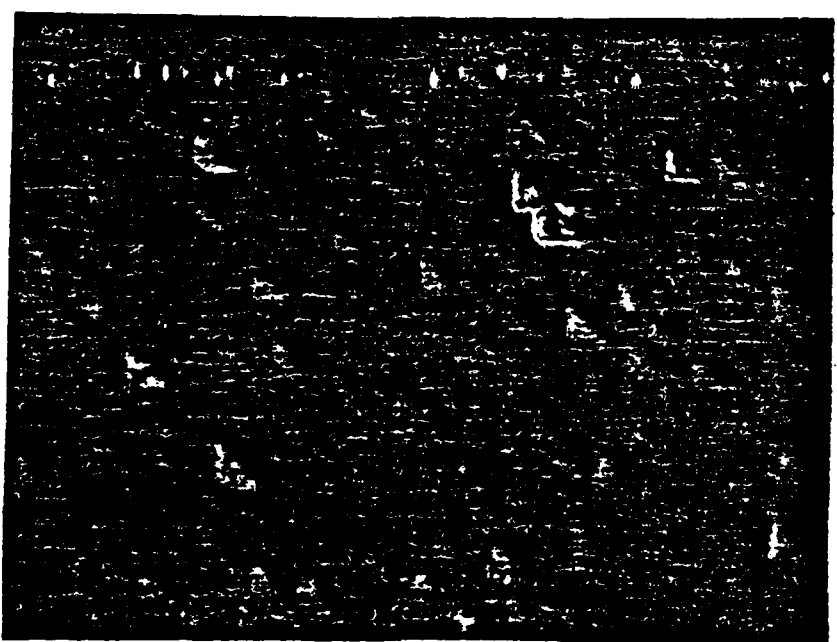
A



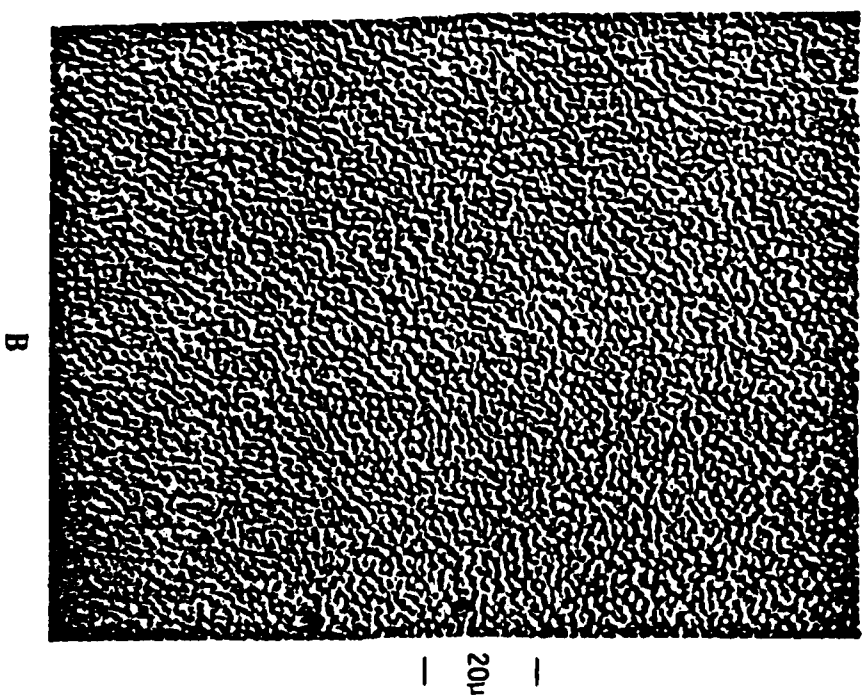
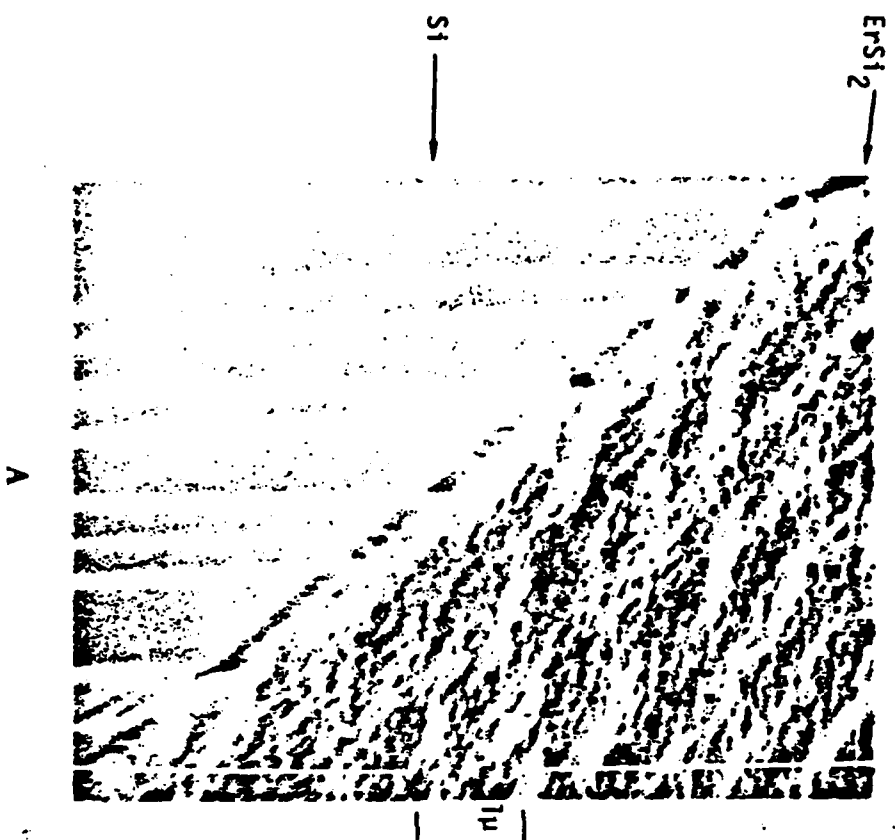
B



A



B



APPENDIX 2

Surface morphology and electronic properties of erbium silicide

C. S. Wu, S. S. Lau

Department of Electrical Engineering and Computer Sciences, University
of California, San Diego, La Jolla, California 92093

T. F. Kuech ^(a) and B. X. Liu ^(b)

California Institute of Technology, Pasadena, California 91125

Abstract

The surface of ErSi_2 , formed by the reaction of thin Er layers with a single crystal silicon substrate, is typically dominated by deep penetrating, regularly shaped pits. These pits are shown to have detrimental effects on the electronic performance of Schottky barrier height diodes. Surface pits may be reduced in density or eliminated entirely by (i) the use of Si substrate surfaces prepared under ultra-high vacuum conditions prior to metal deposition, or (ii) by means of ion irradiation techniques, or (iii) by reacting Er with an

(a) Present address: IBM Research Center, Yorktown Heights, NY 10598

(b) Permanent address: Quinghua University, Beijing, The People's
Republic of China

amorphous Si layer. In this investigation, planar ErSi_2 layers (pit-free) are made using the third approach with a sample structure of $\text{Si(a)}/\text{Er}/\text{Si<crystal>}$. The fast reaction between amorphous Si and Er leads to a planar sample structure of $\text{ErSi}_2/\text{Si<crystal>}$ with little or no reaction between Er and the crystalline Si substrate. The electronic performance of pit-free ErSi_2 diodes made in this manner is shown to be much superior to those made by reacting Er with Si substrates.

I. Introduction

The formation of rare-earth metal silicides is characterized by the following observations: (1) the solid state interactions between rare-earth metals (such as Er and Tb) and single crystal Si exhibit a critical temperature phenomenon [1-3]. Below the critical annealing temperature, interactions are very sluggish. Above the critical anneal temperature, interactions are fast, such that within minutes of annealing a layer of rare-earth metal (typically a hundred to a few thousand Å thick) deposited on Si is consumed completely to form a rare-earth metal silicide; (2) Si is found to be the dominant moving species during interactions; (3) the surface morphology of the silicide is typically dominated by a heavy pitting and the pitting is often crystallographic in nature [2]; (4) the surface pits may be reduced in density or eliminated entirely through either the use of Si substrate surfaces prepared under ultra-high vacuum conditions prior to metal deposition and silicide formation or by means of ion implantation techniques. Silicide layers formed by these techniques possess an almost planar morphology [4]; (5) Silicide formation behavior between Er and amorphous Si is distinctly different from that between Er and crystalline Si. Erbium reacts with amorphous Si to form ErSi_2 in a layer by layer fashion at temperatures as low as $\sim 300^\circ\text{C}$, as compared to the critical temperature for reaction observed for crystalline Si ($\sim 390^\circ\text{C}$). The reaction kinetics are observed to be diffusion controlled [5], and the ErSi_2 layer formed in this manner is laterally uniform without any surface pits [4].

Rare-earth silicides form low Schottky barriers, ϕ_B^n , to n-type Si with $\phi_B^n \approx 0.3 - 0.4\text{eV}$ [6,7]. This suggests the utility of these Schottky barrier diodes in infrared detecting applications. The presence of surface non-

uniformities, such as surface pitting, could prove to have a detrimental effect on the electronic performance of Schottky barrier devices as well as inaccurate determination of barrier heights by I-V measurements.

The objectives of the present study were to form pit-free ErSi_2 layers using amorphous Si, without recourse to ion implantation or ultra-high vacuum techniques; and to compare electronic performance of ErSi_2 diodes with and without surface pitting.

The approach we used to fabricate pit-free ErSi_2 was to utilize the fast reaction kinetic rate between Er and amorphous Si [4,5]. In this case, a layer of Er was first deposited on a <100> Si substrate followed by the deposition of Si on top of the Er layer. A relatively low temperature annealing (300 - 450°C) leads to the formation of pit-free ErSi_2 between the Er layer and the amorphous Si, without silicide formation between Er and crystalline Si. The situation is schematically shown in Figure 1.

II. Experimental

Silicon substrates (p-type, 1-10 Ωcm , <100> in orientation) were used in this study to facilitate barrier height measurements, ($\phi_B^p \sim 0.7 - 0.8\text{V}$). The wafers were first cleaned by organic solvents, followed by an RCA cleaning process with a final rinse in an HF solution. The wafers were loaded immediately into an ion-pumped vacuum chamber. A layer of Er ($\sim 500 \text{ \AA}$) was deposited onto the substrates, followed by the deposition of Si ($\sim 750 \text{ \AA}$ n-type 0.002 $\Omega\text{-cm}$) on top of the Er layer. The Si layer thickness was chosen such that a layer of ErSi_2 would form after thermal annealing. The rate of deposition was $\sim 10 \text{ \AA/sec}$ for Er and 20 - 30 \AA/sec for Si, at a pressure of $\sim 10^{-7}$ torr. A heavily doped n-type Si charge was used for evaporation to increase the conductivity of the deposited Si (amorphous) layer so that electrical measurements could be made before any silicide formation.

For electrical evaluation, diodes with sizes of 0.5 mm, 1 mm and 3 mm in diameter were made on the wafers with mechanical masks. For comparative purposes a similar set of diodes with only Er on p-Si was also made. The samples were analyzed before and after vacuum ($< 5 \times 10^{-7}$ torr) or flowing forming gas (15% H_2 , 85% N_2) annealing with x-ray Read Camera and MeV $^4\text{He}^+$ backscattering techniques. The barrier heights and leakage currents were determined by current voltage measurements.

III. Results

The surface morphologies of ErSi_2 layers formed on Si with the conventional method and with the new approach are shown in Figure 1. It can be seen from the optical micrographs that the ErSi_2 layer formed by reacting Er with amorphous Si on top of Er is much more uniform laterally than that formed by reacting Er with the Si substrate.

The forward and reverse I-V characteristics of these samples before annealing (silicide formation) are shown in Figure 2 (only 3 mm diodes are shown). The barrier heights, ϕ_B^D , of both $\text{Er/Si}\langle p,100 \rangle$ and $\text{Si(a)/Er/Si}\langle p,100 \rangle$ samples are found to be $0.68 \pm 0.01 \text{ eV}$ with an n factor of ~ 1.05 , relatively independent of the size of the diodes. Since these diodes have not been passivated, the reverse currents cannot be determined accurately. However, the lowest reverse currents measured at 10 volts are about seven times (7x) higher than the theoretical reverse current, calculated from considering only the effect of image force lowering.

After silicide formation, the barrier heights of both types of samples are observed to increase. Figure 3 shows the I-V characteristics observed on both types of samples after annealing at 450°C for 30 minutes in forming gas.

The barrier height, ϕ_B^D , of ErSi_2 diodes formed by reacting Er with Si substrate is found to be $0.7 \pm 0.02 \text{ eV}$ with an n factor of ~ 1.1 . The silicide layer formed on this type of sample ($\text{Er/Si}\langle 100 \rangle$) is not laterally uniform as shown in Figure 1. The reverse characteristics show soft break down behavior (see Figure 3). The lowest reverse current measured at 10 V is about 100 times the calculated reverse current. The barrier height, ϕ_B^D , of ErSi_2 formed by reacting Er with amorphous Si is found to be $0.76 \pm 0.02 \text{ eV}$ with an n factor of 1.05. The reverse currents for this type of sample ($\text{Si(a)/Er/Si}\langle p,100 \rangle$)

after silicide formation are usually much smaller than those observed on Er/Si<100> samples after silicide formation. The lowest reverse current measured at 10 V is about 20 times the calculated reverse current (Figure 3).

It is also found that the barrier heights of both types of samples change as a function of annealing temperature for a given annealing time. This behavior is shown in Figure 4 (for a 30 minute annealing period). For samples with a configuration of Si(a)/Er/Si<p,100>, the barrier height increases from an as-deposited value of ~ 0.68 eV to a maximum of ~ 0.77 eV at $\sim 380^\circ\text{C}$ and then gradually decreases to 0.74 eV at 500°C . The initial rise of ϕ_B^p is believed to be due to the reduction of the interfacial oxide and other contaminations, between the Er layer and the Si substrate, by the Er layer without silicide formation, thus allowing intimate contact between Er and the Si substrate. A maximum value of ϕ_B^p is obtained when an ErSi_2 layer is formed between Er and amorphous Si and is in contact with the Si substrate. The temperature and time (380°C , 30 minutes) for this to occur is consistent with reported kinetics [5], and confirmed by backscattering in our case. The reason for the gradual decrease of ϕ_B^p after the maximum is not clear at present. However, this could be due to the very rapid reaction rate between Er and amorphous Si to form silicide at high temperatures, such that the reduction of interfacial oxide could not be completed before the total consumption of Er. For samples with an Er/Si<p,100> configuration, ϕ_B^p increases from 0.68 eV to a maximum of 0.75 eV at $\sim 350^\circ\text{C}$ and then decreases relatively rapidly to ~ 0.68 eV at $\sim 500^\circ\text{C}$. The initial rise of ϕ_B^p can be interpreted as before. The decrease of ϕ_B^p after the maximum is likely to be an effect of silicide formation between Er and the Si substrate. Because of silicide formation, pits begin to form at the $\text{ErSi}_2/\text{Si}<\text{p},100>$ interface, thus affecting the effective area for current density determination. Shallow

pits are visible after annealing at 380°C for 30 minutes. As the annealing temperature increases, surface pits become more pronounced. The barrier height is observed to decrease rapidly between 400°C and 450°C, corresponding to the appearance of a high density of deep penetrating surface pits.

The effect of annealing time at a given temperature on the barrier height is shown in Figure 5 (380°C annealing). For samples with a Si(a)/Er/Si<p,100> configuration, ϕ_B^P increases with annealing time until it reaches a saturation value (~ 0.77 eV) after ~ 0.4 hours of annealing. This corresponds to the total consumption of Er to form ErSi_2 between Er and amorphous Si and the Si substrate is now in contact with a planar ErSi_2 layer. For samples with an Er/Si<p,100> configuration, ϕ_B^P reaches a saturation value of ~ 0.72 eV after ~ 0.1 hours of annealing. We believe that this is the time necessary to reduce the interfacial oxide by Er at 380°C. Shallow surface pits begin to develop after 30 minutes of annealing. The barrier height remains relatively constant at ~ 0.72 eV even after 10 hours of annealing, although shallow surface pits appear to increase somewhat after longer periods of annealing. The electrical properties of Er silicide diodes formed on both types of samples are briefly summarized in Table 1.

IV. Discussion and Summary

The effects of lateral non-uniformity of ErSi_2 layers can be clearly seen by the lowered barrier heights and increased reverse currents (see Figures 1 and 3). These observations can be explained by an increased effective area of diodes for current transport and high electric fields associated with pits in the ErSi_2 layer. Using a sample configuration of $\text{Si(a)}/\text{Er}/\text{Si}\langle\text{xtal}\rangle$, laterally uniform ErSi_2 layers can be formed on single crystal Si substrates. This approach takes advantage of the fact that Er reacts with amorphous Si at temperatures much lower than the critical temperature above which Er reacts with single crystal Si rapidly. Diodes of ErSi_2 with a planar structure are shown to have higher barrier heights and much reduced reverse currents. At temperatures below the critical temperature, the reaction between Er and single crystal Si to ErSi_2 is sluggish, however, we suggest that the Er layer can reduce the native oxide layer and other contaminations located at the $\text{Er}/\text{Si}\langle\text{xtal}\rangle$ interface due to the chemical activity of Er. The reduction of interfacial contamination permits a more intimate contact between Er and the Si surface and leads to increased barrier heights without silicide formation, as shown in the initial rise of ϕ_B^p in Figures 4 and 5. This speculation is supported by the observation that when an HF rinsed Si substrate is backside heated to $500^\circ\text{C} - 600^\circ\text{C}$ in a vacuum of $\sim 1 \times 10^{-8}$ torr and then cooled to room temperature before Er deposition, the barrier height of such a sample is ~ 0.8 eV which is much higher than those obtained on samples without backside heating (~ 0.68 eV). This heating resulted in the desorption of mainly fluorine atoms (originating from HF used on the Si surface), and should lead to a relatively contamination free Si surface [4] (hence the high ϕ_B^p value).

Although high barrier height Schottky diodes of Er on p-Si (hence low barrier heights on n-Si) can be fabricated by proper preparation of the Si

substrate without silicide formation, the elemental Er layer is extremely active and normally oxidizes in room air. Formation of ErSi_2 improves the stability of these diodes significantly, since ErSi_2 is stable up to 800°C and above. Using a sample configuration of $\text{Si(a)}/\text{Er}/\text{Si}\langle\text{xtal}\rangle$ not only allows the formation of laterally uniform ErSi_2 layers, but also relaxes the annealing ambient for silicide formation. In fact, functional planar diodes of ErSi_2 can be obtained by annealing the $\text{Si(a)}/\text{Er}/\text{Si}\langle 100 \rangle$ structure in air at $\sim 400^\circ\text{C}$. This is because the top amorphous Si layer protects the Er layer from oxidation. Once silicide is formed between Er and amorphous Si, the resulting ErSi_2 layer is stable against oxidation at $\sim 400^\circ\text{C}$.

In summary, we have shown that laterally uniform ErSi_2 layers can be easily formed by a simple method. The barrier heights determined by I-V measurements on pit-free ErSi_2 diodes are believed to be more accurate. Schottky diodes of ErSi_2 are stable against oxidation and should prove useful as reliable infrared detectors (on n-type Si).

Acknowledgement

The authors are indebted to R. Fernandez for technical assistance, M. Bartur and M-A. Nicolet (Caltech) for discussion. This work is supported by DARPA (MAA 903-81-C-0348, S. Roosild) at the University of California, San Diego, and by the U.S. Department of Energy through an agreement with the National Aeronautics and Space Administration and monitored by the Jet Propulsion Laboratory at the California Institute of Technology (D. Bickler).

Table 1
Electrical Properties of ErSi₂ Diodes

Sample Configuration	Annealing Condition	Surface Condition	ϕ_B^p (eV)	n
Er/Si<p,100>	as-deposited	planar	0.68 ± 0.01	1.05
Er/Si<p,100>	380°C, 60 min* silicide formed	pits	0.71 ± 0.02	1.1
Si(a)/Er/Si<p,100>	as-deposited	planar	0.68 ± 0.01	1.05
Si(a)/Er/Si<p,100>	380°C, 30 min* silicide formed	planar	0.78 ± 0.02	1.05

* annealing condition for achieving maximum barrier heights

References

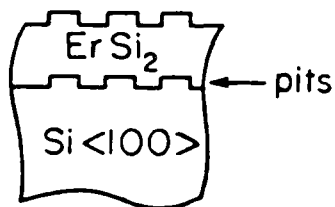
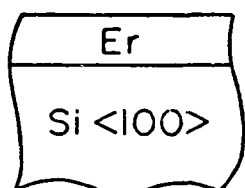
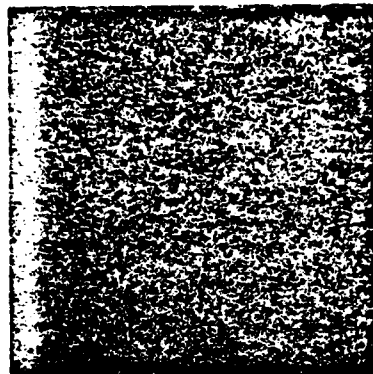
1. J. E. E. Baglin, F. M. d'Heurle and C. S. Petersson, Appl. Phys. Lett. 36, 594 (1980).
2. R. D. Thompson, B. Y. Tsaur and K. N. Tu, Appl. Phys. Lett. 52, 2841 (1981).
3. J. E. E. Baglin, F. M. d'Heurle and C. S. Petersson, J. Appl. Phys. 52, 2841 (1981).
4. S. S. Lau, C. S. Pai, C. S. Wu, T. F. Kuech and B. X. Liu, Appl. Phys. Lett. 41, 77 (1982).
5. B. Y. Tsaur and L. S. Hung, Appl. Phys. Lett. 38, 626 (1981).
6. K. N. Tu, R. D. Thompson and B. Y. Tsaur, Appl. Phys. Lett. 38, 626 (1981).
7. H. Norde, J. de Sousa Pires, F. d'Heurle, F. Pesavento, S. Petersson and P. A. Tove, Appl. Phys. Lett. 38, 865 (1981).

Figure Captions

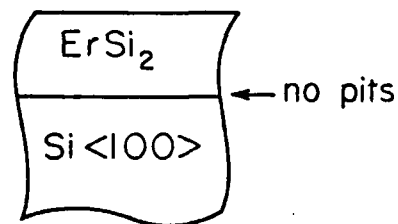
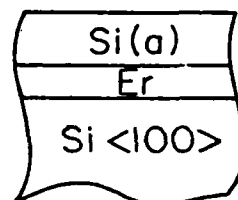
1. Upper portion: Optical micrographs (with Normaski contrast) of top views of ErSi_2 layers formed by two different methods. Lower portion: Schematic showing ErSi_2 Schottky barrier contacts formed by conventional method and the new approach.
2. I-V characteristics of $\text{Er/Si}\langle p,100 \rangle$ and $\text{Si(a)}/\text{Er/Si}\langle p,100 \rangle$ diodes before annealing. The diode size is 3 mm in diameter.
3. I-V characteristics of $\text{Er/Si}\langle p,100 \rangle$ and $\text{Si(a)}/\text{Er/Si}\langle p,100 \rangle$ diodes (3 mm in diameter) after annealing at 450°C for 30 minutes in forming gas.
4. Barrier height vs. annealing temperature (30 minutes annealing time).
5. Barrier height vs. annealing time at 380°C .



10 μm

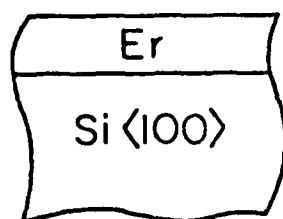
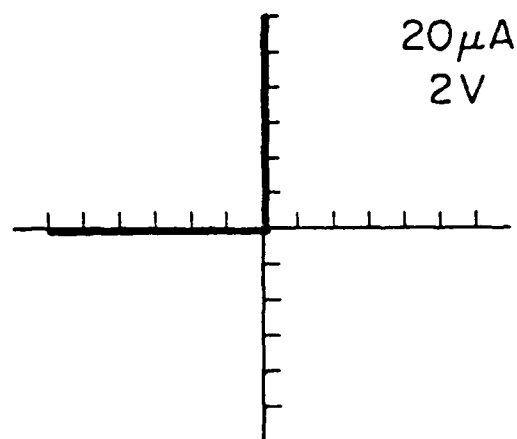


Conventional Method

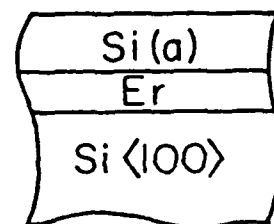


New Approach

450°C
30 min



Before Anneal
3mm diodes

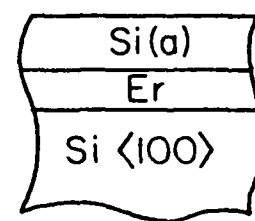
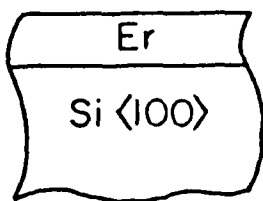
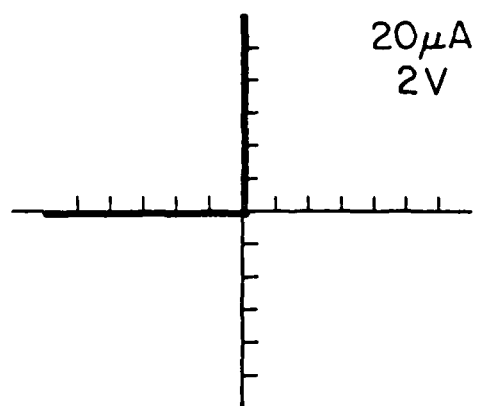
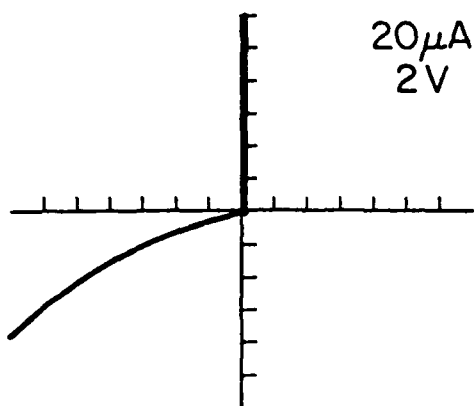


$$\phi_B^p = 0.68 \pm .01 \text{ eV}$$

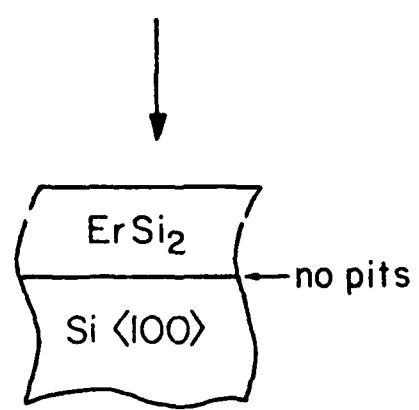
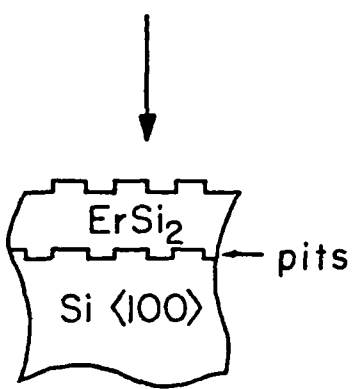
$$n \approx 1.05$$

$$\phi_B^p = 0.68 \pm .01 \text{ eV}$$

$$n \approx 1.05$$



450°C
30min
3mm diodes

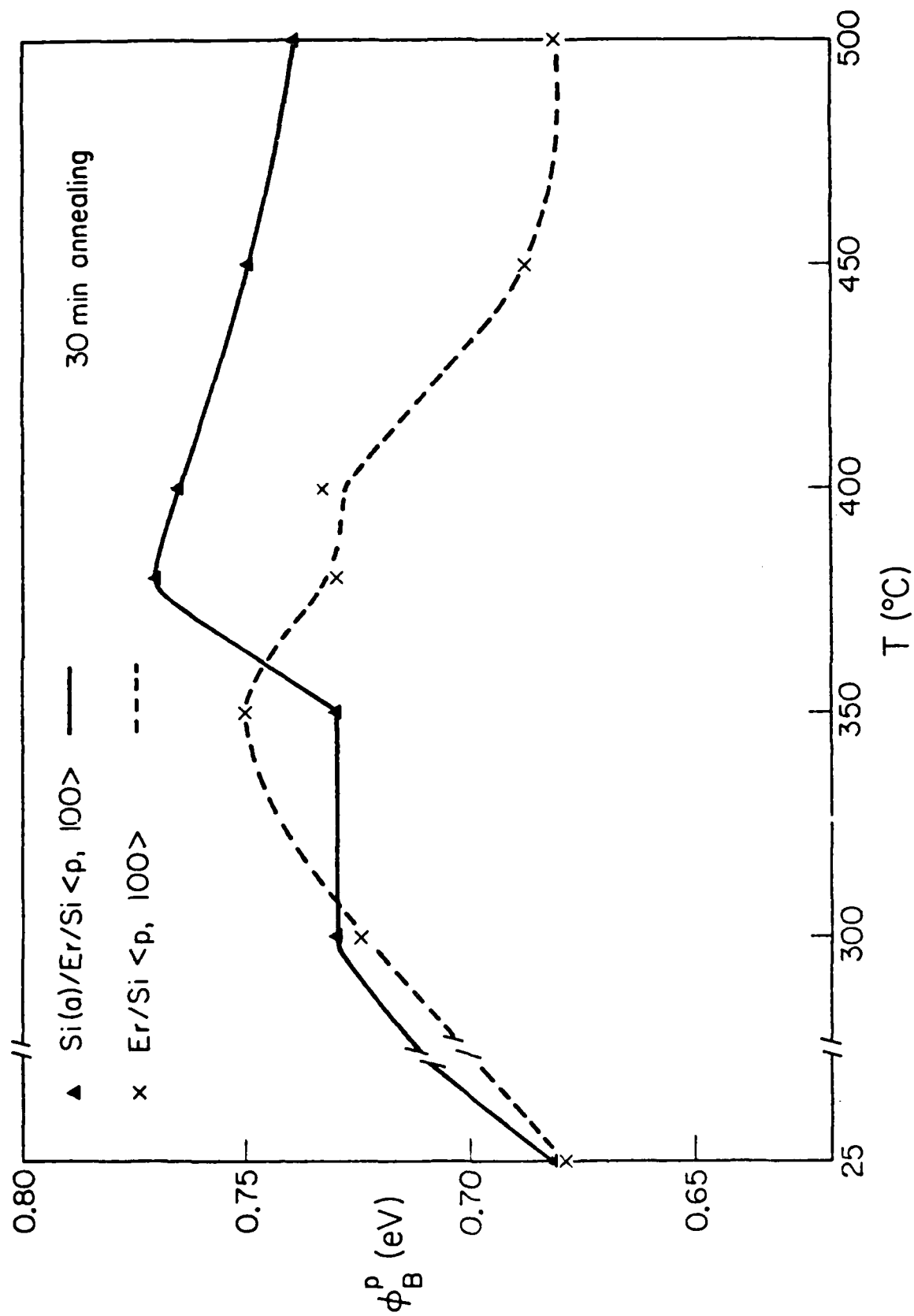


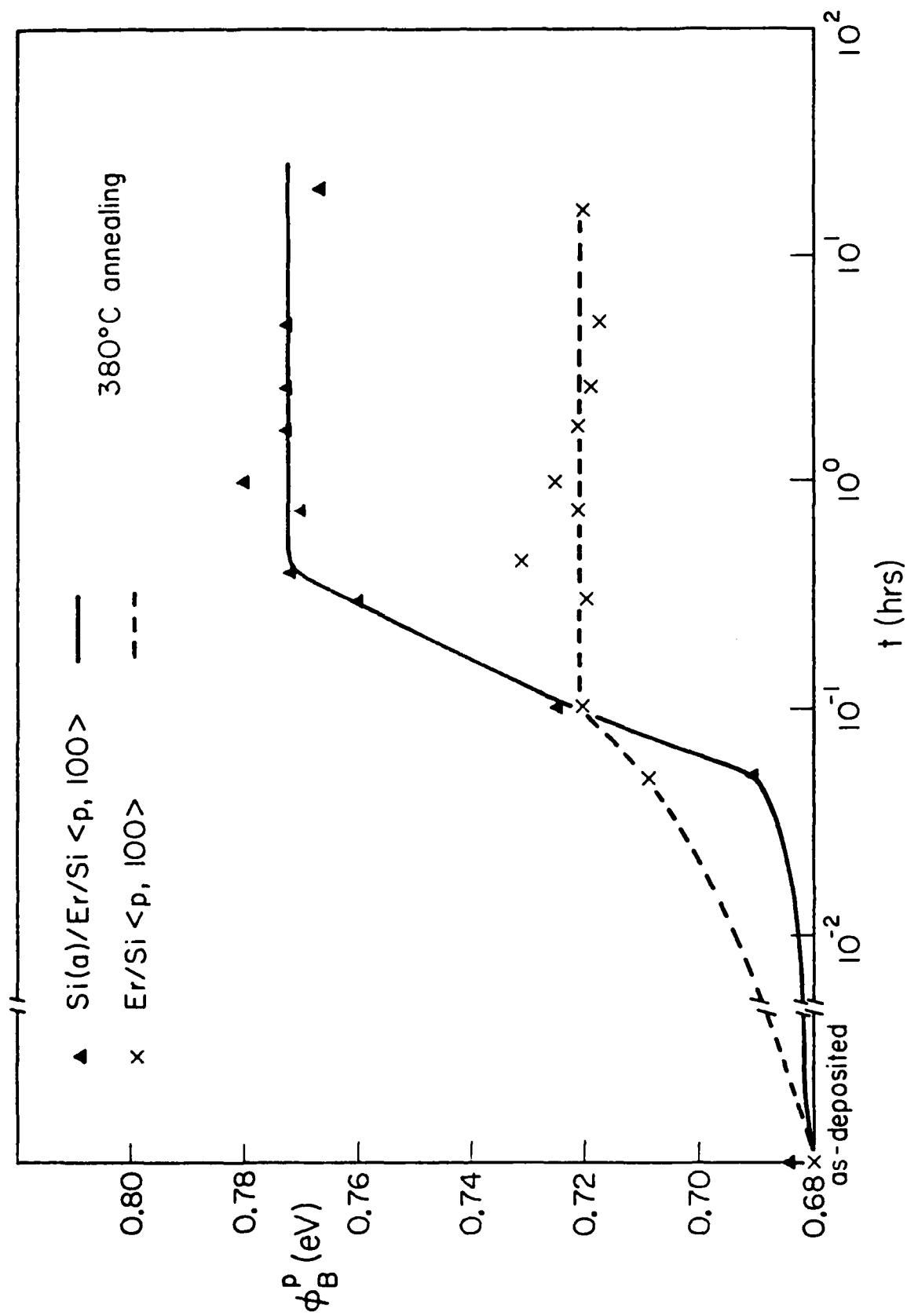
$$\phi_B^p = 0.70 \pm .02V$$

$$n \approx 1.1$$

$$\phi_B^p = 0.76 \pm .02V$$

$$n \approx 1.05$$





APPENDIX 3

ION IRRADIATION EFFECTS ON Pt CONTACTS TO Si WITH AND WITHOUT INTERFACIAL CHEMICAL OXIDE

THOMAS BANWELL, MANUELA FINETTI^{a)}, ILKKA SUNI^{b)} AND MARC-A. NICOLET
California Institute of Technology, Pasadena, California 91125, USA

and

S. S. LAU AND DAVID M. SCOTT
University of California at San Diego, La Jolla, California 92093, USA

ABSTRACT

The electrical properties of ion irradiated metal-semiconductor contacts are investigated. Silicide contacts are fabricated by depositing Pt on chemically clean or slightly oxidized ($\sim 14 \text{ \AA SiO}_2$) n^+ - and n -type $\langle 111 \rangle$ Si, followed by a Si ion irradiation ($10^{14} - 6 \times 10^{15} \text{ Si/cm}^2$) through the metal-Si interface at various substrate temperatures, and a final thermal annealing in vacuum to form the silicide. Forward I-V measurements are employed for electrical characterization. Metal-Si interaction and substrate damage are measured by MeV ion backscattering and channeling, and interfacial oxygen monitored by nuclear $^{16}\text{O}(d,\alpha)^{14}\text{N}$ reaction.

Platinum contacts prepared on clean n -type substrates are Schottky diodes with a barrier height $\phi_{Bn} = 0.83 \text{ eV}$. After Si irradiation, the forward $I(V)$ is a power law whose form is largely independent of the dose. Subsequent thermal annealing induces silicide formation, but at a reduced rate compared to irradiated samples. The dc characteristics is roughly exponential again, but departures from the original Schottky characteristics remain and are largest for the highest Si doses. The effect is attributed to radiation damage in the Si that is not consumed by the silicide reaction.

Platinum contacts prepared on chemically oxidized samples behave differently for different substrate materials, although the total amount of interfacial oxygen is always the same. On n^+ -type samples, the silicide formation at 400°C is laterally uniform for Si doses $> 2 \times 10^{14} \text{ cm}^{-2}$, but is nonuniform for all doses ($< 2 \times 10^{15} \text{ Si/cm}^2$) on n -type samples. For n^+ -type samples at 250°C , a dose of $2 \times 10^{15} \text{ Si/cm}^2$ is required to induce (uniform) silicide formation; the kinetics displays a time delay compared with that of clean n^+ substrates. On oxidized n -type substrates, the $I(V)$ characteristics of Pt contacts before irradiation is not Schottky-like, but power-law-type. After irradiation, the characteristic is the same as for the clean irradiated samples. Thermal annealing induces only incomplete recovery toward an exponential behavior.

^{a)} Permanent Address: LAMEL Laboratory, C.N.R., Via de Castagnoli 1, 40126 Bologna, Italy

^{b)} Permanent Address: Semiconductor Laboratory, Technical Research Centre of Finland, Otakaari 5A, SF-02150 Espoo 15, Finland

These results demonstrate that radiation damage in the unreacted Si remains significant for the electrical behavior of all.

These results demonstrate that radiation damage determines the I(V) characteristics of as-irradiated Pt contacts to n-type Si regardless of the presence of an interfacial oxide layer. After annealing at 400°C for 30 min, radiation damage is still significant, but the oxidized samples recover less than the clean ones. The results are attributed to radiation damage in the unreacted Si substrate.

INTRODUCTION

There is decided interest in ohmic and Schottky barrier contacts to Si using metal silicides because of their stable and reliable characteristics. It is desirable in VLSI technology to minimize the processing temperature employed for silicide formation. Residual contamination at the metal-Si interface can inhibit silicide formation [1] and results in laterally nonuniform silicide formation at low annealing temperatures [2,3]. The room temperature formation of several silicides induced by ion beam has been extensively investigated [4,5], although the electrical properties were not examined. Recent studies have demonstrated that a thin interfacial oxide diffusion barrier can be disrupted by ion irradiation allowing subsequent thermal silicide formation [3]. The ion irradiation also affects the bulk transport process.

We have investigated the influence of Si ion irradiation on the kinetics of Pt₂Si formation and on the forward I(V) behavior of Pt/Si Schottky diodes, both on substrates with and without an interfacial oxide layer produced by wet chemical oxidation. We also briefly examine the role of Si substrate doping level on the interfacial oxide layer's inhibition of Pt diffusion.

EXPERIMENTAL

Two types of Si wafers used in this study were n⁺-type 0.005-0.020 $\Omega \cdot \text{cm}$ <111> Si, and a 10 μm 10-30 $\Omega \cdot \text{cm}$ n-type epilayer on a 0.003 $\Omega \cdot \text{cm}$ n⁺ <111> substrates. Four wafers each were consecutively cleaned ultrasonically in acetone and methanol followed by etching in 12% HF and then slightly oxidized in a boiling solution of 1:H₂O₂:NH₃(aq.):H₂O = 1:1:5. One each of the oxidized wafers were rinsed in distilled water, blow dried with N₂, and loaded into an oil-free e-beam evaporation system. Clean substrates with only the unavoidable native oxide were prepared by dipping the other two wafers in 3% HF prior to loading. A metal mask was used to define square areas of $7.7 \times 10^{-2} \text{ cm}^2$ on the epitaxial wafers for contacts. A $\sim 800 \text{ \AA}$ Pt film was evaporated onto each substrate, during which the pressure was $< 10^{-7}$ torr. The interfacial oxygen on both of the oxidized substrates was measured using the ¹⁶O(d, α)¹⁴N nuclear reaction to be $6.5 \pm 0.8 \times 10^{15} \text{ atoms cm}^{-2}$, corresponding to $\sim 14 \text{ \AA}$ SiO₂. 0.1 μm Al contacts were evaporated onto the back surface of the epi wafers.

Silicon irradiations were made at sample temperatures of -196°C and 27°C with 180 - 200 keV Si⁺ ($R_p(\text{Pt}) \sim 670 \text{ \AA}$, $\Delta R_p(\text{Pt}) \sim 420 \text{ \AA}$) [6] to fluence of 0.2 - $2 \times 10^{15} \text{ cm}^{-2}$. The epi wafer samples were subsequently annealed at 400°C for 30 min in a quartz tube vacuum furnace. Standard forward dc I(V) measurements were made on the contacts after the Si irradiation and after annealing.

Samples studied for thermal reactivity were isothermally annealed over the temperature range 254 - 560°C for periods of 10 - 190 min. The samples were analyzed by 2.0 MeV ⁴He⁺ ion backscattering spectrometry. The Pt was etched from selected unannealed samples with boiling aqua regia and the damaged Si region analyzed by ⁴He⁺ ion channeling measurements.

RESULTS AND DISCUSSION

Figure 1 shows a semi-logarithmic plot of typical forward $I(V)$ curves for un-annealed Pt contacts with and without Si irradiation on both clean and oxidized n-type epi substrates. Schottky diode behavior is observed for as-deposited Pt on clean Si. The Schottky barrier height calculated assuming thermionic emission is $\phi_{bn} = 830$ mV, consistent with previously reported values [7]. The $I(V)$ relation for as-deposited Pt on oxidized Si is not exponential; rather, the curve suggests a power law dependence $I_F = (V_F)^p$ for $V_F > 50$ mV with $p = 2-3$. All of the contacts exhibit the same forward $I(V)$ characteristics after $0.2 - 2 \times 10^{15}$ Si cm^{-2} irradiation, independent of substrate temperature during irradiation. Again, a power law relationship is suggested, with $p = 2 \pm 0.2$, by these characteristics. This uniform behavior after irradiation indicates that electrical transport is dominated by radiation damage in the vicinity of the contact. This is consistent with the fact that a significant fraction of the implanted Si penetrates the Pt-Si interface at the energies employed [6].

The left-hand side of Fig. 2 shows semi-logarithmic plots of the forward $I(V)$ characteristics of typical Si irradiated Pt contacts on the clean n-type epi substrates after 400°C annealing for 30 min. It is evident that diode-like behavior is restored by the annealing. Some dependence on the Si irradiation remains, however, in that the contacts receiving the greatest Si fluence differ most from the unirradiated contacts which exhibit Schottky diode behavior ($\phi_{bn} = 842$ mV, $n = 1.05$). Backscattering spectra of all these samples show laterally uniform silicide formation with PtSi stoichiometry. We believe that the Si damaged by irradiation is not completely consumed during silicide formation. This is consistent with the observed influence of Si dose on the $I(V)$ characteristics after annealing. It is not anticipated that the 400°C annealing will entirely remove the radiation damage [8].

The influence of the Si irradiation on silicide formation kinetics is shown in Fig. 3. These measurements were made on the n^+ doped substrates, and pertain to the first silicide phase formed, namely Pt_2Si . Note the annealing temperature is only 254°C . In contrast, Fig. 2 pertains to n-type substrates and second phase formation at 400°C . Figure 3 shows that silicide formation remains transport limited after Si irradiation with a reduction in the diffusion constant. This concurs with previous observations that Xe irradiation also retards Pt silicide formation [3]. We note that the reaction rate decreases monotonically with increasing Si fluence. Channeling measurements performed on $2 \times 10^{15} \text{ cm}^{-2}$ Si irradiated samples, after Pt removal, show that the Si substrate is heavily damaged ("amorphized") to a depth of $\sim 2000 \text{ \AA}$.

Only 530 \AA of Si is consumed by the complete reaction of the Pt producing Pt_2Si . 1100 \AA of Si is consumed in the formation of PtSi. This supports our contention that a residual underlying damaged Si layer is involved in the

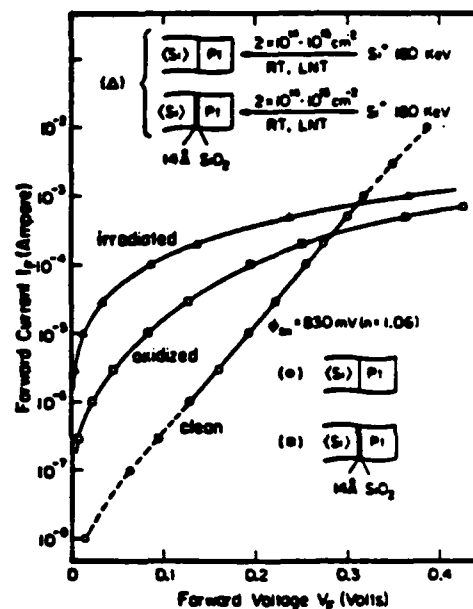


Fig. 1. Typical forward $I(V)$ characteristics of Pt contacts on clean and slightly oxidized n-Si before and after Si^+ irradiation. All contacts exhibit the same $I(V)$ behavior after the Si irradiation.

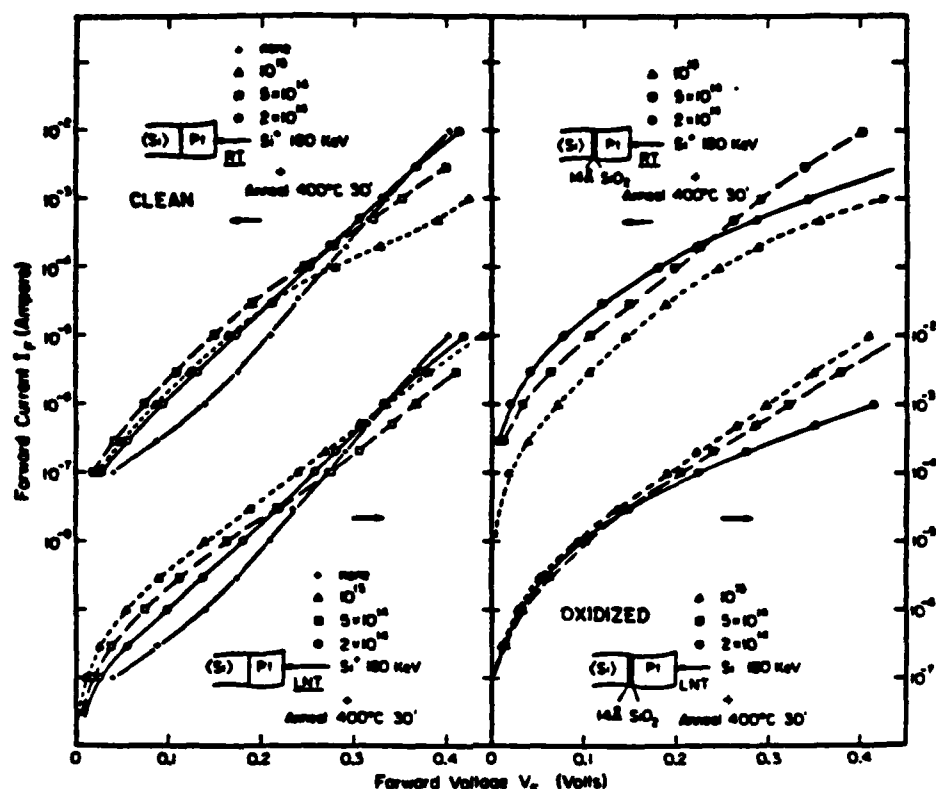


Fig. 2. Typical forward $I(V)$ characteristics of Si irradiated Pt contacts on clean and slightly oxidized n-Si after 400°C annealing for 30 min.

altered $I(V)$ characteristics of irradiated contacts after annealing (left-side of Fig. 2).

We also show in Fig. 3 kinetic studies on oxidized n^+ substrates also made at 254°C. No reaction is observed with as-deposited or $2 \times 10^{14} \text{ cm}^{-2}$ Si irradiated samples. Silicide formation is observed after a 27°C irradiation of $2 \times 10^{15} \text{ Si cm}^{-2}$ at 190 keV. In this case, the lateral uniformity of the moving interface is sufficient to define a kinetic behavior. The first phase silicide formation is again transport limited after a delayed initiation of ~ 27 min. The effective diffusion coefficient is only slightly lower than that observed with clean substrates identically irradiated. We guess that the delay is due to a slow permeation of the oxide barrier followed by its catastrophic failure after which transport is dominated by bulk diffusion.

In contrast to the annealing results at 254°C, Pt silicide formation is observed on the oxidized n^+ substrates after 400°C annealing, although the resulting Si-silicide interface is laterally nonuniform. A uniform interface is obtained with this substrate after 190 keV Si irradiation at fluences of $2 \times 10^{14} \text{ cm}^{-2}$ or more. However, radically different behavior was observed with the oxidized n-type epi wafers. In the later case, no reaction was evident by backscattering spectrometry with unirradiated samples for 30 min annealing at $< 500^\circ\text{C}$. Irradiated samples on the oxidized n-type epi substrates annealed at 400°C for 30 min either did not react or reacted nonuniformly. Typical forward $I(V)$ characteristics of these contacts are shown in the right-side of Fig. 2. It is clear from these curves that Schottky diode behavior is not produced after annealing as in the case with clean substrates. Since the interfacial oxygen is known to be the same for both n and n^+ substrates, we conclude that the oxide on highly doped material is structurally different from that formed on low doped

APPENDIX 4

ION MIXING AND PHASE DIAGRAMS

S. S. Lau^{a)}, B. X. Liu^{b)*}, and M-A. Nicolet^{b)}

a) University of California at San Diego, La Jolla, California 92093, U.S.A.

b) California Institute of Technology, Pasadena, California 91125, U.S.A.

Interactions induced by ion irradiation are generally considered to be non-equilibrium processes, whereas phase diagrams are determined by phase equilibria. These two entities are seemingly unrelated. However, if one assumes that quasi-equilibrium conditions prevail after the prompt events, subsequent reactions are driven toward equilibrium by thermodynamical forces. Under this assumption, ion-induced reactions are related to equilibrium and therefore to phase diagrams. This relationship can be seen in the similarity that exists in thin films between reactions induced by ion irradiation and reactions induced by thermal annealing. In the latter case, phase diagrams have been used to predict the phase sequence of stable compound formation, notably so in cases of silicide formation.

Ion-induced mixing not only can lead to stable compound formation, but also to metastable alloy formation. In some metal-metal systems, terminal solubilities can be greatly extended by ion mixing. In other cases, where the two constituents of the system have different crystal structures, extension of terminal solubility from both sides of the phase-diagram eventually becomes structurally incompatible and a glassy (amorphous) mixture can form. The composition range where this bifurcation is likely to occur is in the two-phase regions of the phase diagram. These concepts are potentially useful guides in selecting metal pairs that form metallic glasses by ion mixing. In this report, phenomenological correlation between stable (and metastable) phase formation and phase diagram is discussed in terms of recent experimental data.

*Permanent Address: Qinghua University, Beijing, The People's Republic of China.

I. Introduction

When an ion impinges on a target, a sequence of ballistic collisions is initiated by the penetrating ion. This initial part of the process has been referred to as the prompt phase of ion mixing and lasts about 10^{-12} sec. As the energy of the primary particle is distributed over a progressively larger number of atoms, one reaches a state where an average local energy or temperature may be defined. During the prompt event period, the displacement of atoms is presumed to be largely random, so that a correlation between ion-induced mixing of two chemically distinct species and their phase diagram is not expected. As the relaxation process proceeds, a quasi-equilibrium condition may exist locally. If phase diagrams were to be pertinent in this regime, one would expect that they should be diagrams for high pressures, on account of the confinement exerted by the surrounding material. After further relaxation of the excited regions, atoms and defects move toward a configuration that is even closer to thermal equilibrium. The temperature and pressure eventually reach conditions near those of commonly available phase diagrams. In this region a correlation with available phase diagrams may be expected.

Along the path toward equilibrium, metastable states may exist where atoms can be arrested. Without sufficient thermal energy to provide mobility, the system may be frozen in these metastable states and form metastable phases. If a correlation between ion-induced reactions and phase diagrams exists, it appears, then, that this correlation should result from effects that take place during the relaxation of the system after the primary impact (delayed effects).

In the following, we shall examine if indeed there is experimental evidence to indicate that ion-induced reactions between two elements can be correlated to the commonly available binary phase diagrams of the system in question.

II. Sample Configuration for Ion Mixing Experiments

In general, three types of sample configurations have been used to investigate ion mixing: (1) bilayered samples, where a thin film is deposited onto a substrate. At the early stages of ion irradiation, there is basically an unlimited supply of the top layer material and of the substrate material to interact and form a mixture. Under the conditions of unlimited supply of both components, there is a possibility for the mixed region to seek a preferred composition during the delayed phase of the mixing process; (2) multilayered samples, where interposing thin films ($\leq 100 \text{ \AA}$) of component A and B are deposited onto an inert substrate (e.g. SiO_2 or sapphire). The average and final composition of the sample in this case is fixed, barring sputtering effects. These samples are sometimes referred to as having a limited supply configuration; (3) thin marker samples, where a very thin marker ($\leq 10 \text{ \AA}$) is imbedded in a matrix of host atoms. The first type of samples (bilayered, unlimited supply) are usually used to compare ion-induced reactions with thin-film reactions that proceed under steady-state annealing conditions. The second type of samples (multilayered, limited supply) are usually used to investigate metastable and amorphous phase formation of a given composition. The third type of samples (thin marker) are used to investigate the basic aspects of ion mixing.

The presently accepted view is that for significant mixing to occur at a given interface, the ions must have sufficient energy to penetrate that interface.

III. The Q-Curve

In ion mixing experiments, it is often observed, especially in compound forming systems, that the amount of intermixing has two relatively distinct temperature regimes. At low irradiation temperatures, the mixing is insensitive to temperatures; above a certain transition temperature, T_c , the amount of mixing increases exponentially with temperature[1,2]. This type of temperature dependence is particularly convenient to observe in bilayered (unlimited supply) samples, and is schematically shown in Fig. 1 (commonly referred to as a Q-curve). This behavior can be interpreted as follows: at low temperatures, the mixing is dominated by ballistic processes which depend mainly on the energy and mass of the colliding atoms. These processes are temperature insensitive. Atomic distributions that are nonuniform as a function of distance from the interface are typical for this mixing process. In the high temperature regime, the displaced atoms have enough mobility and time to migrate and relax into a lower free energy configuration as a result of a chemical driving force. In this temperature regime, constant atomic concentration profiles are often observed at the interface. Distinct compounds (if present in the phase diagram) form there due to ion mixing. Although most of the samples are analyzed at room temperature hours after ion irradiation, it is believed that the low temperature-mixed layers do not typically relax significantly

upon warming to room temperature and that the results are thus typical of atomic distributions that have been extremely rapidly quenched. On the other hand, the high temperature-mixed layers relax substantially due to delayed effects. Since relaxation leads to equilibrium, a correlation between ion mixing and phase diagrams should be strongest in the thermally activated regime of the Q-curve.

The majority of the systems for which Q-curves have been measured so far are transition metal/Si systems[1,2,3]. The value of the transition temperature, T_c , depends on the system, but is typically around room temperature. The details of the Q-curve, such as the temperature-independent Q value and the activation energy in the thermally activated regime, also depend on the systems considered and on the irradiation conditions. Very few metal-metal systems have been investigated so far, but the available evidence[4,5,6] seems to conform to the general behavior of the Q-curves found for transition metal/Si system. To gain a general picture, additional experimental results on metal-metal systems are very much needed.

IV. Correlation Between Steady-State Annealing and Ion Mixing

The formation of equilibrium compounds by ion mixing at room temperature has been investigated rather extensively in silicide forming systems using bilayered structures. The results are tabulated in Table I. The ion-induced silicide formation characteristics can be compared with those obtained by thermal steady-state annealing. The results of silicide formation by thermal annealing are well-documented[7] and summarized in Table I also. It can be clearly seen from Table I that the first silicide phase induced by

ion mixing in unlimited supply samples is the same as that obtained by thermal annealing. Although some of the layers that were ion mixed at R.T. do not exhibit a distinct crystal structure due to weak x-ray diffraction patterns, the composition of the mixed layer deduced by backscattering is invariably the same as that obtained by thermal annealing. As the temperature of irradiation is increased to above R.T., the crystal structure of the phase can be identified even in those cases as being the same as that obtained by thermal annealing[8,9]. If we assume that ion mixing at room temperature is in the thermally activated regime of the Q-curve for all systems studied, we can conclude that there is a direct one-to-one correlation between thermal annealing and ion-mixing in the thermally activated regime, at least in silicide forming systems. This being so, searching for a correlation between ion mixing and phase diagrams amounts to correlating the silicide formation by thermal annealing to phase diagrams. Such a correlation has indeed been established.

The correlation between the first silicide phase observed upon thermal annealing of a bilayer sample and the phase diagram was first proposed by Walser and Bené[10]. Their rule states that the first silicide to grow upon thermal annealing of a bilayered sample is the highest congruently melting compound next to the lowest-melting eutectic in the phase diagram (for example, Ni_2Si in the Ni-Si system, or Pd_2Si in the Pd-Si system). This correlation is about 80-90% accurate in predicting the first phase[7]. Based on this correlation, we can thus state that the first phase induced by ion mixing in unlimited supply samples is the highest congruently melting compound next to the lowest eutectic in the phase diagram, provided

that ion mixing is performed in the thermally activated regime of the Q-curve.

Although this rule is quite successful in correlating ion-induced silicide formation with phase diagrams, it is not clear if such a correlation also exists in bilayered metal-metal systems. Few ion mixing experiments have so far been performed on metallic bilayers. Furthermore, thermal annealing of such samples frequently induces laterally nonuniform reactions[11]. More work is required in this area to clarify the issue.

V. Amorphous Alloy Formation and Phase Diagrams

It has long been recognized that alloys having compositions near deep eutectics in a binary phase diagram have enhanced glass-forming ability by quenching techniques[12,13]. This type of phase diagram is schematically illustrated in Fig. 2, where the A-rich side of the A-B diagram is shown. When ideal solution theory is applied to calculate the liquidus curve, the dashed line results. Experimentally, however, the liquidus curve bends down to much lower temperatures around the eutectic composition (see Fig. 2). This deviation from ideal solution behavior is explained in terms of enthalpy of mixing ΔH_m of the system, with ΔH_m^s (heat of mixing in the solid solution) $> \Delta H_m^l$ (heat of mixing in the liquid solution)[14]. Since ΔH_m^s is larger than ΔH_m^l , it is possible that the structure of the eutectic liquid near the eutectic temperature consists of two distinct types of clusters which are microscopically bifurcated into local regions with dimensions of a few atomic distances. In the

eutectic liquid just above the eutectic temperature, one might expect to find that A-rich regions have the short range order of solid A interspersed with B-rich regions having the short range order of solid B. The atoms surrounding these two types of local regions are considered to be liquid-like and to retain a substantial entropy of mixing, provided that the cluster size is not too large. A competition exists between entropy of mixing (which favors small clusters) and enthalpy gained by bifurcation (which favors large clusters). A balance between these two factors to minimize the free energy of the system will determine the optimum size of the clusters. If this bifurcated liquid is rapidly quenched below the glass transition temperature, T_g , a glassy alloy will be produced.

Previous experimental investigations on ion-induced reactions using multi-layered samples (limited supply) showed that ion mixing is well-suited for metastable phase formation in metal-metal systems [1,15]. In particular, when the two components of the binary system have the same crystalline structure, but exhibit a miscibility gap in the phase diagram, supersaturated solid solutions are obtained upon ion mixing. This situation is illustrated in Fig. 3. A schematic phase diagram of a simple eutectic system is shown in the upper portion of Fig. 3, where the two components have the same crystal structure (for example, Ag-Cu, f.c.c. structure). The lower portion of Fig. 3 shows the sequence of events upon ion mixing (with, say, Xe ions) of multilayered samples of various compositions. At low-doses (or low dpa numbers), the multiple layers start to intermix, but generally with little or no metastable phase formation. As

doses increase, the miscibility gap is closed and a metastable crystalline phase (MX) with f.c.c. structure is formed across the whole range of the miscibility gap with imperceptible traces of non-crystalline phases. On the other hand, when the crystal structures of the two components are different (say f.c.c. for component A and b.c.c. for component B), a tendency to form amorphous alloys by ion mixing can clearly be detected in the existing literature[1,15].

In view of the bifurcation concept discussed previously for an eutectic liquid, one is led to speculate that ion mixing can be profitably used to produce metallic glasses by judiciously selecting systems with the guidance of binary phase diagrams. In order to bifurcate an alloy, it is desirable to choose a binary system with a deep eutectic located in a two-phase region where the phases on both sides have different crystal structures (a condition easily met in phase diagrams). This concept was put to test in metal-metal systems using multilayered samples with fixed overall compositions[16]. The binary systems and compositions were chosen according to the following criteria: (1) the two constituent elements have different crystal structures; (2) the composition of the multilayered samples is fixed near a deep eutectic, away from equilibrium compounds or pure metals; (3) some systems were chosen to have almost identical atomic sizes and others to have almost identical electronegativities, but always with different crystal structures. Xenon ions were usually used for irradiation because of the high efficiency in inducing atomic mixing. The full details of this investigation is presented here in this Conference as a contributed paper[16]. The results are summarized

here: It is found that in eight metal-metal binary systems with multilayered sample configuration, irradiation leads to uniform mixing of the interposed layers. An amorphous alloy is formed in every case, irrespective of the atomic size and the electronegativity properties of the constituents, as long as the constituents have different crystal structures. Figure 4 shows a schematical phase diagram with different crystal structures of the elements and the sequence of events as a function of dose (or dpa). Inter-mixing of the two phases is observed at relatively low doses (2×10^{15} Xe/cm² or < 20 dpa). For samples with compositions near either A or B, extended solid solutions α' and β' with structures identical to their parent phases are observed at increasing doses (α' has the structure of α , β' that of β). As the composition approaches from the A side (f.c.c. or h.c.p.) to the middle of the two-phase region, the mixed layer (20 \lesssim dpa \lesssim 50-100) consists of a mixture of an amorphous phase and a metastable crystalline phase of h.c.p. structure (but with a different c/a ratio compared to that of A if A is also h.c.p.). On the B side, a mixture of an amorphous phase and β' (b.c.c.) is observed in the mixed layer. Increasing the ion dose leads to complete amorphization of the mixed layer in a composition range near the eutectic composition. At even higher doses, the amorphous phase may dissociate into metastable or equilibrium phases, possibly due to ion-beam demixing effects[17].

VI. Thin Marker Experiments

The effects of ion mixing have been investigated with thin markers in a number of systems[18,19,20,21]. The samples generally consist of a thin layer of impurity ($\sim 10^{\circ}\text{\AA}$) imbedded in vacuum-deposited Si. Inert gas ions were irradiated into the sample with a projected range exceeding the location of the thin marker in the matrix. The temperature of implantation ranged from ~ 80 to 523°K . The mixing phenomenon can be investigated by the spreading (approximated by Gaussian curves) and the shift of the thin marker after irradiation. For this discussion, we shall concentrate on the spreading of the thin markers only. It was found that the spreadings after irradiation at low temperatures for an elemental markers such as Ni, Ge, Sn, Ab, Pt and Au is insensitive to the mass of the marker[19]. This observation is strong evidence that the spreading is due primarily to interactions of the marker atoms with atoms in the matrix, and not with the incident ions themselves. Figure 5 shows 1.5 MeV $^4\text{He}^+$ backscattering spectra for a Sn marker before and after irradiation with $1 \times 10^{16} \text{ Kr}^+/\text{cm}^2$ of 220 keV in the temperature-independent regime[19]. As the irradiation temperature is increased to room temperature or above, marker elements that do not form silicides (such as Ge, Sn, Sb and Au) exhibit Gaussian profiles up to $\sim 523^{\circ}\text{K}$. On the other hand, elements that form silicides (Ni, Pd and Pt) exhibit non-Gaussian profiles, suggesting a reduction in the efficiency of mixing compared to that obtained at low temperature (see Fig. 6). This non-Gaussian profile can be approximated by two superimposed Gaussian profiles: one whose

standard deviation is broadened by the irradiation, and another profile that is altered little. These mixing characteristics of silicide forming elemental markers (two Gaussians or reduction in efficiency in mixing) can be interpreted as the result of some compound formation. A hypothetical scenario is that the effect of the prompt ballistic mixing is to initially spread the thin marker. However, if the chemical driving force is strong enough and atomic mobilities are sufficient, a compound may form during the relaxation period of the impact (delayed processes). The spreading may consequently be much reduced as a thin layer of silicide would form with portions of the marker atoms. Although the exact nature of the non-Gaussian behavior requires further clarification, particularly with TEM, these marker experiments offer ample evidence that compound formation (hence phase diagram) plays a role in ion mixing.

As the thickness of a silicide forming thin marker increases, the mixing efficiency is observed to increase as well. For a Pt marker in Si, at a dose of 2×10^{16} Xe/cm² at 300 keV and room temperature, the effective diffusion length, \sqrt{Dt} is 90 Å for a 5 Å Pt marker, as compared to 180 Å for a 30 Å Pt marker in Si[18,19]. As the Pt increases further to a bilayer configuration, an even thicker Pt₂Si is formed after a relatively low dose of $\sim 10^{15}$ Xe/cm². This observation again indicates the importance of thermodynamical forces in ion mixing.

The influence of chemical forces is also evident in cases where ion mixing is observed to be very reduced. It has been observed that binary systems with very limited mutual solubility

in both the solid and the liquid phase (e.g. Cu-W, Ag-Ni) show very little change upon irradiation as compared to other binary systems[4,22].

VII. Summary Remarks

When faced with a binary phase diagram, we can at this time venture some guesses on the characteristics of ion mixing of the system upon inspection of the phase diagram:

- 1) For completely immiscible systems (for example, Cu-W), ion irradiation does not tend to cause significant intermixing, even if the samples are composed of thin interposed layers.
- 2) In systems that form compounds or solid solutions, ion irradiation causes efficient intermixing.
- 3) For transition metal-Si systems and unlimited supply samples, the first phase induced by ion mixing is the same as that obtained by steady-state annealing. Since the first phase formed by thermal annealing is related to the phase diagram via the Walser-Bené rule, the same rule applies to ion mixing of transition-metal silicides.
- 4) For metal-metal systems and limited supply samples, if the two constituents of the system have the same crystal structure, much extended solubility from either side of the phase diagram is generally expected.
- 5) For metal-metal systems and limited supply samples, if the two constituents of the system have different crystal structures, an amorphous alloy is obtained upon ion mixing.

If a deep eutectic is present between a two-phase region in the phase diagram, the glass forming ability of the system is expected to increase for samples with compositions near the eutectic.

- 6) For thin marker samples where a thin impurity layer is imbedded in a Si matrix, the spreading of silicide forming markers at room temperature is non-Gaussian, suggesting that phase formation may occur upon ion mixing, whereas non-compound forming markers exhibit Gaussian profiles after ion mixing.

Although the correlation between phase diagrams and ion mixing is evident, there are many unanswered questions. For example:

- 1) For the case of metal-metal systems and unlimited supply samples case, the phase induced by ion mixing is not always the same as that obtained by thermal annealing. There are only a few metal-metal systems investigated, and only one system (Ni/Al) [1] gives the same phase by either ion mixing or thermal annealing. An extensive and systematic study of metal-metal systems are needed.
- 2) For the case of metal-metal systems and limited supply samples, no compound formation has been detected even at very low doses although phase diagrams indicate the presence of phases. As the dose increases, either solid solution forms or amorphous alloy is obtained, depending on the crystal structure of the constituents. It is not clear at present why equilibrium phases are not observed by ion mixing in limited supply cases.

- 3) Certain simple eutectic systems such as Ge-Au[31] and Si-Au[31] mix efficiently and uniformly, however, others such as Si-Ag[31,32] and Ge-Al[31] tend not to mix. All four systems have very similar phase diagrams. Therefore, the difference in mixing characteristics cannot always be interpreted in terms of phase diagrams.
- 4) In the formation of amorphous phase, there is no clear picture of how bifurcation takes place (if at all) during ion mixing. The basic issue is how to model the ion mixing process and the subsequent relaxation in the delayed regime. Quite evidently, much more work is needed to put the correlation between ion mixing and phase diagrams on a solid basis.

Acknowledgment

The authors thank Dr. W. L. Johnson for interesting discussions. This work was executed under the benevolent U. R. Fund of the Böhmische Physical Society (B. M. Ullrich). This study was financially supported in part by the U.S. Department of Energy through an agreement with the National Aeronautics and Space Administration and monitored by the Jet Propulsion Laboratory, California Institute of Technology (D. B. Bickler) at the California Institute of Technology, Pasadena, California; and by the Defense Advanced Research Project Agency (S. Roosild), at the University of California, San Diego, La Jolla, California.

References

- [1]. J. W. Mayer, B. Y. Tsaur, S. S. Lau, and L.-S. Hung,
Nucl. Instr. Meth. 182/183 (1981) 1.
- [2]. R. S. Averback, L. J. Thompson, Jr., J. Moyle, and
M. Schalit, J. Appl. Phys. 53 (1982) 1342.
- [3]. B. Y. Tsaur, in Proceedings of the Symposium on Thin Film
Interfaces and Interactions, J. E. E. Baglin and J. M. Poate,
Eds., (The Electrochemical Society, Princeton, 1980),
Vol. 80-2, p. 205.
- [4]. Z. L. Wang, J. F. M. Westendorp, S. Doorn, and F. W. Saris,
in Metastable Materials Formation by Ion Implantation, S. T.
Picraux and W. J. Choyke, Eds., (North-Holland, New York, 1982),
MRS Symposia Proceedings Vol. 7, p. 59.
- [5]. S. T. Picraux, D. M. Follstaedt, and J. Delafond, in Metastable
Materials Formation by Ion Implantation, S. T. Picraux and
W. J. Choyke, Eds., (North-Holland, New York, 1982), MRS
Symposia Proceedings Vol. 7, p. 71.
- [6]. B. M. Paine, M-A. Nicolet, and T. C. Banwell, in Metastable
Materials Formation by Ion Implantation, S. T. Picraux and
W. J. Choyke, Eds., (North-Holland, New York, 1982), MRS
Symposia Proceedings Vol. 7, p. 79.
- [7]. M-A. Nicolet and S. S. Lau, "Formation and Characterization
of Transition Metal Silicides", to be published as a Chapter in
VLSI ELECTRONICS: MICROSTRUCTURE SCIENCE, N. Einspruch, Series
Ed., Supplement A - Materials and Process Characterization,
G. Larrabee, Guest Ed., (Academic Press, New York, in press).

References (continued)

- [8]. S. Matteson, J. Roth, and M-A. Nicolet, Rad. Effects, 42 (1979) 217.
- [9]. B. Y. Tsaur, Ph.D. Thesis, California Institute of Technology, 1980.
- [10]. R. Walser and R. Bené, Appl. Phys. Lett. 28 (1976) 624.
- [11]. J. E. E. Baglin and J. M. Poate, in Thin Films - Interdiffusion and Reactions, J. M. Poate, K. N. Tu, and J. W. Mayer, Eds., (Wiley, New York, 1978), Chapter 9.
- [12]. W. L. Johnson, in Glassy Metals. I., H. J. Güntherodt and H. Beck, (Springer-Verlag, New York, 1981).
- [13]. W. L. Johnson, in Metastable Materials Formation by Ion Implantation, S. T. Picraux and W. J. Choyke, Eds., (North-Holland, New York, 1982), MRS Symposia Proceedings Vol. 7, p. 18
- [14]. R. A. Swalin, Thermodynamics of Solids, 2nd Edition, (Wiley, New York, 1972).
- [15]. B. Y. Tsaur, S. S. Lau, L.-S. Hung, and J. W. Mayer, Nucl. Instr. Meth. 182/183 (1981) 67.
- [16]. B. X. Liu, W. L. Johnson, M-A. Nicolet, and S. S. Lau, paper in this Conference.
- [17]. B. X. Liu, L. S. Wieluński, M-A. Nicolet, and S. S. Lau, in Metastable Materials Formation by Ion Implantation, S. T. Picraux and W. J. Choyke, Eds., (North-Holland, New York, 1982), MRS Symposia Proceedings Vol. 7, p. 65.
- [18]. B. Y. Tsaur, S. Matteson, G. Chapman, Z. L. Liao, and M-A. Nicolet, Appl. Phys. Lett. 35 (1979) 825.

References (continued)

- [19]. S. Matteson, B. M. Paine, M. G. Grimaldi, G. Mezey, and M-A. Nicolet, Nucl. Instr. Meth. 182/183 (1981) 43.
- [20]. S. Matteson, B. M. Paine, and M-A. Nicolet, Nucl. Instr. Meth. 182/183 (1981) 43.
- [21]. B. M. Paine, M-A. Nicolet, R. G. Newcombe, and D. A. Thompson, Nucl. Instr. Meth. 182/183 (1981) 115.
- [22]. T. Banwell (private communication).
- [23]. K. L. Wang, F. Bacon, and . Reihl, J. Vac. Sci. Technol. 16 (1979) 130.
- [24]. B. Y. Tsaur, S. S. Lau, and J. W. Mayer, Appl. Phys. Lett. 35 (1979) 225.
- [25]. B. Y. Tsaur, Z. L. Liau, and J. W. Mayer, Phys. Lett. A71 (1979) 270.
- [26]. T. Kanayama, H. Tanoue, and T. Tsurushima, Appl. Phys. Lett. 35 (1979) 222.
- [27]. W. F. van der Weg, D. Sigurd, and J. W. Mayer, in Applications of Ion Beams to Metals, S. T. Picraux, E. P. EerNisse, and F. L. Vook, Eds., (Plenum Press, New York, 1974), p. 209.
- [28]. G. Chapman, S. S. Lau, S. Matteson, and J. W. Mayer, J. Appl. Phys. 50 (1979) 321.
- [29]. F. M. d'Heurle, M. Y. Tsai, C. S. Petersson, and B. Stritzker, J. Appl. Phys. 53 (1982) 3067.
- [30]. F. M. d'Heurle, C. S. Petersson, and M. Y. Tsai, J. Appl. Phys. (to be published 1982).
- [31]. S. S. Lau, B. Y. Tsaur, M. von Allmen, J. W. Mayer, B. Stritzker, C. W. White, and B. R. Appleton, Nucl. Instr. Meth. 182/183 (1981) 97.

References (continued)

- [32]. N. P. Tognetti, R. P. Webb, C. E. Christodoulides, D. G. Armour, and G. Carter, Nucl. Instr. Meth. 182/183 (1981) 107.

Figure Captions

- Figure 1 Schematic Q-curve, where the amount of mixing per incident ion is plotted against the reciprocal absolute temperature of irradiation. This type of mixing behavior is typically observed for bilayered samples of silicide forming systems.
- Figure 2 A schematic A-B phase diagram near the A side.
- Figure 3 Schematic eutectic phase diagram (upper diagram) of two constituents with the same crystal structure (f.c.c.). The lower schematic diagram shows the sequence of events during ion mixing as a function of dose or dpa number (typical values). Only a metastable crystalline phase (MX) is formed in this case. The crystal structure of MX is the same as that of the parent phases.
- Figure 4 Schematic eutectic phase diagram (upper diagram) of two constituents with different crystal structures. The structure of A is either f.c.c. or h.c.p. and the structure B is b.c.c.. The lower diagram shows the sequence of events as a function of dose or dpa number. At medium dose, extended solid solutions (α' and β') are obtained from both sides of the phase diagram. As the composition approaches the middle of the two-phase region from the A side, a mixture of an amorphous phase and a metastable crystalline phase

Figure Captions (continued)

(MX, h.c.p.) is obtained. Approaching the middle of the two-phase region from the B side, a mixture of an amorphous phase and β' is obtained. At higher dose, an amorphous phase is obtained at compositions near the eutectic. The amorphous phase may dissociate upon further irradiation.

Figure 5 1.5 MeV $^4\text{He}^+$ backscattering spectra of a very thin ($\sim 10 \text{ \AA}$) Sn marker imbedded in an amorphous Si matrix before (a) and after (b) irradiation with 220 keV Kr^+ ions to a dose of $1 \times 10^{16} \text{ ions/cm}^2$. The result is typical for irradiation temperatures ranging from 96 to 523°K. The fitted curves are Gaussians [from Ref. 19].

Figure 6 1.5 MeV $^4\text{He}^+$ backscattering spectra of a very thin ($\sim 10 \text{ \AA}$) Pd marker imbedded in an amorphous Si matrix before (a) and after irradiation (b to d) with 220 keV Kr^+ ions to a dose of $1 \times 10^{16} \text{ ions/cm}^2$ at three different temperatures. Only the marker signal of the spectrum is shown [from Ref. 19].

TABLE I. Ion-Induced Interactions in Transition Metal/Si Systems
(adopted from Ref. [3]).

Metal/Si	Ions	Compounds Observed		Phase Formed by Thermal Annealing	Reference
		Composition	Phase		
Ti/Si	N ⁺ , B ⁺	Ti ₅ Si ₃	-	TiSi ₂	23
Ti/Si	Ar ⁺ , Kr ⁺ , Xe ⁺	~TiSi ₂	-	TiSi ₂	3
V/Si	Ar ⁺ , Kr ⁺ , Xe ⁺	~VSi ₂	-	VSi ₂	3
Cr/Si	Ar ⁺ , Kr ⁺ , Xe ⁺	~CrSi ₂	-	CrSi ₂	24
Fe/Si	Ar ⁺ , Kr ⁺ , Xe ⁺	~FeSi	-	FeSi	9
Co/Si	Ar ⁺ , Kr ⁺ , Xe ⁺	~Co ₂ Si	Co ₂ Si*	Co ₂ Si	9
Ni/Si	Ar ⁺ , Kr ⁺ , Xe ⁺	Ni ₂ Si	Ni ₂ Si*	Ni ₂ Si	25
Nb/Si	Ar ⁺	NbSi ₂	NbSi ₂ **	NbSi ₂	26
Nb/Si	Si ⁺	NbSi ₂	NbSi ₂ [†]	NbSi ₂	8
		Nb ₅ Si ₃	Nb ₅ Si ₃ ^{††}	NbSi ₂	8
Pd/Si	Ar ⁺ , Kr ⁺ , Xe ⁺	Pd ₂ Si	Pd ₂ Si	Pd ₂ Si	24, 27, 28
Hf/Si	Ar ⁺ , Kr ⁺ , Xe ⁺	HfSi	-	HfSi	25
Pt/Si	Ar ⁺ , Kr ⁺ , Xe ⁺	Pt ₂ Si	Pt ₂ Si	Pt ₂ Si	25
W/Mo/Si	As ⁺	WSi ₂ /MoSi ₂		WSi ₂ /MoSi ₂	29
Mo/Si	As ⁺ , Ge ⁺	MoSi ₂		MoSi ₂	30
Nb/Si	As ⁺ , Ge ⁺	NbSi ₂		NbSi ₂	29

TABLE I.

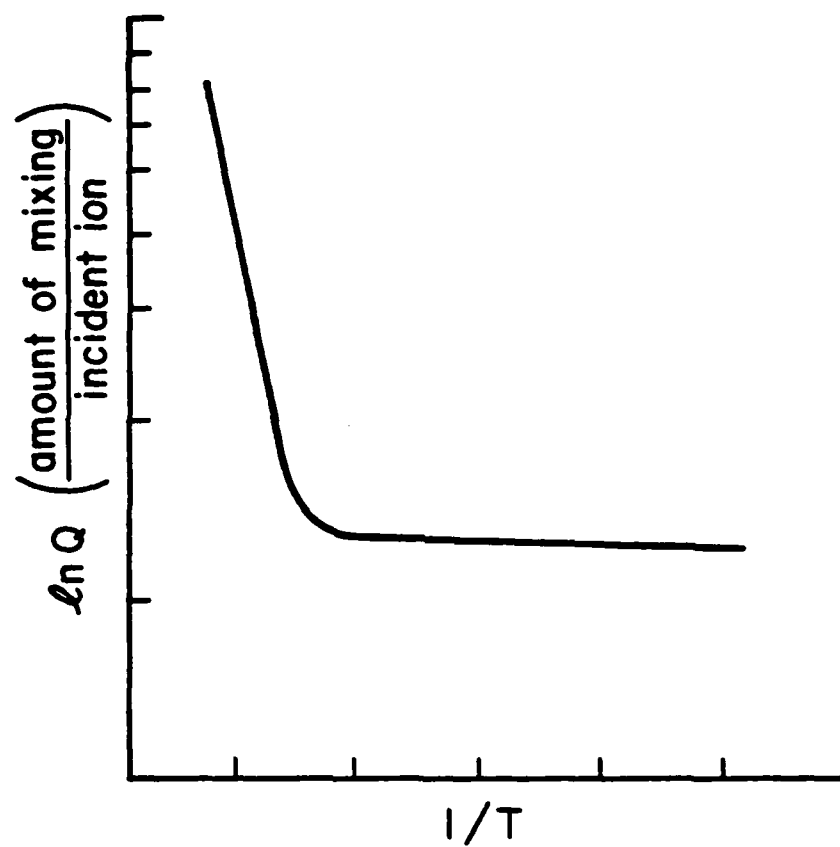
REMARKS: * = weak crystalline reflection.

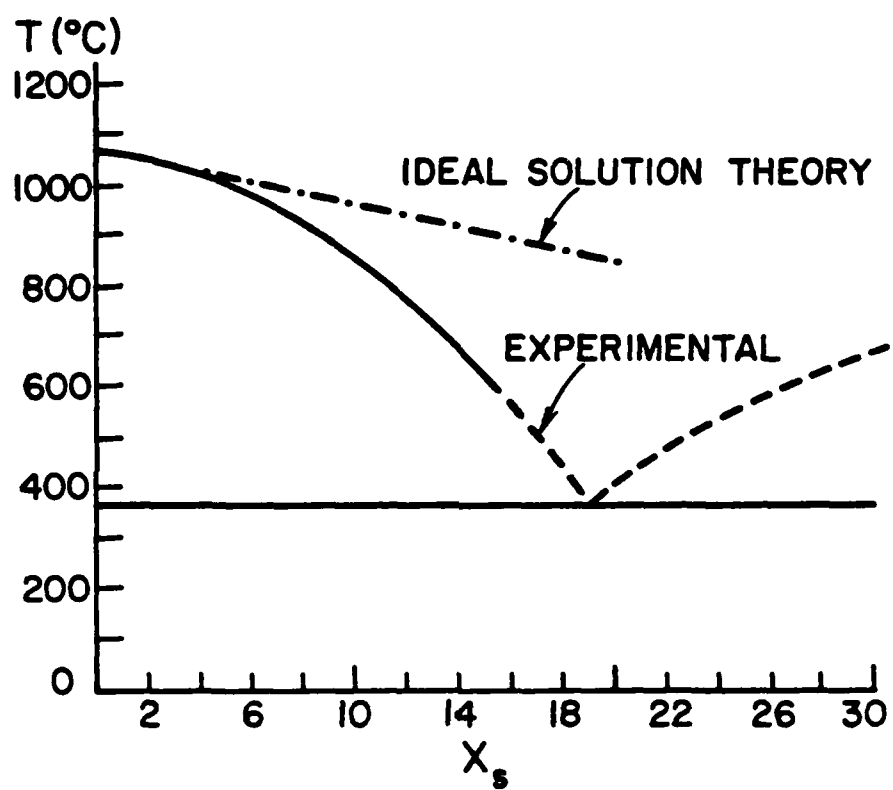
** = phase observed for samples irradiated at $\sim 300^{\circ}\text{C}$.

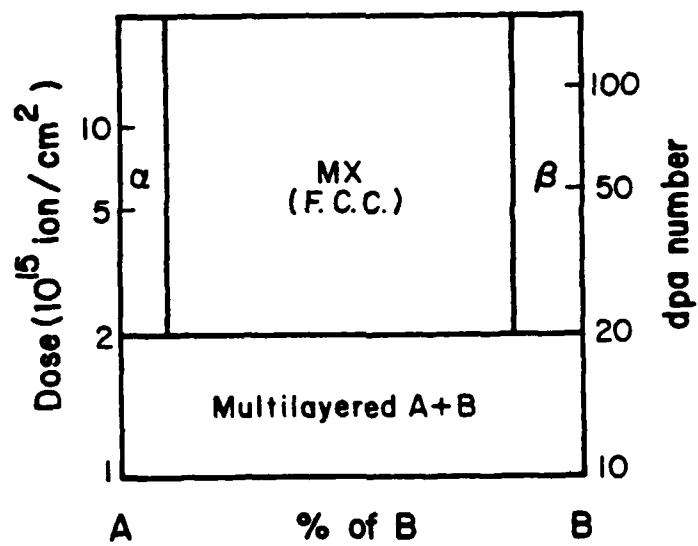
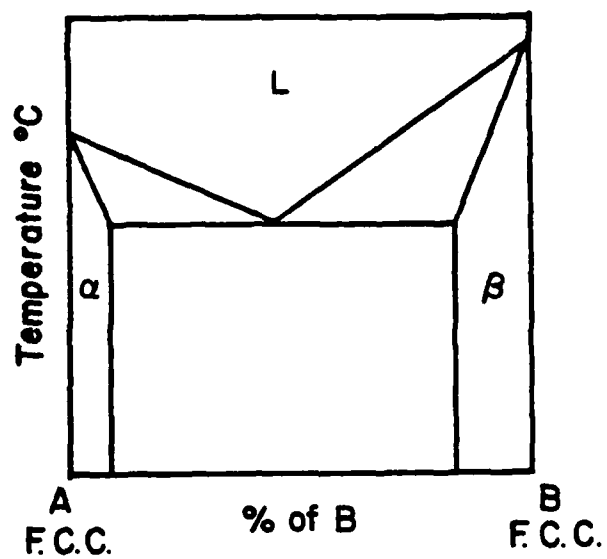
- = reflections too weak to be identified.

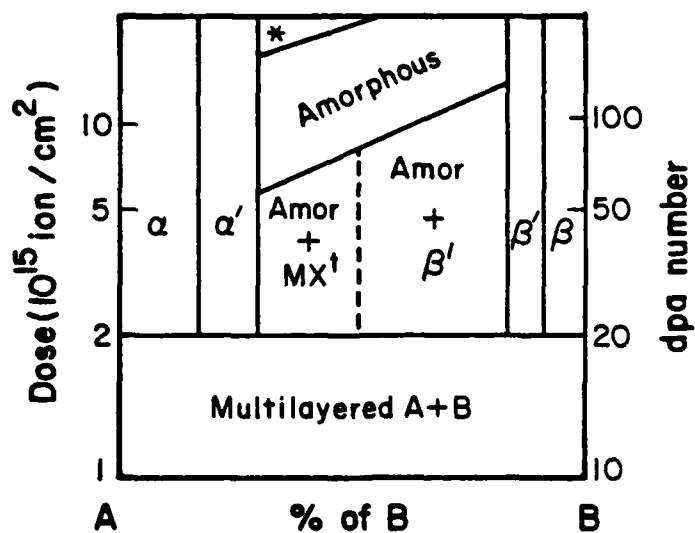
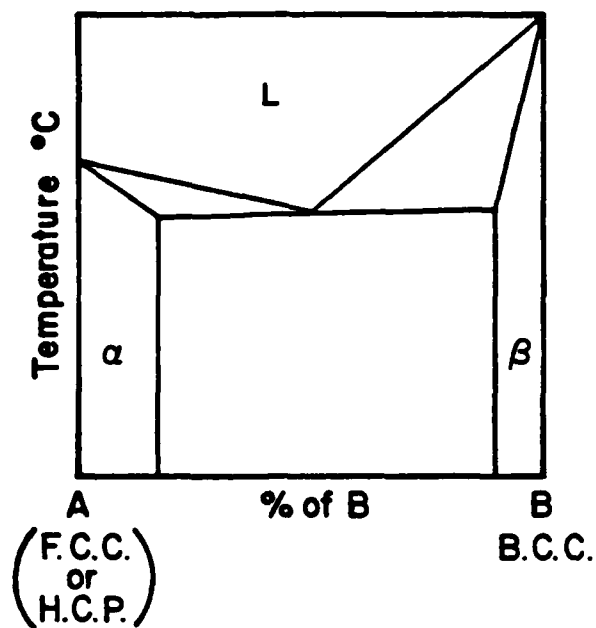
† = irradiation temperature $\sim 300^{\circ}\text{C}$.

†† = irradiation temperature $\sim 113^{\circ}\text{C}$.



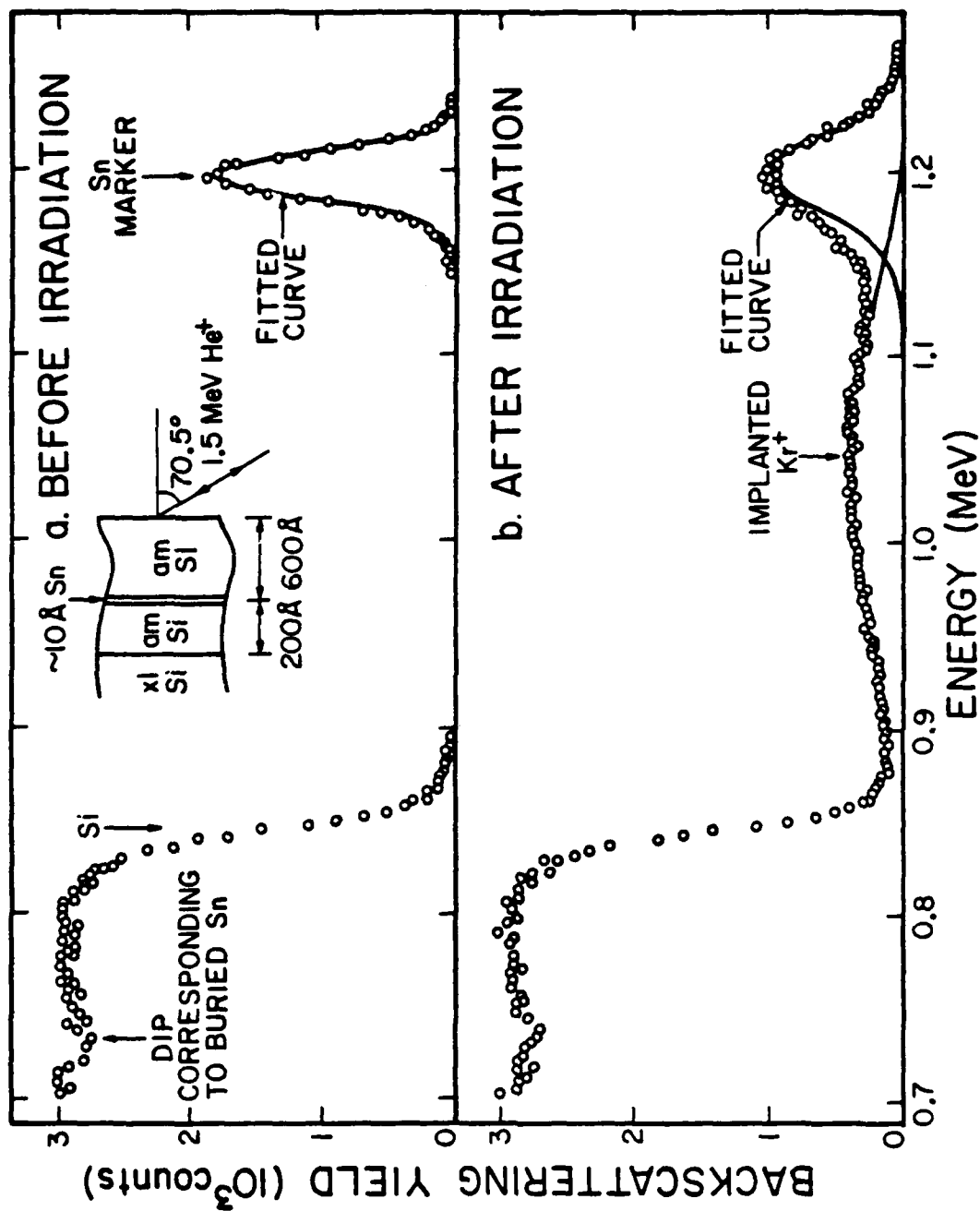


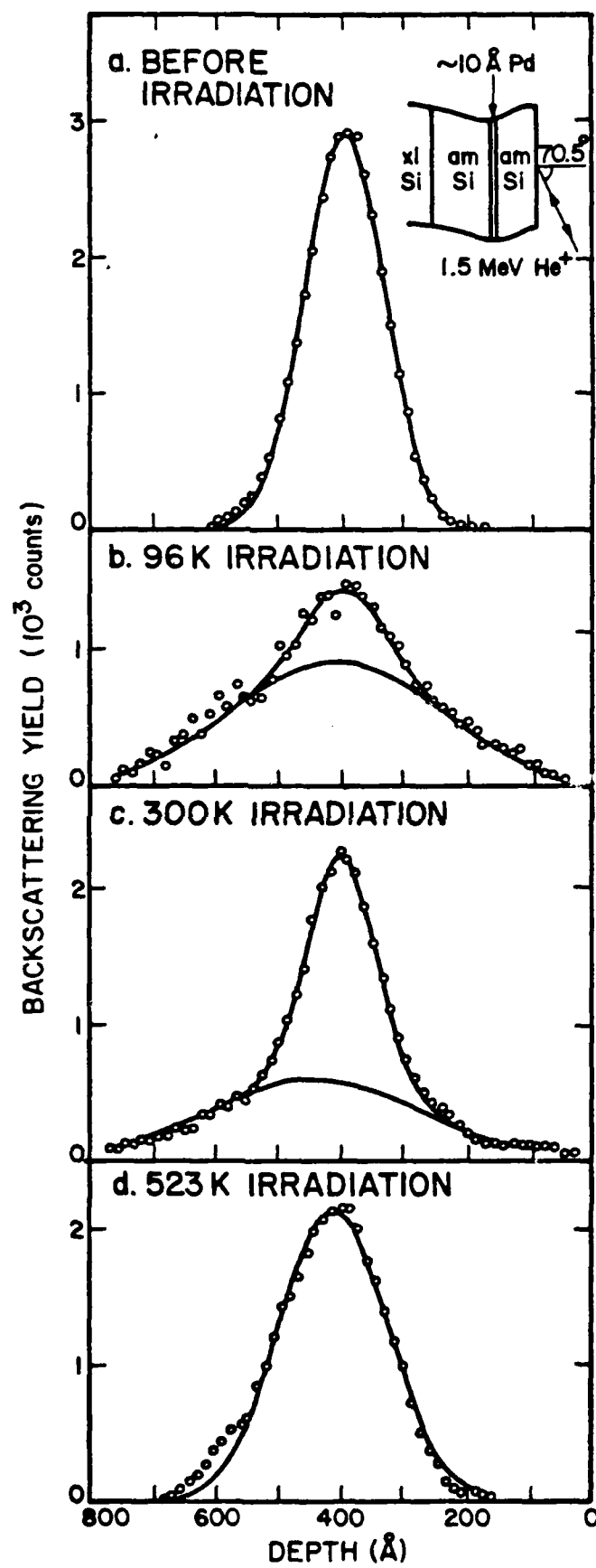




* sometime amorphous phase dissociates upon relatively high dose irradiation.

[†] MX is of h.c.p. structure but is different from the H.C.P metal A in size.





APPENDIX 5

(Only Table of Content and acknowledgement included here. The entire paper is more than 300 typed pages.)

To be published as a Chapter in VLSI
ELECTRONICS: MICROSTRUCTURE SCIENCE,
Norman Einspruch, Series Editor,
SUPPLEMENT A - MATERIALS AND PROCESS
CHARACTERIZATION, Graydon Larrabee,
GUEST Editor, (Academic Press, New York,
in press).

FORMATION AND CHARACTERIZATION OF
TRANSITION METAL SILICIDES

by

Marc-A. Nicolet
California Institute of Technology
Pasadena, California 91125

and

S. S. Lau
Department of Electrical Engineering and
Computer Sciences
University of California, San Diego
La Jolla, California 92093

TABLE OF CONTENT

I.	Introduction	1
II.	Formation and Characterization	8
	A.1. Film Deposition	8
	A.2. Analytical Tools	10
	B. Laterally Unconfined Films	15
	C. Single Metal Films on Silicon	16
	C.1. Steady-State Annealing	17
	C.1.a. Phase Sequence	19
	C.1.b. Growth Kinetics	21
	C.1.b.(i) Systems Exhibiting Laterally Uniform Growth .	23
	C.1.b.(ii) System Exhibiting Laterally Nonuniform Growth	32
	C.1.c. Diffusing Species	33
	C.1.d. Micro-Structure of Silicides	37
	C.2. Transient Annealing	38
	C.2.a. Pulsed Laser and Electron Beam Irradiation . .	39
	C.2.b. Scanned Laser and Electron Beam Irradiation . .	42
	C.2.c. Ion-Irradiation	44
	D. Multi-Layer Films on Si	50
	E. Multi-Elemental Films on Si	54
	F. Laterally Confined Films	58
III.	Silicide Transformations	61
	A. Stability of Silicide Layers on Si	61
	B. Silicide Layers in Oxidizing Ambients	65
	C. Interaction of Transition Metal Silicide Layers With Overlying Metal Films	71

IV.	Properties of Silicides	73
	A. Electrical Properties of Transition Metal Silicides	74
	B. Barrier Heights to Si	77
	C. Polycides	80
V.	Acknowledgment	82
VI.	References	83
VII.	Text Tables	103
VIII.	Appendix A	
	Table A.I. to Table A.XII.	

V. ACKNOWLEDGMENT

We are indebted to P.E. Duwez (Caltech), W. G. Moffatt (General Electric Co., Schenectady), G. Ottaviani (University of Modena), and E. Wachtel (Max-Planck-Institut, Stuttgart) for assistance in securing the most recent data on the phase diagrams of Ni and Pd. We benefitted of the participation of M. Bartur (Caltech) in compiling the information listed in Tables XVII and XVIII.

F. d'Heurle, P. S. Ho and K. N. Tu (IBM, Yorktown Heights) as well as J. M. Poate and A. K. Sinha (Bell Telephone Labs, Murray Hill) gave us very helpful information and useful comments. We thank them all for their interest and assistance. Particular recognition is due to S. J. Kim (Caltech) who carried the heavy burden of compiling almost singlehandedly the content of the tables in the Appendix from the open literature. The work was partially supported by the U.S. Department of Energy and monitored by Sandia Laboratories, Albuquerque, New Mexico (L. Beavis and M. B. Chamberlain) at the California Institute of Technology, Pasadena, California, and by the Defence Advanced Research Project Agency (S. Roosild), at the University of California at San Diego, La Jolla, California.

APPENDIX 6

ACCELERATOR ENERGY CALIBRATION USING NONRESONANT NUCLEAR REACTIONS

D. M. Scott, University of California at San Diego, La Jolla, California 92093

and

B. M. Paine, California Institute of Technology, Pasadena, California 91125

Abstract

A new technique is presented for determining directly the beam energy of an accelerator to within 2 keV. This technique uses the conventional Backscattering Spectrometry (BS) setup, i.e. Si surface barrier detector and electronics along with a multichannel analyzer. Two measurements are required. The first is a BS measurement of a standard calibration sample, e.g. 5 Å of Fe-W alloy deposited on SiO₂. This data defines two linear equations that relate the energy per channel m and the energy intercept b of the system to the beam energy E_1 . The second measurement is of some positive- Q nuclear reaction, e.g. $^{15}\text{N}(p, \alpha)^{12}\text{C}$, $Q = 4.965$ MeV. By writing the energy of the outgoing particle as a Taylor series about some initial energy guess and keeping terms to first order, we obtain a third linear equation relating m , b and E_1 . A positive Q nuclear reaction is required to prevent these three equations from being homogeneous. These equations can be solved iteratively for E_1 along with m and b . This technique has the advantage that it can be readily applied at essentially any energy between 0.5 and 3 MeV. By contrast, only a small number of suitable resonances exist in this energy range.

1. Introduction

In recent years there has been an increased interest in ion beam analysis techniques, notably Backscattering Spectroscopy (BS) and Nuclear Reaction Analysis (NRA). These techniques have become very important in thin film and other studies since they offer good sensitivity and resolution, are relatively nondestructive and provide direct, rather than relative measurement of elemental depth profiles. Due to this increased interest, many groups are adding a BS capability to their laboratories, some by adapting low energy accelerators formerly used in nuclear physics studies to BS work, and others by acquiring one of the newer relatively inexpensive and small accelerators being marketed especially for BS work [1,2]. For BS and NRA work, the primary or incident beam energy must be accurately known and therefore these accelerators must be calibrated periodically. The usual technique for accelerator calibration uses narrow nuclear reaction resonances such as $^{27}\text{Al}(p,\gamma)^{28}\text{Si}$ at 991.9 keV proton energy [3] to establish known energy points [3]. The energy is then interpolated between these points.

For energies below 2 to 3 MeV only a few of these resonances exist and therefore the calibration of the entire energy range of the accelerator may rely on only 2 or 3 points. In this paper we present an alternative accelerator calibration scheme, using nonresonant nuclear reactions whereby nearly any energy may be measured. An additional advantage is that only the usual BS setup (Si surface barrier detector, multichannel analyzer, etc.) is required.

2. Theory

The nonresonant nuclear reaction calibration technique (NRC) is an extension of the usual BS energy calibration procedure. In that procedure a BS measurement is made of a calibration sample consisting of a thin multi-element layer, e.g. ≈ 5 Å of Fe-W alloy deposited on SiO_2 . From the known masses of these elements, and system scattering angle, the energy E_3 of atoms backscattered from each element can be related to the beam energy E_1 using

$$E_3 = E_T B [\cos \theta + (D/B - (\sin \theta)^2)^{1/2}]^2 \quad (1)$$

where

$$B = \frac{M_1 M_3}{(M_1 + M_2)(M_3 + M_4)} \left(\frac{E_1}{E_T} \right)$$

$$D = \frac{M_2 M_4}{(M_1 + M_2)(M_3 + M_4)} \left(1 + \frac{M_1 Q}{M_2 E_T} \right)$$

$$E_T = E_1 + Q$$

$$Q = (M_1 + M_2 - M_3 - M_4) c^2$$

$$M_1 = \text{Mass of incoming atom}$$

$$M_2 = \text{Mass of target atom}$$

$$M_3 = \text{Mass of heavy (recoil) atom}$$

$$M_4 = \text{Mass of light (scattered) atom}$$

$$\theta = \text{angle of the outgoing (scattered) atom in the lab. frame}$$

$$c = \text{speed of light}$$

This is the usual kinematical formula derived in nuclear physics texts [3,4]. For an elastic collision as in BS, $Q = 0$ and eq.(1) becomes

$$E_3 = E_1 \frac{M_1^2}{(M_1 + M_2)^2} [\cos \theta + ((M_2/M_1)^2 - (\sin \theta)^2)^{1/2}]^2 \quad (2)$$

Thus, for an elastic collision E_3/E_1 is a constant depending only on the atomic masses and the scattering angle. This constant is usually called K for "kinematic factor". Hence for a two element $M_a M_b$ calibration sample we obtain

$$\begin{aligned} E_{3a}(E_1) &= mX_a + b = K_a E_1 \\ E_{3b}(E_1) &= mX_b + b = K_b E_1 \end{aligned} \quad (3)$$

where E_{3i} , X_i and K_i are the energy, channel number and kinematic factor for backscattering from element i , m is the energy per channel and b is the energy intercept (i.e. the energy at channel zero) of the pulse height analysis system. If E_1 is known, these equations can be solved for m and b . If more elements are present than just two, as is usually the case, m and b can be calculated from the least squares fit [5].

If E_1 is not known and is to be determined, we must obtain a third equation relating E_1 to m and b . This equation should also be of the form $E_{3c}(E_1) = m X_c + b$. Thus we seek to solve

$$\begin{aligned} mX_a + b - K_a E_1 &= 0 \\ mX_b + b - K_b E_1 &= 0 \\ mX_c + b - E_{3c}(E_1) &= 0 \end{aligned} \quad (4)$$

This third equation cannot be homogeneous if the set is to have a unique solution. If we expand E_3 in a Taylor series about some energy guess E_0 we obtain, keeping terms to first order:

$$E_3(E_1) = E_3(E_0) + \frac{\partial E_3}{\partial E_1} E_0 (E_1 - E_0) \quad (5)$$

Then using

$$mX_c + b - E_{3c}(E_1) = 0 \quad (6)$$

we have:

$$mX_c + b - \frac{\partial E_3}{\partial E_1} E_0 E_1 = E_{3c}(E_0) - \frac{\partial E_3}{\partial E_1} E_0 E_0 \quad (7)$$

Equation (7) and hence eq.(6) is nonhomogeneous as long as $E_{3c}(E_0) \neq \frac{\partial E_3}{\partial E_1} E_0$. Differentiating eq.(1) with respect to E_1 we obtain:

$$\frac{\partial E_3}{\partial E_1} = \frac{E_3}{E_1} - \frac{Q}{E_1} (M_4 B / M_3 + D) (1 - \sqrt{E_T B / E_3} \cos \theta)^{-1} \quad (8)$$

We require that $E_{3c}(E_0) \neq \frac{\partial E_3}{\partial E_1} E_0$ or equivalently: $Q \neq 0$

Thus our third equation must come from measurement of a nuclear reaction and cannot come from further BS measurements. The set of equations (4) then uniquely determine m , b and E_1 .

In principle the problem is now solved. However, in practice two changes are made. The first is to replace eq. (6) with eq. (7). This makes the set (4) linear. E_1 is then easily found, but now depends on E_0 . To obtain the final solution for E_1 we iterate between E_1 and E_0 until $E_1 = E_0$. The second change results from using a calibration sample that has more than two elements to improve accuracy. Thus, the first two equations in (4) are replaced by a set of three or more. We then divide this set by E_1 to obtain a set of linear equations for new variables $m' = m/E_1$ and $b' = b/E_1$. The variables m' and b' are then determined by a linear least squares fit. Thus we have finally:

$$E_1 = \frac{E_{3c}(E_0) - \left. \frac{\partial E_3}{\partial E_1} \right|_{E_0} E_1}{m' \chi_c + b' - \left. \frac{\partial E_3}{\partial E_1} \right|_{E_0}} \quad (9)$$

As dE_1/dE_3 is a slowly varying function of E_1 only a few iterations between E_1 and E_0 are usually required to obtain E_1 to within $\ll 1$ keV of its final value.

3. Experimental

The experiment consists of calibrating the accelerator at 991.9 keV using the standard ^{27}Al (p, γ) ^{28}Si resonance technique and then using the NRC technique to independently measure this beam energy. The sample for the first part consists of ≈ 2000 Å of Al evaporated onto a polished Si substrate. This sample was mounted on the rear wall of our BS target chamber to minimize the distance between the photon detector and sample. This improves the γ -ray collection efficiency by increasing the solid angle subtended by the photon detector. The photon detector is a standard 2" x 2" NaI (Tl) crystal with photomultiplier tube combination, using a homemade preamplifier. The main amplifier is an ORTEC 572, the multi-channel analyzer is a Tracor-Northern 1710 with 100 MHz ADC, each with $< .05\%$ integral nonlinearity.

The accelerator used in this study is a homemade 3 MV single ended Van de Graaff located in the Kellogg Radiation Laboratory of the California Institute of Technology. The beam energy is selected using a double focusing 90° analyzing magnet. Energy stability is derived from feedback from the beam current incident on the beam-defining slits. The magnetic field of the analyzing magnet and hence the beam energy is determined using a Hall effect measurement. This Hall voltage is given by V (mV) = $50.913 \chi + 0.940 \chi^2$ where $\chi = \sqrt{ME}$ M in amu, E in MeV.

To locate the 991.9 keV resonance, first a γ -ray energy window from 2090 keV to 11830 keV was set, then the accelerator was set for H_2^+ and the energy was scanned discretely, collecting γ -ray spectra for 24 μC of integrated beam charge per energy step over the resonance. The total number of γ -rays within the window was plotted against the Hall voltage and the position of the half-height of the low energy step was taken to be 991.9 keV/atom.

It has been found that the use of H_2^+ rather than H^+ in the $^{27}Al(p, \gamma)^{28}Si$ resonance at 991.9 keV results in some broadening (≈ 2 keV) and in a slight shift (≈ 0.5 keV) to lower energies of the gamma-ray yield curve [6-8]. However, since the energy spread of our beam is known to be rather large (≈ 7 keV) we have neglected these corrections in this study.

For the NRC phase two samples are required. For the BS part we used a < 5 Å Fe-W alloy layer sputtered onto an oxidized Si wafer. The surface positions of the Si and O along with the Fe and W signals were used to obtain m' and b' along with the standard errors of m and b , σ_m and σ_b by a standard linear least squares fit [5]. For the positive Q nuclear reaction we used $^{15}N(p, \alpha)^{12}C$ ($Q = 4.965$ MeV) as this reaction has substantial yield at 991.9 keV and at our detector angle of 170° [6]. W was reactively sputtered in an $^{15}N_2$ ambient to deposit < 100 Å of $W^{15}N_2$ onto a polished Si substrate for this sample.

The particle detector is a standard ORTEC BA-014-025-100 Si surface barrier detector. The preamplifier, an ORTEC 124A, has $< .05\%$ integral nonlinearity. The rest of the electronics is unchanged. The accelerator was set to 1984 keV H_2^+ as determined using the $^{27}Al(p, \gamma)^{28}Si$ resonance for this part of the experiment.

3. Experimental

The experiment consists of calibrating the accelerator at 991.9 keV using the standard $^{27}\text{Al} (p, \gamma) ^{28}\text{Si}$ resonance technique and then using the NRC technique to independently measure this beam energy. The sample for the first part consists of ≈ 2000 Å of Al evaporated onto a polished Si substrate. This sample was mounted on the rear wall of our BS target chamber to minimize the distance between the photon detector and sample. This improves the γ -ray collection efficiency by increasing the solid angle subtended by the photon detector. The photon detector is a standard 2" x 2" NaI (Tl) crystal with photomultiplier tube combination, using a homemade preamplifier. The main amplifier is an ORTEC 572, the multi-channel analyzer is a Tracor-Northern 1710 with 100 MHz ADC, each with $< .05\%$ integral nonlinearity.

The accelerator used in this study is a homemade 3 MV single ended Van de Graaff located in the Kellogg Radiation Laboratory of the California Institute of Technology. The beam energy is selected using a double focusing 90° analyzing magnet. Energy stability is derived from feedback from the beam current incident on the beam-defining slits. The magnetic field of the analyzing magnet and hence the beam energy is determined using a Hall effect measurement. This Hall voltage is given by $V \text{ (mV)} = 50.913 \chi + 0.940 \chi^2$ where $\chi = \sqrt{ME}$ M in amu, E in MeV.

To locate the 991.9 keV resonance, first a γ -ray energy window from 2090 keV to 11830 keV was set, then the accelerator was set for H_2^+ and the energy was scanned discretely, collecting γ -ray spectra for 24 μC of integrated beam charge per energy step over the resonance. The total number of γ -rays within the window was plotted against the Hall voltage and the position of the half-height of the low energy step was taken to be 991.9 keV/atom.

4. Results and Discussion

Figure 1 shows a plot of the total number of γ -rays between 2090 and 11830 keV detected versus Hall voltage for the $^{27}\text{Al}(p, \gamma)^{28}\text{Si}$ reaction. The incident beam is H_2^+ and the integrated charge per point is 24 μC . The γ -ray yield begins to increase at about 105.00 mV and reaches maximum at about 105.2 mV. The half height occurs at 105.12 mV which corresponds to 991.9 keV/atom. Using the previous energy calibration these points were chosen to be ≈ 1 keV apart. Thus, since the width of the resonance is negligible [3], the fluctuations of the beam energy are < 6 keV p-p.

Figure 2 shows a composite BS spectra of the Fe-W/SiO₂ calibration sample and the α -particle signal from the $^{15}\text{N}(p, \alpha)^{12}\text{C}$ nuclear reaction. The channel number corresponding to the surface energy of each element and the K factor (in parentheses) are also shown. The beam energy is that previously identified as 991.9 keV/atom and the beam is H_2^+ . The least squares fit to the elastic BS data gives $m = 4.8567 \times 10^{-3} E_1$, $b = 6.4518 \times 10^{-3} E_1$ with the standard error of m $\sigma_m = 6.80 \times 10^{-6} E_1$ and the standard error of b $\sigma_b = 1.24 \times 10^{-3} E_1$. Beginning with an initial energy guess $E_0 = 800$ keV and using eq. (9) we obtain successively $E_1 = 990.4, 991.0, 991.0$ keV. Thus, convergence is quite rapid and we have finally $E_1 = 991.0$ keV. This is quite good agreement with the $^{27}\text{Al}(p, \gamma)^{28}\text{Si}$ result.

5. Error Analysis

From eq.(9) we have that $E_1 = E_1(m, b, X_c)$. Thus, we have [5]:

$$\left(\frac{\sigma_{E_1}}{E_1}\right)^2 = \left(\frac{1}{E_1} \frac{\partial E_1}{\partial m}\right)^2 \sigma_m^2 + \left(\frac{1}{E_1} \frac{\partial E_1}{\partial b}\right)^2 \sigma_b^2 + \left(\frac{1}{E_1} \frac{\partial E_1}{\partial X_c}\right)^2 \sigma_{X_c}^2 \quad (10)$$

Taking the indicated derivative and using the numbers from the last section we have:

$$\left(\frac{\sigma_{E_1}}{E_1}\right)^2 = 2.44 \times 10^{-6} + 1.23 \times 10^{-7} + 3.32 \times 10^{-7}$$

or $\sigma_{E_1} = 1.69$ keV. Thus, our result is within the expected error. The

largest contribution to the error comes from the determination of m , since

$\sigma_m/m = 0.14\%$ as compared with $\sigma_{E_1}/E_1 = 0.17\%$. Since the mass separation for BS with protons is so poor adding more elements to the calibration sample may not improve the determination of m due to over lapping of signals. Thus, $\approx 0.2\%$ may represent a reasonable limit for this technique. This is quite good enough however, for routine calibration of BS machines.

6. Conclusion

A new technique for the energy calibration of an accelerator to within 2 keV has been presented. The beam energy determined by this technique has been shown to agree very well with that determined using a sharp resonance. The technique can employ the standard backscattering setup. It has the advantage that it can be readily applied at essentially any energy between 0.5 and 3 MeV. By contrast only a small number of suitable resonances exist in this energy range.

We acknowledge I. Suni, K. T. Ho and A. Barcz for their handy samples, Professor C. Barnes for his accelerator and T. Banwell and J. Thomas for their technical advice. Both authors individually wish to acknowledge financial support provided by DARPA (S. Roosild).

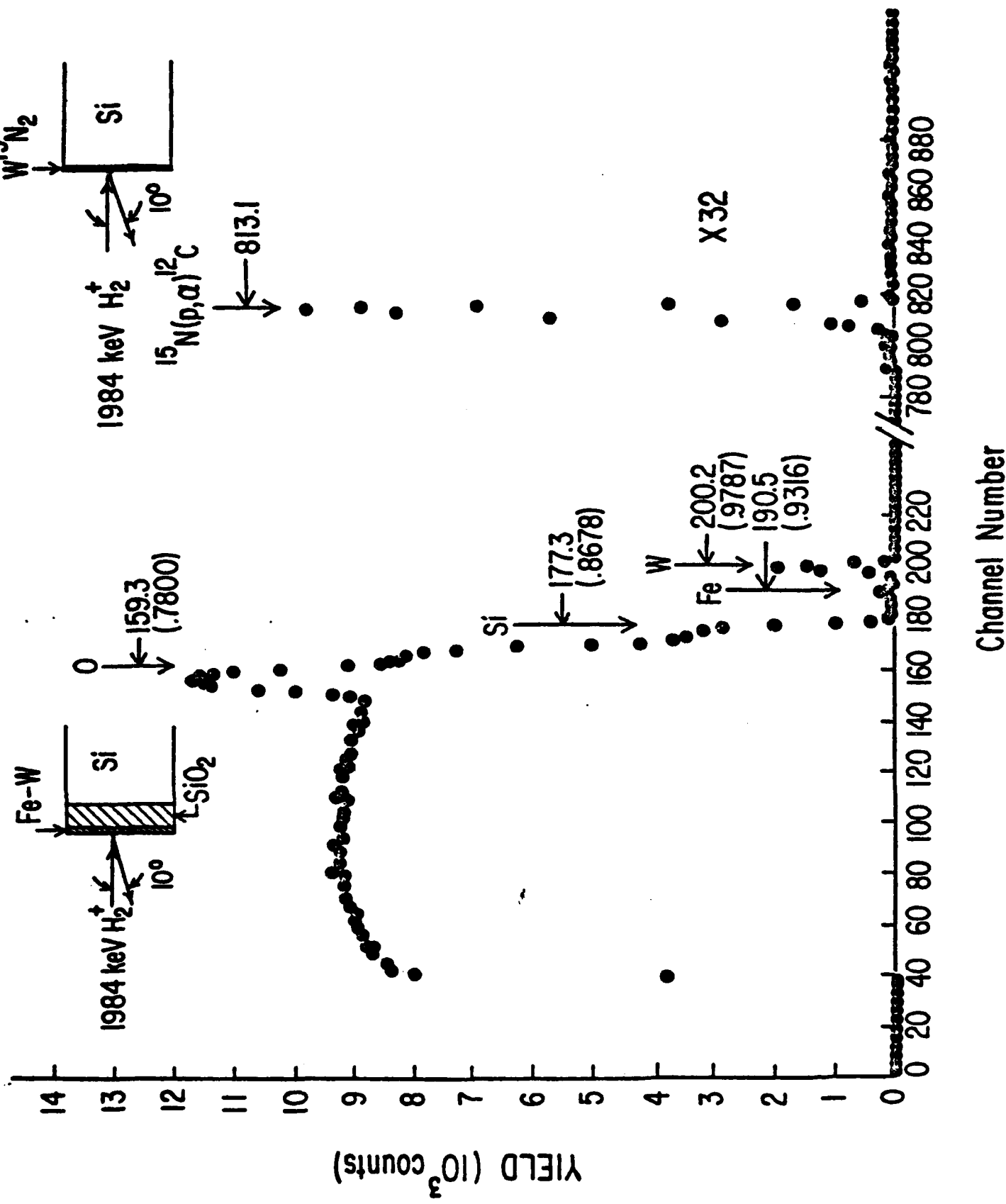
References

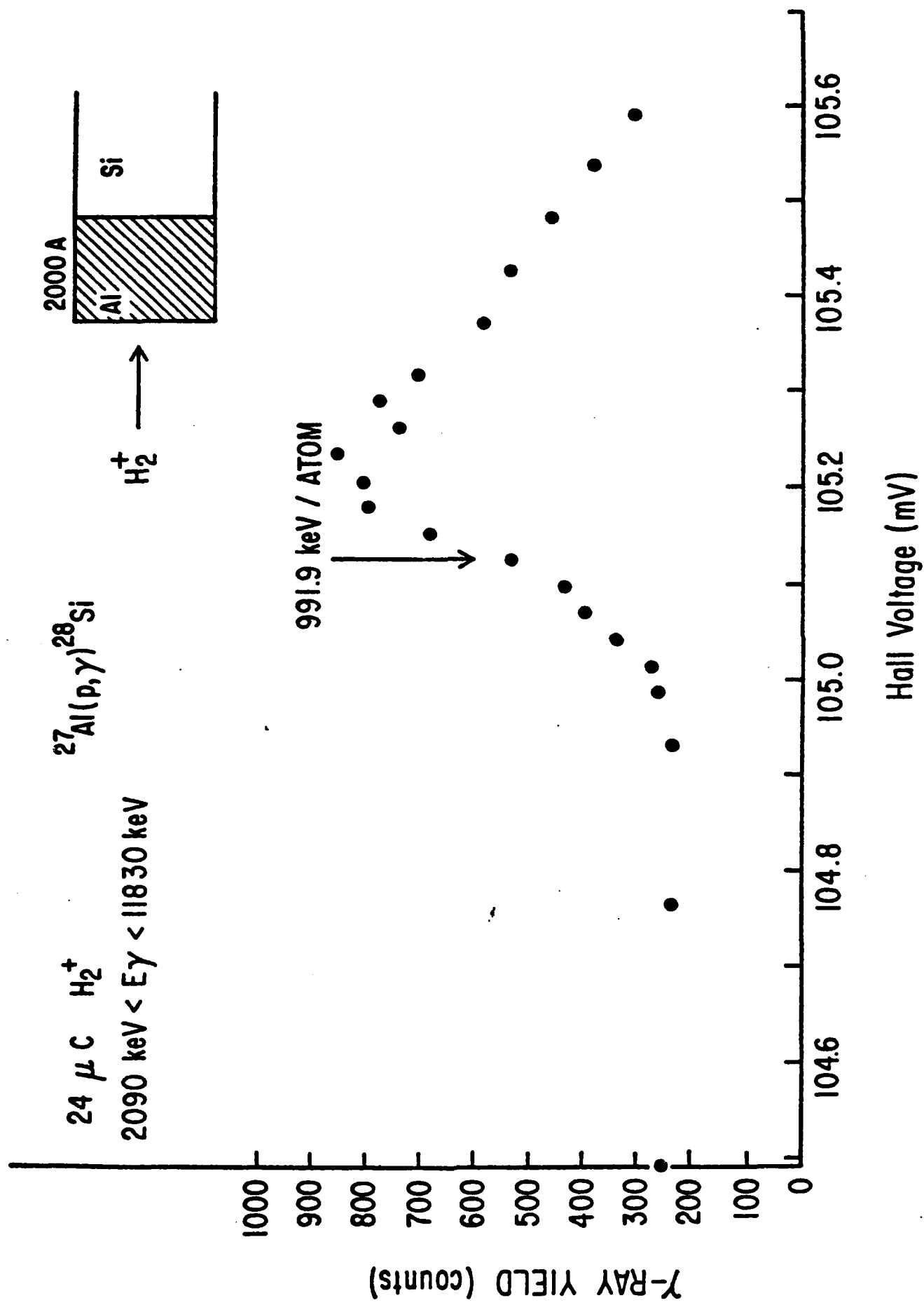
1. General Ionex Corporation, Newburyport, Mass.
2. National Electrostatics Corporation, Middleton, Wisconsin.
3. J. B. Marion and F. C. Young, "Nuclear Reaction Analysis: Graphs and Tables", North-Holland, Amsterdam (1968).
4. F. K. Richtmeyer, E. H. Kennard and J. N. Cooper, "Introduction to Modern Physics", 6th ed., McGraw-Hill, N.Y. (1969).
5. P. R. Bevington, "Data Reduction and Error Analysis for the Physical Sciences", McGraw-Hill, N.Y. (1969).
6. P. F. Dahl, D. G. Costello and W. L. Walters, Nucl. Phys. 21 (1960) 106.
7. W. L. Walters, D. G. Costello, J. G. Skofronick, D. W. Palmer, W. E. Kane and R. G. Herb, Phys. Rev. 125 (1962) 2012.
8. J. W. Butler and C. M. Davisson, Nucl. Inst. Meth. 149 (1978) 183.
9. J. W. Mayer and E. Rimini, Eds., "Ion Beam Handbook for Material Analysis", Academic Press, N.Y. (1977), p.154.

Figure Captions

Figure 1 Plot of γ -ray yield versus Hall voltage for the $^{27}\text{Al}(p, \gamma)^{28}\text{Si}$ reaction. The γ -ray energy window is $2090 \text{ keV} < E_\gamma < 11830 \text{ keV}$ with $24 \text{ } \mu\text{C}$ per point. 105.12 mV corresponds to $1984 \text{ keV } \text{H}_2^+$.

Figure 2 A composite plot of the BS spectra from a $< 5 \text{ } \text{\AA}$ Fe-W layer deposited on SiO_2 , also showing the α -particle signal from the $^{15}\text{N}(p, \alpha)^{12}\text{C}$ nuclear reaction for a H_2^+ beam of energy 1984 keV . The position of each element is shown by a vertical arrow, the channel number by the adjacent horizontal arrow with the K factor given in parentheses below.





APPENDIX 7

Continuation sheets : begin typing on this line

MEV ION BACKSCATTERING SPECTROMETRY APPLIED TO THE ANALYSIS OF BEAM PROCESSED SEMICONDUCTORS

S. S. Lau only : type author's name(s) here
University of California, San Diego
La Jolla, California 92093

Abstract

In this report pulsed laser beam and ion beam induced interdiffusions between metals and semiconductors are summarized. For laser induced reactions, emphasis is placed on the condition under which amorphous alloys can be formed. Experimental results seem to suggest that the cooling rate necessary to quench a liquid binary mixture into a glass state is highest for compositions close to those of congruently melting compounds. For ion induced reactions, both equilibrium compound and amorphous alloy formation are discussed. The phase formation characteristics of these two techniques are compared.

1. Introduction

The techniques of Rutherford backscattering come directly from the field of low-energy nuclear physics. In principle, energetic ion beams in the range of a few hundred keV to several MeV are produced in the accelerator and analyzed, magnetically or electrostatically to give an energetically well defined beam of particles. The ions are then passed along a beam tube through collimating apertures to the target chamber (at typical pressures of 10^{-6} to 10^{-7} torrs) with a typical beam spot size of the order of 1 mm in diameter. The backscattered particles from the sample are energy analyzed, usually with a surface barrier semiconductor detector. The energy spectrum (so called backscattering spectrum) contains chemical information as a function of depth into the sample. The typical sampling depth by MeV $^4\text{He}^+$ particles is about 1 μm ; therefore, backscattering spectrometry is well suited for near surface chemical analysis. When channeling and blocking techniques are used in conjunction, structure as well as lattice location can be investigated. For further information on these techniques, the reader is referred to two books (Chu et al. 1978, Feldman et al. 1982) devoted to the subject of backscattering spectrometry. The advantages of using backscattering spectrometry to beam processed semiconductors come from the fact that (i) the probed depth is commensurate with the thickness of the reacted layer induced by beam processing, and (ii) backscattering is a non-destructive, convenient and fast technique for depth profiling with a typical depth resolution of 300 \AA for most solids. Although backscattering spectrometry is capable of structural analysis, for amorphous phase identification diffraction techniques (such as x-rays and electron diffraction) are necessary.—In the following, we give examples of backscattering spectrometry applied to the analysis of beam processed semiconductors. The focus is placed in the area of metastable and equilibrium phase formation between metals and Si.

2. Glass Formation by Laser Pulse

The research activity of metastable phase formation was first initiated by Pol Duwez in early 1960 (Duwez, 1967). Duwez and his co-workers obtained solid solubility extension and new metastable crystalline or amorphous phases in certain binary alloy systems by rapid cooling from the liquid to the solid state. These rapid solidification techniques are commonly known as splat cooling techniques. The quenching rate of splat cooling generally ranges between 10^4 and 10^6 K/sec. With these quenching rates, Duwez and others have found that metastable alloy phases can be formed near the eutectic composition in binary systems where deep eutectic troughs are present. In Duwez's original thinking, metastable phases are formed as a result of "fooling" the atoms by freezing them into unconventional positions by rapid cooling from the liquid state. Subsequently, Turnbull and others (Cohen and Turnbull, 1961; Davies and Lewis, 1975; Sinha et al., 1976) have dealt with the theoretical and experimental aspects of splat cooling, and the field of rapid solidification has progressed in the interim to a very active, well documented area of research.

With the advent of pulsed laser processing of materials, quenching rates on the order of 10^{10} K/sec are now achievable. These much faster rates open up new dimensions for the formation of metastable phases. In a typical experiment, the sample is a planar, laterally uniform structure containing some distribution of two elements A and B (typically Si and a metal) as a function of depth. The sample surface is heated by a heat pulse with a duration in the range 10^{-9} to 10^{-6} sec. Heat flow in this time regime is essentially one-dimensional, since the thickness of the heated region (on the order of micrometers or less) is small compared to the lateral dimensions of both the sample and the beam. The absorbed fluence is on the order of 1 J/cm^2 , enough to melt several 100 nm of the sample while creating thermal gradients in the 10^6 to 10^8 K/cm range. The maximum surface temperature may exceed the melting point by several 100 K, but it should not approach the boiling point.

Figure 1 shows a one-dimensional heat flow calculation for the position of the liquid-solid interface as a function of time. The film is deposited on a substrate of much higher melting point.

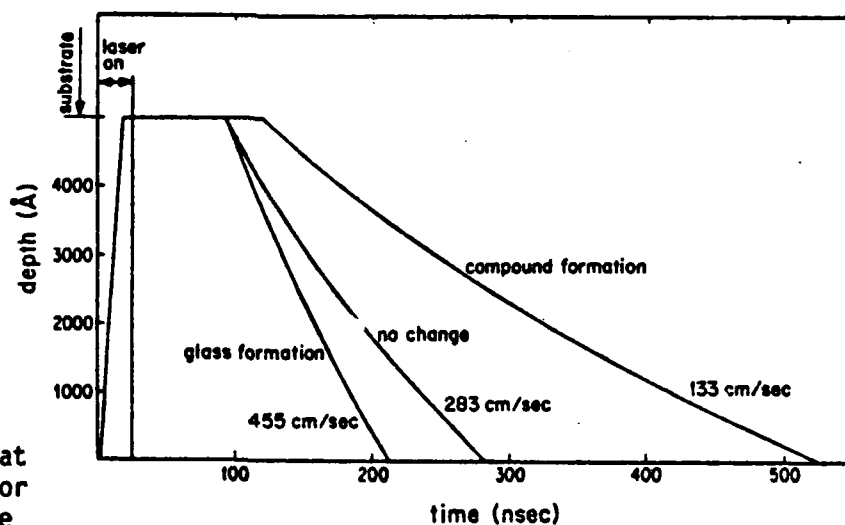


Figure 1. Calculated melt front position as a function of time in a laser-irradiated 5000-Å alloy film on top of an inert substrate. The three curves result from different assumptions on the nature of the solidifying phase, as explained in the text. (From von Allmen et al. 1981.)

For this particular calculation, film thickness and laser pulse duration were chosen to be 500 nm and 25 nsec, respectively; the values for conductivity, specific heat, and melting heat were selected to be about halfway between those of Si and those of Pt. Since the function of the calculation was to obtain some insight into the relevance of various parameters (rather than to obtain accurate temperature values), the melting temperature was arbitrarily set at 1000°C. For the substrate, a constant conductivity κ of 0.24 W/(cm K) was assumed. The three different solidification curves in Figure 1 result from three different assumptions about the solidification process:

(i) For the curve labeled "no change", the same values for transition temperature and latent heat as for melting were used. This corresponds to the case of an elemental sample or, alternatively, to recrystallization of a mixture without a reaction between the components.

(ii) For the curve labeled "compound formation", the latent heat for freezing was 1.5 times that for melting. This describes a case in which a compound is formed with a heat of formation of 50% of the average melting heat of the elements. (The corresponding value for formation of PtSi would be 46%; see Figure 5 for the Pt-Si phase diagram.) Further, the freezing temperature of the compound was set at 800°C. The consequence of this reduction in liquid-solid interfacial velocity due to compound formation is discussed in more detail later.

(iii) For the curve "glass formation", it was assumed that latent heat of two-thirds of the melting heat was liberated upon solidification. The freezing temperature was 1000°C in this case. (This procedure neglects the presence of the freezing interval.)

As is evident from Figure 2, rather different values for the interface velocity during solidification can result under otherwise identical conditions, depending on the thermodynamics of the solidification process. As a rule, the interface velocity is roughly proportional to the inverse of the total latent heat liberated at the interface if all other parameters are left unchanged.

Processing times in heat pulse annealing are usually small fractions of a second, thereby making the solid state diffusion negligible. However, the atoms in the melt have high mobilities, corresponding to diffusivities on the order of 10^{-4} cm²/sec as compared to 10^{-9} to 10^{-12} cm²/sec in a solid. This allows mass transport over tens of nanometers even for heat pulses in the nanosecond range, and composite samples will necessarily undergo redistribution of the elements.

The diffusivities D in liquids depend on composition as well as on temperature, but generally far less so than in solids. If D is taken to be a constant, concentration distributions due to diffusion in the melt can be readily calculated.

Figure 2 gives concentration distributions for three different initial sample configurations often found in practice:

Figure 2 shows three cases, including this one:

- (1) The Gaussian (describing a profile obtained by ion implantation of a dopant B in a semiconductor A).
- (1.1) The rectangular distribution (occurring in the case of a deposited

Continuum layer B on top of a substrate A).

(iii) The square wave profile (describing a multilayer of alternating deposited films of A and B).

Cases (ii) and (iii) will also be referred to as "unlimited supply" and "limited supply" of the element A, respectively.

It can be seen that the initial concentration peaks are broadened by an amount of approximately $2\sqrt{Dt_1}$. For more accurate calculations, t_1 is allowed to vary within the molten layer as a function of depth, taking into account the finite velocity of the liquid-solid interface (Lau et al., 1979).

As the conditions governing heat flow during melting establish a boundary condition for atomic diffusion (via the duration of existence of the melt), the latter, in turn, results in an initial condition for solidification:

It defines the local thermo-physical properties (melting point, latent heat) of the molten layer at the instant of solidification and influences the structure of the solid, as well as the velocity of the l-s interface, as demonstrated in Figure 1.

Experiments on silicide and metastable phase formation are usually based on sample configurations shown in Figure 2b and 2c.

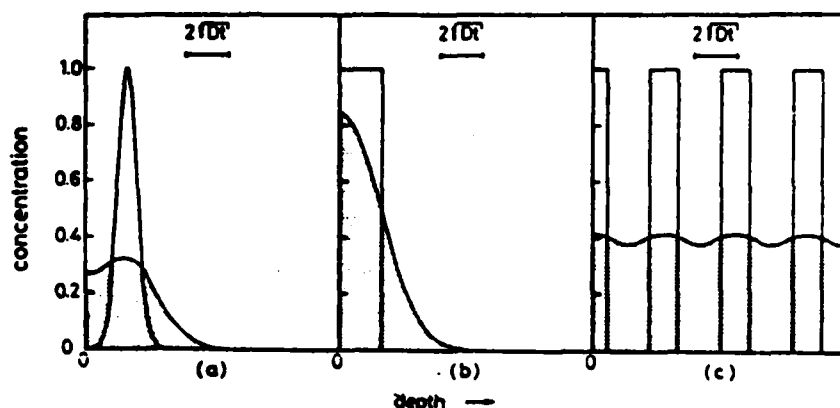


Figure 2. Calculated diffusion profiles in the melt for three different initial concentration profiles. (a) Gaussian (as produced by ion implantation of an impurity into a substrate). (b) Rectangular profile (vapor-deposited thin film). (c) Square wave profile (alternating multilayer).

In principle, an alloy melt can be cooled too fast for either nucleation or growth to take place. If the undercooling is great enough, the melt will, in this case, retain its structure indefinitely and be called a glass (Turnbull, 1969). The question then is, what cooling rate (or what interface velocity) is required for glass formation from a melt of given properties?

These two limiting situations (nucleation and growth limited) have been analyzed by numerous workers and are summarized recently for thin film cases by Von Allmen and Lau (1982). In the following we will discuss two cases: (i) metal semiconductor eutectic systems (Au-Si as an example) and (ii) silicide forming systems (Pt-Si and Pd-Si as examples).

2.1 Metal-Eutectic Systems begin typing on this line

Since the first demonstration of an Au-Si metallic glass made by splat cooling in 1960, a multitude of metastable phases (amorphous or crystalline) have been obtained by rapid quenching of the melts. With the extremely high cooling rate made available by short laser pulses, it was a natural consequence to investigate the glass-forming characteristics of classical deep eutectic systems under laser irradiation. The configuration of a metal layer deposited on a semiconductor substrate is suitable for the study of glass formation at the metal-semiconductor interface under unlimited supply conditions. Figure 3 shows the

schematics and backscattering spectra for an Au-Si sample before and after laser irradiation (Lau et al., 1981).

The thin Si layer (~300 Å) on top of the Au layer (~2500 Å) was to facilitate the absorption of laser power (Nd-glass, 30 nsec pulse). After irradiation, the Au signal spread in width in both directions, indicating that the Au layer had reacted with crystalline as well as amorphous Si. From the decrease in the

height of the Au signal near the Au-Si substrate interface, the mixed layer has a composition of $\text{Au}_{82}\text{Si}_{18}$ with an amorphous structure. It is interesting to note that the composition of the mixed layer, $\text{Au}_{82}\text{Si}_{18}$, is the eutectic composition of the Au-Si system.

With the limited supply approach, the extent of glass-forming ability of Au-Si can be investigated at extremely fast quench rates which are induced by pulsed laser irradiation and are not accessible with splat cooling techniques. Experiments of this kind have been done using samples where multiple layers of Au and Si were vacuum-deposited on sapphire substrates. The thicknesses of the layers were adjusted such that the average film composition ranged between AuSi_{10} and Au_{10}Si , i.e. from 9 to 91 at % Au. The individual layer thickness was not more than a few hundred angstroms, with a total layer thickness of about 2000 Å. The surface layer was chosen to be Si and served the purpose of an antireflection coating.

The composition of the irradiated samples remained the same as the initial

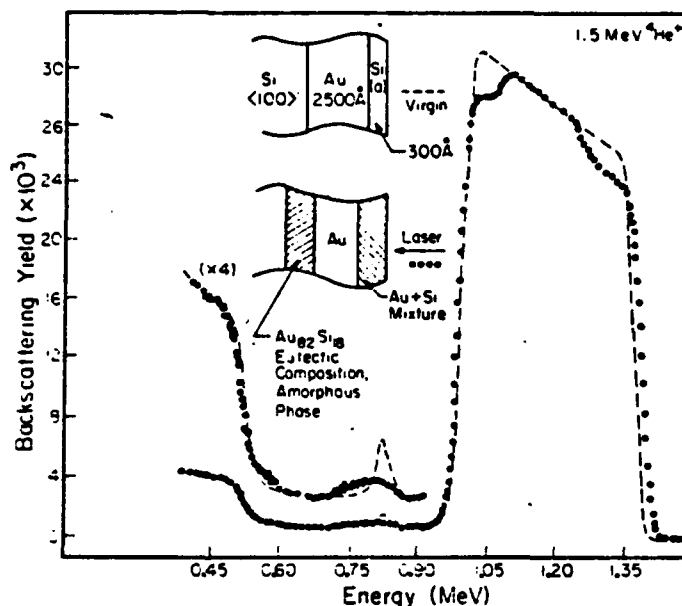


Figure 3. Backscattering spectra of an Au-Si sample (unlimited supply) before and after pulsed laser irradiation. (From Lau et al., 1981.)

average film composition, as monitored by backscattering. As an example, Figure 4 shows backscattering spectra for a sample with the composition AuSi_5 before and after irradiation with a 30-nsec pulse. In general, the layers mixed by 30-nsec pulses showed some residual waviness in composition versus depth, whereas those obtained with 300- μsec pulses were very uniform.

X-ray diffraction analysis of films irradiated by 30-nsec pulses

revealed an amorphous structure in all but the most Au-rich (91 at.%) samples, usually together with traces of a metastable Au-Si compound. The films irradiated with 300- μsec pulses were polycrystalline and consisted of the same metastable compound, generally together with precipitates of the predominant component.

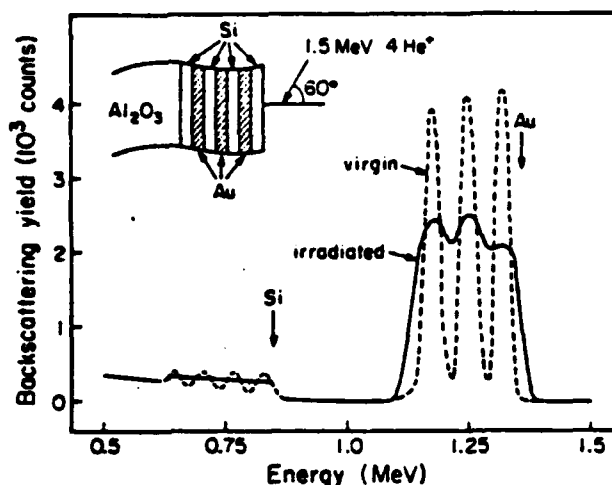


Figure 4. Backscattering spectra of an AuSi_5 sample before and after irradiation with a Q-switched pulse of 30-nsec duration, Nd-glass laser. (From von Allmen et al., 1980a.)

The compositional range of Au-Si glasses induced by laser processing greatly exceeds previously established limits for glass formation by liquid quenching. Glass-forming ability is believed to be related to melting point depression (Donald and Davies, 1978), which is largest at the eutectic point. The only Au-Si glasses reported so far have eutectic compositions (Klement et al., 1960).

2.2 Silicide-Forming Systems

Laser annealing as a means of forming metal silicide contacts on Si provides the advantage of transferring energy to only a very localized region instead of heating up the whole wafer. Because of this practical aspect, a wealth of experimental investigations have been reported in the literature (for a summary, see von Allmen and Lau, 1982). For the limited-supply case, a variety of compounds for a number of metal-Si systems, usually not observed under thermal annealing conditions, have been found. However, glass formation is usually not induced by pulsed laser processing.

The application of the limited-supply techniques to the Pt-Si and Pd-Si systems lead to interesting phase transformation under the influence of pulsed laser processing.

Unlike the case of Au-Si, not all the compositions tested could be quenched into an amorphous state. Generally speaking, polycrystalline films resulted from samples with compositions at or close to those of the congruently melting compounds, Pt_2Si , PtSi and Pd_2Si , PdSi , respectively. Figure 5 shows the phase diagrams of the two systems along with arrows marking the compositions of the films studied. The letters beneath the arrows give the structure of the as-irradiated films.

Intimate mixing of the components by laser irradiation was found to be essential in obtaining amorphous films; incompletely mixed films containing local compositions too close to that of a congruently melting compound were not amorphous after irradiation but rather showed the presence of the congruently melting compound. The reason for this could lie in the liberation of the heat of formation of the compound, which reduces the cooling rate as discussed previously. The fact of a composition-dependent cooling rate notwithstanding, it seems clear that the cooling rate necessary to quench a liquid binary mixture into a glassy state is highest for compositions close to those of congruently melting compounds, as well as to those of the pure components.

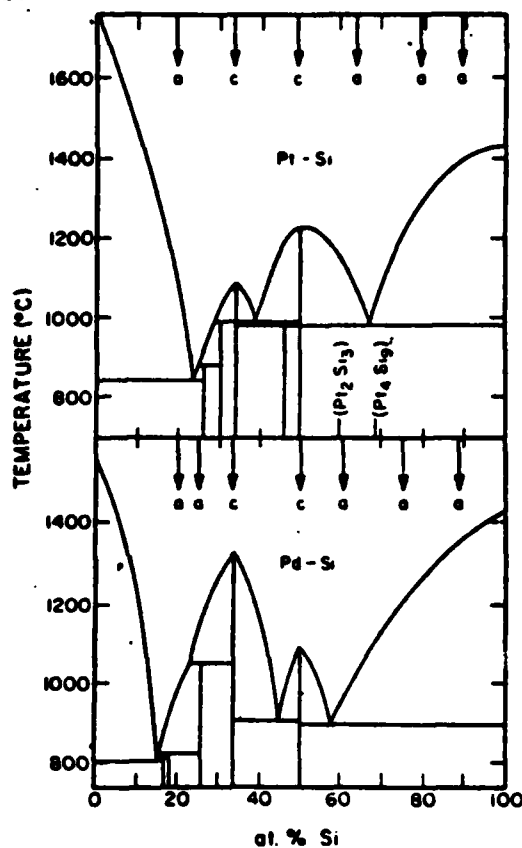


Figure 5. Phase diagrams of the Pt-Si and Pd-Si systems. The arrows mark the compositions of films used in this study. Small letters indicate the structure of the As-quenched films (a, amorphous; c, polycrystalline). (From von Allmen et al., 1980b.)

3. Ion Mixing Experiments

Ion-induced mixing not only can lead to stable compound formation, but also to metastable alloy formation. In some metal-metal systems, terminal solubilities can be greatly extended by ion mixing. In other cases, where the two constituents of the system have different crystal structures, extension of terminal solubility for both sides of the phase diagram eventually becomes structurally incompatible and a glassy (amorphous)

mixture can form. The composition range where this bifurcation is likely to occur is in the two-phase regions of the phase diagram. These concepts are potentially useful guides in selecting metal pairs that form metallic glasses by ion mixing.

3.1 Equilibrium Compound Formation by Ion Mixing

The formation of equilibrium compounds by ion mixing at room temperature has been investigated rather extensively in silicide forming systems using bilayered structures. The ion-induced silicide formation characteristics can be compared with those obtained by thermal steady-state annealing. It can be clearly seen that the first silicide phase induced by ion mixing in unlimited supply samples is the same as that obtained by thermal annealing. Although some of the layers that were ion mixed at room temperature (RT) do not exhibit a distinct crystal structure due to weak x-ray diffraction patterns, the composition of the mixed layer deduced by backscattering is invariably the same as that obtained by thermal annealing. As the temperature of irradiation is increased to above RT, the crystal structure of the phase can be identified even in those cases as being the same as that obtained by thermal annealing. If we assume that ion mixing at room temperature is in the thermally activated regime for all systems studied, we can conclude that there is a direct one-to-one correlation between thermal annealing and ion mixing in the thermally activated regime, at least in silicide forming systems (Tsaur 1980). This is in marked contrast to the case of pulsed laser processing of bilayered samples where the induced reactions are of a rather complex nature (von Allmen and Lau, 1982).

3.2 Glass Formation by Ion Mixing

Previous experimental investigations on ion-induced reactions using multilayered samples (limited supply) showed that ion mixing is well-suited for metastable phase formation in metal-metal systems (Mayer et. al, 1981). In particular, when the two components of the binary system have the same crystalline structure, but exhibit a

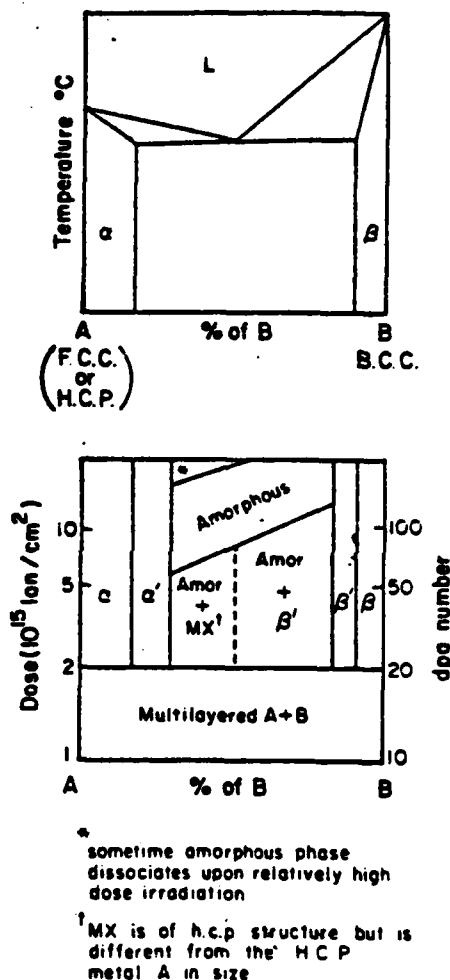


Figure 6. See text for explanation.

miscibility gap in the phase diagram, supersaturated solid solutions are obtained upon ion mixing (for example, Ag-Cu, f.c.c. structure). On the other hand, when the crystal structures of the two components are different (say f.c.c. for component A and b.c.c. for component B), a tendency to form amorphous alloys by ion mixing can clearly be detected.

Figure 6 shows a schematical phase diagram with different crystal structures of the elements and the sequence of events as a function of dose (or dpa). Intermixing of the two phases is observed at relatively low doses ($< 2 \times 10^{15}$ Xe/cm² or < 20 dpa). For samples with compositions near either A or B, extended solid solutions α' and β' with structures identical to their parent phases are observed at increasing doses (α' has the structure of α , β' that of β). As the composition approaches from the A side (f.c.c. or h.c.p.) to the middle of the two-phase region, the mixed layer ($20 \lesssim \text{dpa} \lesssim 50 - 100$) consists of a mixture of an amorphous phase and a metastable crystalline phase of h.c.p. structure (but with a different c/a ratio compared to that of A if A is also h.c.p.). On the B side, a mixture of an amorphous phase and β' (b.c.c.) is observed in the mixed layer. Increasing the ion dose leads to complete amorphization of the mixed layer in a composition range near the eutectic composition. At even higher doses, the amorphous phase may dissociate into metastable or equilibrium phases, possibly due to ion-beam demixing effects.

It is found that in eight metal-metal binary systems with multilayered sample configuration, irradiation leads to uniform mixing of the interposed layers. An amorphous alloy is formed in every case, irrespective of the atomic size and the electronegativity properties of the constituents, as long as the constituents have different crystal structures (Liu et al. 1983).

4. Summary

In summary, glass formation in binary systems requires (i) uniform intermixing between different components in a given system and (ii) fast quench rates after the mixing is completed. MeV backscattering spectrometry provides a very convenient way to examine the mixing phenomenon after energetic beam processing. There are numerous other applications of backscattering spectrometry to material analysis which are well discussed in the two books and many articles reported in the literature on this subject.

Acknowledgement

The financial support of DARPA (S. Roosild) is greatly appreciated.

References

- Chu W K, Mayer J W and Nicolet M A 1978 Backscattering Spectrometry (Academic Press)
- Cohen M H and Turbull D 1961 Nature (London) 189, 132
- Davies H A and Lewis B G 1975 Scr. Metall. 9, 1107
- Donald I W and Davies H A 1978 J. Non-Cryst. Solid 30, 77
- Duwez P 1967 ASM Trans. Q. 60, 83
- Feldman L C, Mayer J W and Picraux S T 1982 Materials Analysis by Ion Channeling (Academic Press)
- Klement W, Willen R H and Duwez P 1960 Nature (London) 187, 869

- Lau S S, Tsaur B Y, von Allmen M, Mayer J W, Stritzken B, White C W and Appleton B 1981 Nucl. Instr. Meth. 182/183, 79
- Liu B X, Johnson W L, Nicolet M A and Lau S S 1983 Appl. Phys. Lett. 42(1), 45
- Mayer J W, Tsaur B Y, Lau S S and Hung L S 1981 Nucl. Instr. and Meth. 182/183, 1
- Sinha A K, Giessen B C and Polk D E 1976 Treatise on Solid State Chemistry (N B Hannay Ed. Plenum, NY) Vol.1 pp.1
- Tsaur B Y 1980 Proc. Symp. on Thin Film Interfaces and Interactions, (J. E. E. Baglin and J. M. Poate, Eds.) The Electrochemical Society, Princeton Vol.80-2, pp.205
- Turbull D 1969 Contemp. Phys. 10, 473
- von Allmen M, Lau S S, Maenpaa M and Tsaur B Y 1980a Appl. Phys. Lett. 36, 205
- von Allmen M, Lau S S, Maenpaa M and Tsaur B Y 1980b Appl. Phys. Lett. 37, 84
- von Allmen M, Affolter K and Wittmer M 1981 Laser and Electron Beam Solid Interactions and Materials Processing (J. F. Gibbons, L. D. Hess and T. W. Sigmon, Eds. North-Holland, NY) pp.559
- von Allmen M, Lau S S 1982 Laser Annealing of Semiconductors (J. M. Poate and J. W. Mayer, Eds. Academic Press, NY) pp.439-478

You have 5 lines left including this one

APPENDIX 8

Characterization of Tantalum-Silicon Films on GaAs
at Elevated Temperatures

W. F. Tseng, B. Zhang, D. Scott, S. S. Lau,
A. Christou and B. R. Wilkins*

Abstract

R.f. sputter-deposited tantalum-silicon films on GaAs have been investigated using four-point probe, glancing x-ray diffraction, Auger electron spectroscopy and MeV $^4\text{He}^+$ backscattering spectrometry as a function of annealing up to 850°C. Experimental results show that (1) there is no observable Ta or Si migration from the TaSi_2 overlayer into the GaAs substrate; (2) the structure of the as-sputtered film is amorphous and crystallization into a polycrystalline TaSi_2 layer occurs at ~500°C accompanied by a reduction in electrical resistivity. After annealing at 650°C, As and/or Ga appear to have migrated into the TaSi_2 layer. The amount of this migration remains unchanged up to an annealing temperature of 850°C. On the other hand, migration of Ta and/or Si into the GaAs substrate is not detected up to 850°C. This absence of the Ta and/or Si migration contributes to the stability of the Schottky diode characteristics against annealing reported previously.

*B. Zhang, D. Scott and S. S. Lau are with the University of California at San Diego, La Jolla, CA 92093. W. F. Tseng, A. Christou and B. R. Wilkins are with the Naval Research Laboratory, Washington, D.C. 20375.

The Schottky barrier height of a metal/GaAs contact has been found to be invariant with respect to the metal overlayer [1,2]. Thus, Schottky barrier devices on GaAs (such as MESFETs) with a constant and reproducible barrier are fabricated relatively easily. However, it is difficult to select a single metallization system that will not degrade the electrical properties after annealing at the temperatures required for post-ion implantation heat treatment (850°C). This degradation of the device performance after high temperature annealing is usually a result of interactions between the metal layer (such as Pt, Cr, Ti, W and Ti/W) and the GaAs substrate [2,3,4]. It has been found recently that refractory metal silicides (such as Ti/W silicide [3] and tantalum silicide[5]) can replace metal layers as Schottky barrier contacts on GaAs with much improved stability after high temperature annealing. Experimental results show that the barrier height and ideality factor remain stable at values of ~0.8 eV and ~1.1, respectively for these two co-sputtered silicides on n-type GaAs even after annealing at 800-850°C [3,5]. In this study, our objectives are to characterize the TaSi₂ and to correlate the contact properties of r.f. sputtered tantalum-silicon films on GaAs with the interactions between these films and GaAs as a function of annealing temperature.

Thin layers (1500 Å) of tantalum-silicon were deposited on semi-insulating GaAs and on SiO₂ substrates by r.f. sputtering. The target for sputtering was a hot-pressed tantalum-silicon mixture with 76.32 wt% (33.7 at%) of Ta and 23.33 wt% (66.3 at%) of Si. The samples were annealed for 30 minutes in a flowing forming gas (10% H₂ - 90% N₂) ambient up to 850°C. Each sample was annealed at a given temperature only once. Before and after annealing, the samples were analyzed using a four-point probe, glancing angle x-ray diffraction (Read camera), Auger electron spectroscopy and MeV ⁴He⁺ backscattering spectrometry.

The results of the x-ray diffraction measurements are shown in Fig. 1. The as-deposited Ta-Si film is amorphous in structure. The films remain amorphous after annealing up to and including 450°C. At annealing temperatures at or above 500°C the amorphous Ta-Si film crystallized into a polycrystalline TaSi₂ (hexagonal, C40) layer. The film remained as a single phase TaSi₂ without any other compounds (i.e. products from a Ta-Si and GaAs reaction) being detected by x-ray diffraction up to 850°C.

The crystallization is accompanied by a decrease in resistivity, shown in Fig. 2. The initial resistivity of the as-deposited film is 480 μΩ-cm (ρs=32Ω/). The electrical resistivity begins to decrease at 500°C and continues to decrease with increasing temperature. At 850°C the resistivity was found to have decreased to 120 μΩ-cm, about 1/4 of the initial value. Over the annealing range up to and including 850°C the barrier height was found to remain stable at ~0.8 eV [5]. It is interesting to note that this barrier height is independent of the crystal structure (amorphous or polycrystalline) of the overlying film in this case.

Figure 3 shows the Auger profiles for a sample before and after annealing at 800°C. Comparison of Figs. 3a and 3b does not show any detectable interaction between TaSi₂ and GaAs. The reaction between the Ta-Si film and the GaAs is further investigated by MeV ⁴He⁺ backscattering spectrometry. Figure 4 shows the backscattering spectra (in linear scales) for three samples after annealing at different temperatures. The overall composition of the TaSi₂ layer remains unchanged and the interface between the TaSi₂ layer and the GaAs substrate remains sharp up to an annealing temperature of 850°C. These spectra also suggest that neither Ta nor Si appear to migrate into the GaAs substrate. Figure 5 shows the region of two backscattering spectra from 1.3 to 1.9 MeV, with the yield expressed in a logarithmic scale for a sample

before and after annealing at 850°C for 30 min. After annealing at 850°C for 30 minutes, a signal appears between ~1.5 and ~1.6 MeV, indicating that As and/or Ga have migrated into the TaSi₂ layer to a concentration of about 2 at.%. The trailing edge of the Ta signal remains very sharp, again confirming that there is little or no migration of Ta into the GaAs substrate. It is interesting to note that this migration of As and/or Ga first appeared after annealing at 650°C for 30 minutes, having the same concentration in the TaSi₂ layer as that observed for the sample annealed at 850°C (Fig. 5). The temperature at which this migration of As and/or Ga occurs may be related to the recrystallization of the as-deposited (amorphous) TaSi₂ film which occurs at or above 500°C.

The stability of TaSi₂ layers on GaAs shown in this investigation is consistent with the reported stable Schottky barrier characteristics of TaSi₂ on GaAs. Barrier heights are not expected to change if the metal and/or Si migration does not occur between the metallization and the GaAs substrate. This has been found to be the case for Ti-W silicide [3] and for TaSi₂ on GaAs in the present study. On the other hand, excessive metal migration as observed in the case of Pd [7] or Au [2] on GaAs between the metallization and the GaAs does lead to degradation of device performance. The advantage of using silicides as metallization for GaAs therefore relies on the ability of the silicides to resist reactions with the substrate. The migration of As and/or Ga does not appear to affect the Schottky barrier characteristics. In principle, more stable silicides (i.e. large negative heat of formation) should yield more reliable Schottky contacts on GaAs. If one accepts this view, NiSi₂ ($\Delta H = -6.9$ Kcal/gm-atom) [6] would yield a less stable Schottky contact and VSi₂ ($\Delta H = -24.6$ Kcal/gm-atom [6]) would yield a more stable Schottky contact compared to that of TaSi₂ ($\Delta H = -8.0$ Kcal/gm-atom) [6],

assuming all other heats of formation (i.e. between metals and GaAs) are relatively the same. More work is now in progress to test the validity of this concept.

In summary, there was no observable Ta and/or Si migration from the r.f. sputtered TaSi₂ films into the GaAs substrate up to temperatures of 850°C although some migration of As and/or Ga was observed. Crystallization of the amorphous (as-sputtered) TaSi layer occurs at 500°C. This phase transformation did not cause any change in the Schottky barrier characteristics. The accompanying reduction of resistivity of the TaSi₂ layer is beneficial to device operations.

Acknowledgement

The work at UCSD was partially supported by DARPA (S. Roosild). We also wish to acknowledge Prof. Marc Nicólet (CalTech) for encouragement and hospitality. The investigations at NRL were supported by the Office of Naval Research.

References

1. W. E. Spicer, I. Lindau, P. Skeath, C. Y. Su and P. Shye, "Unified Mechanism for Schottky-Barrier Formation and III-V Oxide Interface States," *Phys. Rev. Lett.* 44, 420 (1980).
2. D. V. Morgan, "Interdiffusion of Metal Films on GaAs and InP," in Reliability and Degradation, Semiconductor Devices and Circuits, ed. M. J. Howes and D. V. Morgan, Wiley (1981).
3. N. Yokoyama, T. Ohnishi, K. Odani, H. Onodera and M. Abe, "Ti/W Silicide Gate Technology for Self-Aligned GaAs MESFETs VLSIs," *IEDM*, 80 (1981).
4. A. K. Sinha and J. M. Poate, "Metal-Compound Semiconductor Reactions," in Thin Films - Interdiffusion and Reactions, ed. J. M. Poate, K. N. Tu and J. W. Mayer, Wiley (1978).
5. W. F. Tseng and A. Christou, "Stable High Temperature Tantalum Silicide Schottky Barrier on Gallium Arsenide," *IEDM*, 174 (1982).
6. R. Pretorius, J. M. Harris and M. A. Nicolet, "Reaction of Thin Metal Films with SiO_2 Substrates," *Solid State Electron.* 21, 667 (1978).
7. J. O. Olowolafe, P. S. Ho, H. J. Hovel, J. E. Lewis and J. M. Woodall, "Contact Reactions in Pd/GaAs Junctions," *J. Appl. Phys.* 50, 955 (1979).

FIGURE CAPTIONS

- Fig. 1. X-ray diffraction (Read camera) patterns of three samples annealed at (a) 400°C, TaSi₂ is amorphous, the spot pattern is from the GaAs substrate; (b) 500°C, onset of crystallization of TaSi₂; and (c) 850°C, TaSi₂ is fully recrystallized. Every diffraction ring can be identified as hexagonal TaSi₂ and indexed according to ASTM card file #8-53.
- Fig. 2. Sheet resistance ratio [R (after anneal)/R(before anneal)] versus annealing temperature. Each sample was annealed once at a given temperature in a flowing forming gas ambient for 30 minutes.
- Fig. 3. Auger profiles for (a) an as-deposited sample and (b) a sample after annealing at 800°C. No interdiffusion between the TaSi₂ and the GaAs was observed after annealing.
- Fig. 4. Backscattering spectra for three samples after annealing at different temperatures. The shape and the height of the Ta and Si signal remain relatively unchanged after annealing up to 850°C.
- Fig. 5. Backscattering spectra of Fig. 4 plotted in logarithmic scale. The trailing edge of Ta signal remains unchanged after annealing up to 850°C. About 2 at.% of As and/or Ga have been incorporated into the crystallized TaSi₂ film as the annealing temperature was increased beyond 650°C.

1500Å TaSi₂ on (100) GaAs

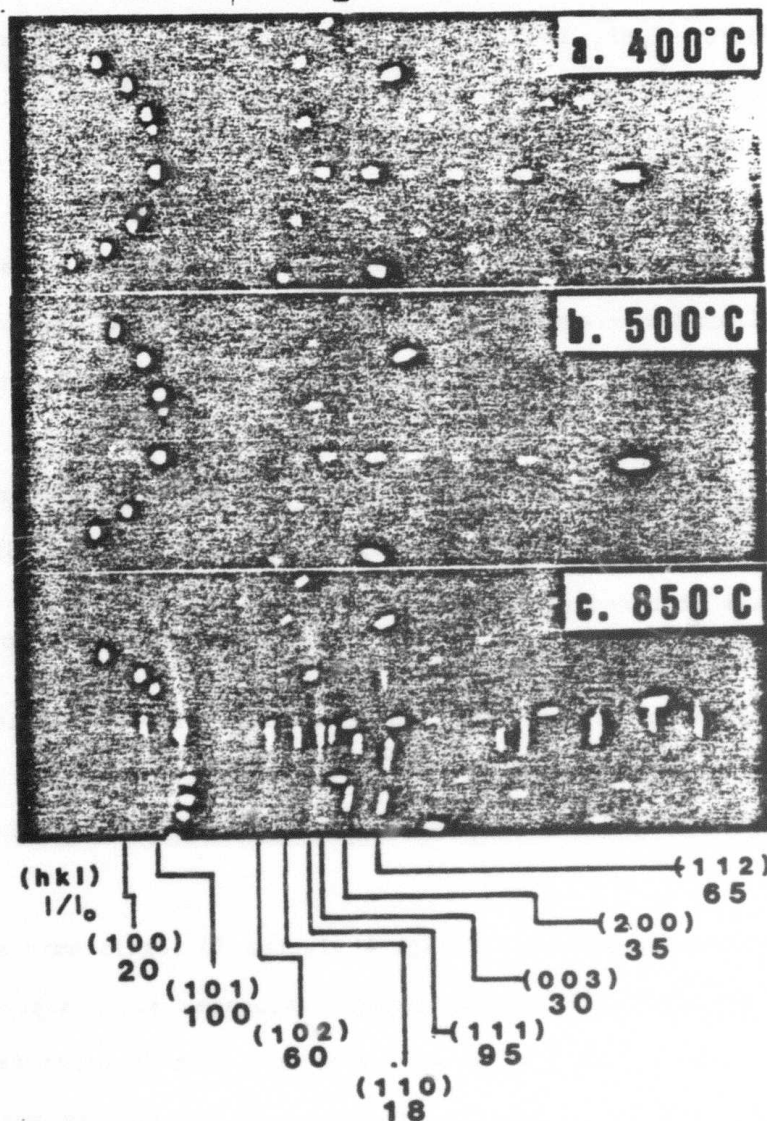


Fig. 1.
Tseng, et. al

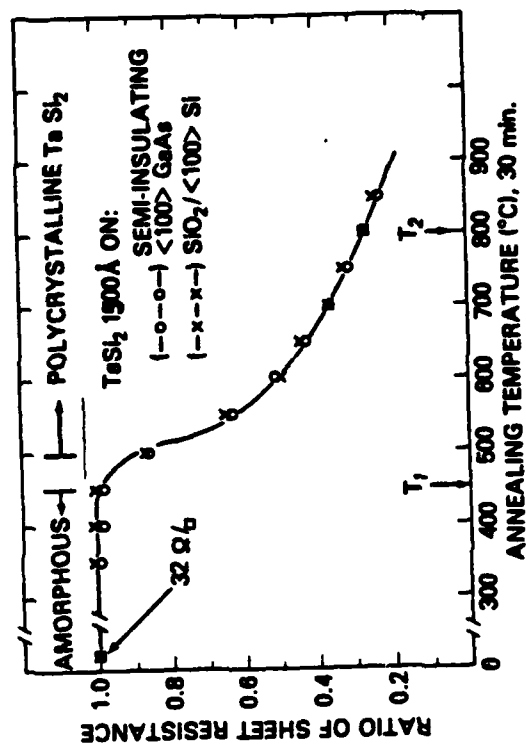


Fig. 2.
Tseng, et. al

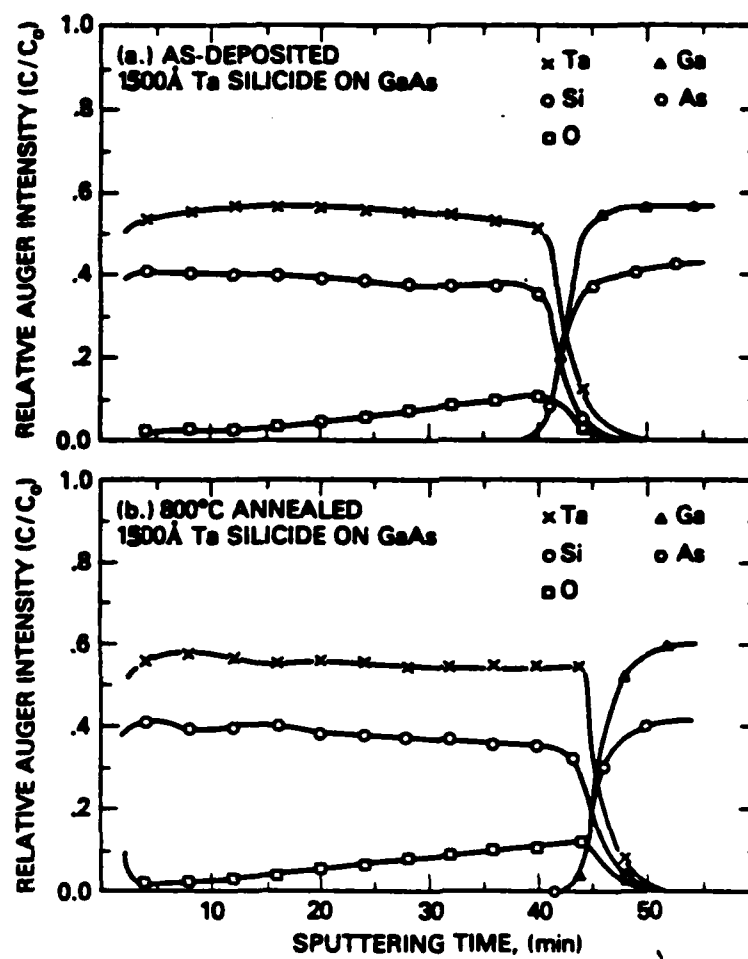


Fig. 3.
Tseng, et al.

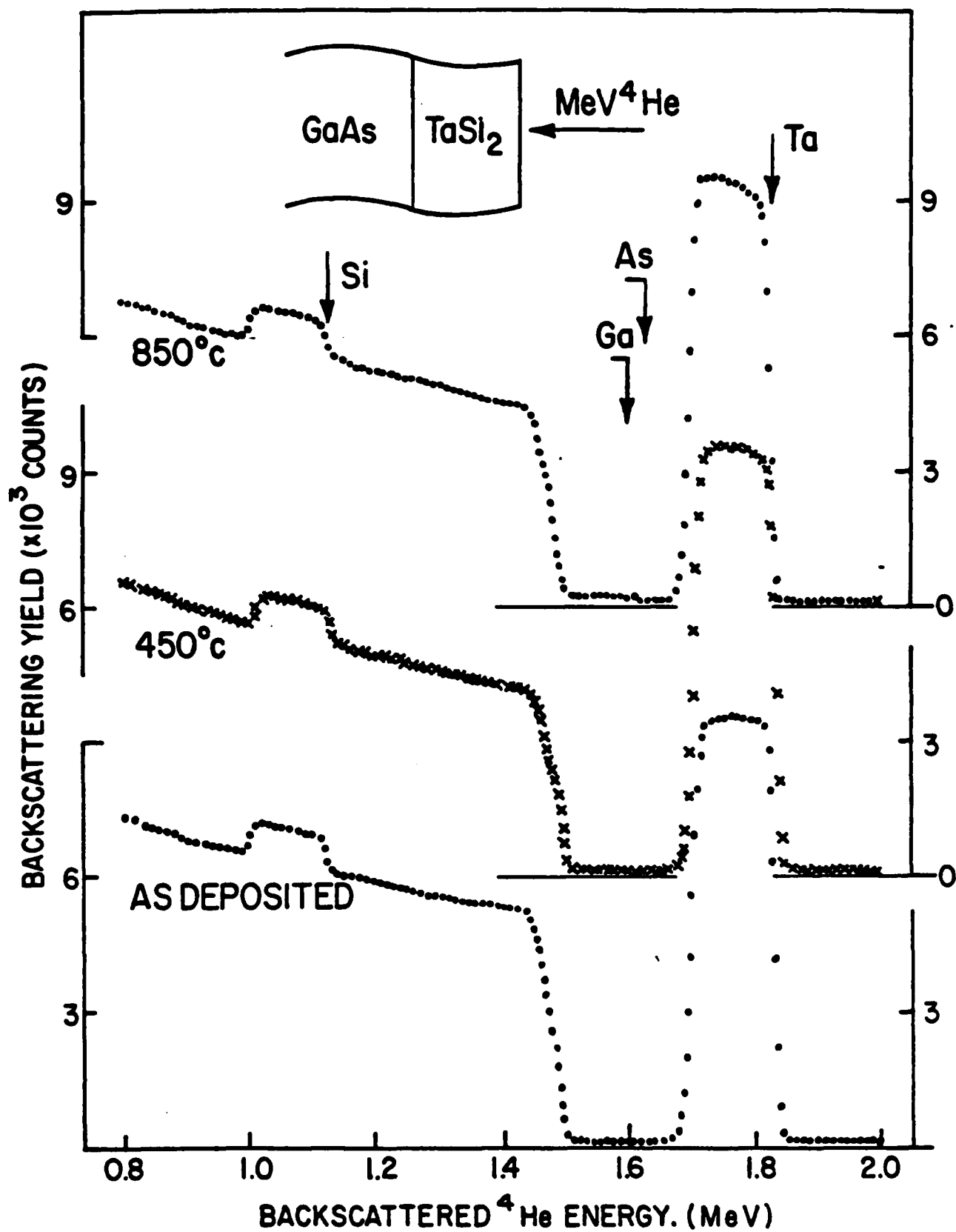


Fig. 4
Tseng, et al

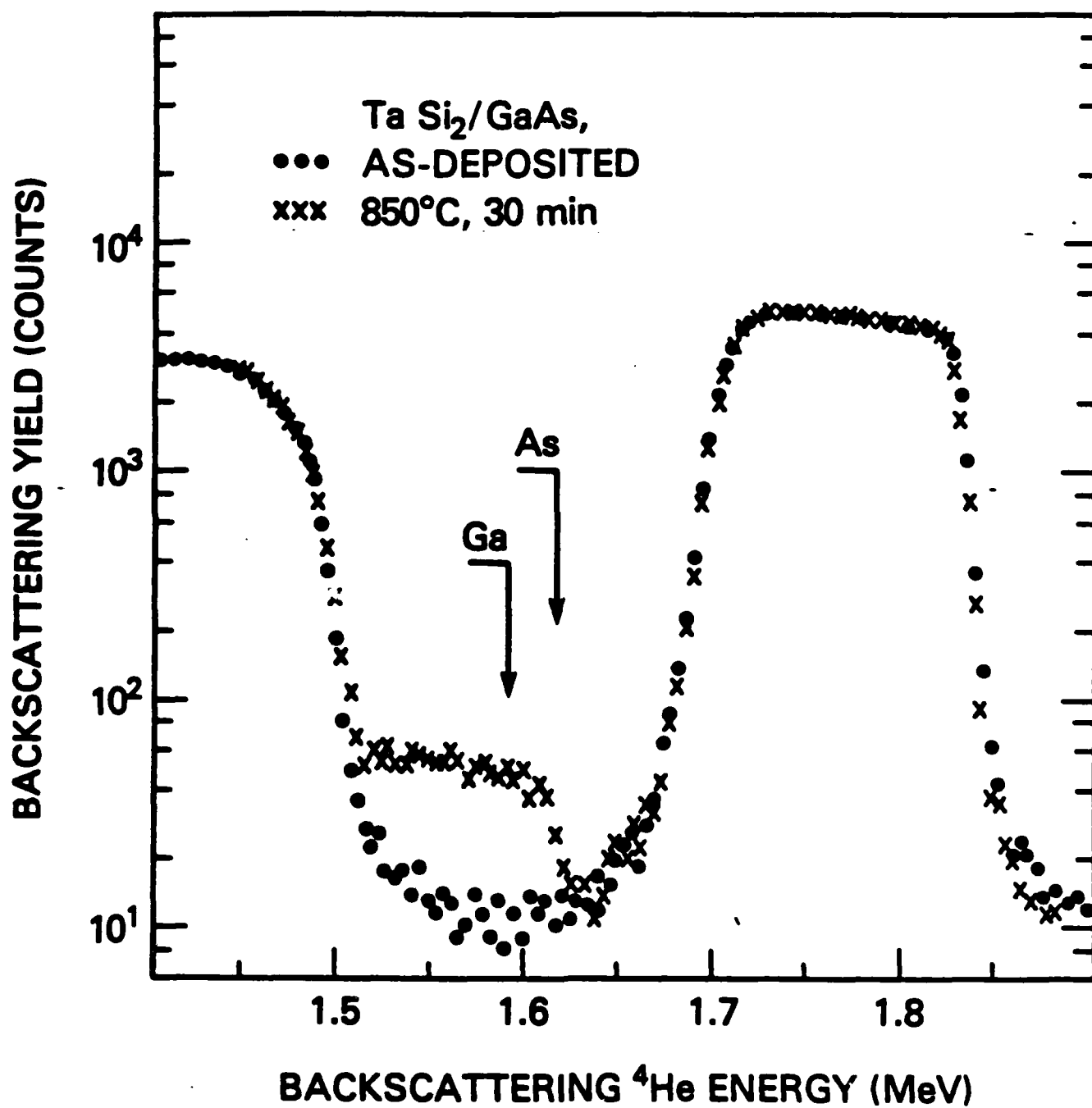


Fig. 5.
Tseng, et al.

APPENDIX 9

Interaction of Pd-Er Alloys With Silicon

G. Ottaviani,^(a) K.N. Tu, R.D. Thompson
IBM Thomas J. Watson Research Center
Yorktown Heights, N.Y. 10598

J.W. Mayer
Dept. of Material Science, Cornell University
Ithaca, N.Y. 14853

S.S. Lau
University of California at San Diego
La Jolla, CA 92093

Abstract:

In situ resistivity measurements together with MeV $^4\text{He}^+$ backscattering, x-ray diffraction, barrier height measurements and Auger electron spectroscopy combined with Ar sputtering have been used to investigate the interaction of silicon with alloys of rare-earth and near-noble metals with annealing at temperatures up to 650°C. Alloys of Pd-Er with three different compositions have been prepared by dual electron-gun coevaporation on both n and p-type silicon and Pd/Er bilayers have been deposited on SiO_2 . The results show that as-deposited these alloys are amorphous and the initial stages of the reaction with silicon upon annealing is controlled by the metal-metal interaction as well as the metal-silicon interaction. The Er-rich alloy ($\text{Pd}_{15}\text{Er}_{85}$) segregates Er to the silicon interface and forms Pd_2Er_5 . The segregated Er reacts with silicon producing ErSi_2 . For the Pd-rich alloy ($\text{Pd}_{65}\text{Er}_{35}$) the excess Pd is segregated at the silicon surface forming Pd_2Si . The near 50-50 alloy forms PdEr and a slightly higher temperature is necessary to promote the reaction with silicon to form the silicide of the excess component.

^(a)Permanent Address: Istituto di Fisica, 213/A via Campi, 4110 Modena, Italy.

I. Introduction

Silicide formation has provided much of our information on thin-film solid-phase reactions.^{1,2,3} Silicon technology has given the media and the impetus for the investigation. Silicide forming systems are generally well-behaved with uniform layers formed with single phases having clearly defined boundaries.

The reaction between silicon and metal can be broken down into three categories:⁴ near-noble, refractory and rare-earth metal silicides with the silicides in each category following distinct patterns. The near-noble metals (M) react at low temperatures forming M_2Si as the initial phase and have high barrier heights on n-type silicon. The refractory metals form the disilicide as the initial phase at high temperatures ($T \sim 600^\circ C$) and have medium barrier heights on n-type silicon. The rare earth metals also form the disilicide first at low temperatures ($T \sim 200-300^\circ C$) but have the lowest barrier heights on n-type silicon.

There have been investigations of reactions of Si with binary alloys of near noble and refractory metals,⁵⁻⁸ rare-earth and refractory metals,⁹ and rare-earth and near noble metals. In the first two cases the initial reaction is phase separation and the silicide formed is determined by the species with the lowest formation temperature. For example, an alloy of PdV reacts to form Pd_2Si at the Si/alloy interface.⁸ In these cases the kinetics of metal-silicon reactions determine the formation of the initial phases. In the third case, the trend of the initial phase formation is unclear since both rare-earth and near noble metals have similar silicide formation temperatures.^{1,4,10,11} In addition the rare-earth and near-noble metals react strongly with each other forming intermetallic phases¹² at a temperature which is comparable to their initial silicide formation temperatures. However, the large difference in barrier heights between rare-earth/silicon and near-noble/silicon structures provides

a sensitive identification method for determining the presence of either silicide at the silicon-alloy interface.

We have chosen to investigate Pd-Er as a representative system. Furthermore codeposited Pd-Er alloys are amorphous. Therefore upon annealing on silicon, two competitive reactions occur: interfacial reaction with silicide formation and crystallization of intermetallic Er-Pd compound phases. With this in mind we have used *in situ* resistivity measurements to characterize the crystallization and the initial interfacial reaction. In addition we have used the standard array of techniques (x-ray diffraction, Rutherford backscattering, and Auger electron spectroscopy) to determine the thickness and structure of the initial phases.

II. Experimental

The samples were prepared by electron-beam codeposition in a 10^{-7} torr vacuum at $10\text{\AA}/\text{sec}$ deposition rate. The thicknesses of the film were around 1000\AA and three different concentrations $\text{Pd}_{65}\text{Er}_{35}$, $\text{Pd}_{45}\text{Er}_{55}$, $\text{Pd}_{15}\text{Er}_{85}$ have been prepared. The substrates were Si wafers, n and p-type, $10\Omega\text{-cm}$. Some of the wafers were blank for metallurgical analysis and some had diodes with diameters ranging from 12 to $400\mu\text{m}$. The diodes were obtained by opening holes on 4000\AA thermally grown SiO_2 layer. Alloys were also deposited on SiO_2 for monitoring their crystallization without interfacial reaction. In addition, bilayers of Pd-Er on SiO_2 were prepared for intermetallic compound formation. The samples were annealed up to 650°C in a purified He furnace. To prevent the oxidation of the rare earth an etched polished silicon blank was placed on the alloy sample in close contact with the sample surface during the annealing. As a further precaution, Ti sponge was placed in the near vicinity. Subsequent analysis showed that oxidation was minimal.

In situ resistivity measurements were made with four, spring-loaded, tungsten probes in contact with the sample. The sample surface between the probes was covered with a silicon blank and in some cases Ti sponge was near by in the flowing helium ambient. When these precautions were not taken oxidation occurred and the resistivity showed a strong increase after the initial drop.

The reaction products were mainly analyzed with MeV $^4\text{He}^+$ backscattering and Seeman Bohlin x-ray diffraction techniques. Pd-Er forms seven intermetallic compounds^{12,13}; for four of them the lattice parameters and structure are known. One ternary $\text{Pd}_2\text{Er}_1\text{Si}_2$ has been identified.¹⁴ The stopping cross section for Er is unknown and an extrapolation was used in backscattering analysis.. This extrapolation may lead to a systematic error in our listed values of thicknesses and to a lesser-extent in the composition values. I-V characteristics both on n and p-type material were used to measure the apparent barrier heights and hence to investigate the initial stage of the reaction. Norde plots¹⁵ and extrapolation to zero voltage of a $1/n I$ vs. V plot were used in order to evaluate the Schottky barrier values.

Auger electron spectroscopy combined with an Ar sputter was used to verify the cleanliness and absence of contaminants at the alloy-silicon interface.

III. Results

A. Overview

The results are summarized in Fig. 1. The initial stages of the reaction on silicon are mainly driven, at low temperatures (~350 to 400°C), by the formation of the Er-Pd intermetallic compound: the compound having the composition closest to the original alloy tends to form and the excess of material is depleted from the alloy to react with silicon forming a silicide. It is

possible to have three different cases: no reaction with silicon, formation of ErSi_2 or of Pd_2Si . For the Pd-Er bilayer on SiO_2 the intermetallic compound PdEr is formed at 250°C , a temperature well below that at which silicide formation occurs at the alloy-silicon interfaces.

The annealing at 350°C of the $\text{Pd}_{45}\text{Er}_{55}$ alloy produces the crystallization of the PdEr phase which has a composition almost identical to the starting alloy film. At higher temperatures a ternary silicide is formed.

In the case of $\text{Pd}_{15}\text{Er}_{85}$ alloy the compound Pd_2Er_5 is the closest to that of the as-deposited alloy. The excess of Er reacts with silicon forming a layer of ErSi_2 on the silicon wafer. Similar behavior has been observed in the $\text{Pd}_{65}\text{Er}_{35}$ alloy. Now Pd is the excess specie and Pd_2Si forms at the interface between the alloy and silicon. At 650°C , a strong intermixing among Pd, Er and Si is found for the three alloy compositions.

B. Backscattering Spectrometry

Figures 2(a) and (b) show the backscattering spectra of the sample $\text{Pd}_{65}\text{Er}_{35}$ as deposited and after annealing at 350°C for 1 hour and 450°C for 1 hour. The heights of the Pd and Er signals in the spectrum for the sample as deposited indicates a Pd to Er concentration of 65 to 35; the energy widths suggests that the layer is 1000\AA thick. After the 350°C annealing the silicon signal presents a change toward higher energy and the Pd signal develops a change in the low energy side indicating that some reaction has occurred. These changes together with an increase in height of the Er signal in the backscattering spectra are consistent with the formation of a very thin Pd_2Si layer at the silicon-alloy interface and the formation of a layer at the surface having a composition of $\text{Pd}_{60}\text{Er}_{40}$. Annealing at 450°C for 1 hour leads to the formation of a layer having a nonuniform composition with an average

value of about $\text{Pd}_{40}\text{Er}_{25}\text{Si}_{35}$ interposed between the inner Pd_2Si and the outer $\text{Pd}_{60}\text{Er}_{40}$ layer.

The formation of Er silicide at the silicon-Er rich alloy interface is shown in Fig. 3a and b. Figure 3a shows the spectrum for a $\text{Pd}_{15}\text{Er}_{85}$ sample annealed at 350°C for 1 hour. The Pd signal is shifted toward the surface away from the interface. The Er signal broadens inward and the Er-Si height ratio at the interface is close to that of ErSi_2 . The composition of the outer layer is between that of $\text{Pd}_{20}\text{Er}_{80}$ and $\text{Pd}_{30}\text{Er}_{70}$. Subsequent annealing at 450°C for 1 hour produces (Fig. 3b) an increase in the thickness of the Er-silicide layer. The composition of the layer is not uniform with the Er distribution representing an average value of ErSi_2 and with the Pd distribution graded down from the surface. Some Pd has penetrated into the ErSi_2 .

The intermediate alloy $\text{Pd}_{45}\text{Er}_{55}$, Fig. 4, shows only a small reaction with silicon at 450°C for 1 hour. The reaction is so limited that we cannot rely upon backscattering to identify the interfacial composition. The composition of the outer layer is $\text{Pd}_{50}\text{Er}_{50}$.

Annealing at 650°C produces in all three alloy compositions a strong intermixing between Pd, Er and Si. In the case of $\text{Pd}_{65}\text{Er}_{35}$, Fig. 5a, the reacted layer is uniform and has a composition very close to that of $\text{Pd}_{40}\text{Er}_{20}\text{Si}_{40}$. The composition shown in the schematic in Fig. 5a represents the best fit by computer simulation. This composition corresponds to that of the ternary $\text{Pd}_2\text{Er}_1\text{Si}_2$. The other cases show the presence of two well defined layers with different compositions of Pd, Er and Si. An example is shown in Fig. 5b for the Er rich case. The step in the Pd signal is clearly visible in the spectrum.

C. X-ray Diffraction

The analysis of the x-ray diffraction spectra based on the structures available, allows us to identify ErSi_2 , Pd_2Si , four Er-Pd compounds of the seven possible¹² and one ternary, $\text{Pd}_2\text{Er}_1\text{Si}_2$.¹⁴ Fig. 6 shows the x-ray diffraction spectra of the three samples as deposited. The broad peaks show the amorphous nature of the films.

Annealing at 350°C for 1 hour produces the crystallization of the Pd-rich and Er-rich alloys as well as the formation of Pd_2Si and ErSi_2 , Fig. 7. The peaks have been identified on the basis of the crystalline structures of the various compounds as given in Ref. 12. In the almost 50-50 Pd Er alloy the annealing produces the formation of the PdEr compound, Fig. 7b. For the Er-rich alloy nearly all the peaks can be identified and show the presence of ErSi_2 and Pd_2Er_5 . Three of the peaks given in Fig. 7a for the Pd-rich alloy are identified with Pd_2Si and the rest cannot be identified; we believe that these belong to either Pd_3Er_2 or Pd_5Er_4 which have been reported as compounds but their structures are unknown. This belief is based on the backscattering spectra and on the fact that the peaks cannot be attributed to PdEr or to Pd_3Er . The annealing at 450°C for 1 hr. enhances the formation of Pd_2Si and ErSi_2 in the richest Pd and Er alloys.

The annealing at 650°C produces, at least in the case of $\text{Pd}_{65}\text{Er}_{35}$, a compound which has been identified as a ternary.¹⁴ Nearly all the peaks in Fig. 8 correspond to the ternary $\text{Pd}_2\text{Er}_1\text{Si}_2$. In the other two cases the peaks cannot be attributed to any known Pd, Er, Si, O compound. If ternaries are formed their structures are not known. Moreover, the analysis is even more complicated since the backscattering data suggests the presence of two well defined layers, both contributing to the x-ray diffraction.

D. Bilayer Results

Backscattering measurements on Pd-Er bilayers deposited on SiO_2 indicated that the reaction between Pd and Er starts around 250°C . By increasing either the time or the temperature the reaction proceeds with the formation of a single intermetallic compound PdEr. Fig. 9a and b shows the x-ray diffraction spectra for the as-deposited and annealed sample. In the as-deposited case the Pd and Er are polycrystalline. After the sample was annealed at 250°C for 5 hours PdEr is clearly identified in the x-ray diffraction spectra. The unlabelled lines in Fig. 9b correspond to unreacted Pd and Er.

E. Barrier Height Measurements

The values, in eV, of the barrier heights, measured at room temperature, are summarized in Table 1. The data have been obtained from I-V characteristics and have been analyzed using two different methods. Extrapolation to zero voltage was used in almost all cases. In cases where the ideality factor was greater than 1.1, Norde plot analyses¹⁵ were used to measure the barrier height value. Where the I-V characteristics allowed comparison of barrier height values, both methods give the same results. The major source of error is the scattering of the experimental data due mainly to the presence of a high series resistance. The error in the worse case is around 0.05eV. The data for Pd (and Er) rich alloys show that annealing at 400°C or 450°C produces the formation of Pd_2Si (or ErSi_2) at the original silicon-alloy interface. The barrier height approaches very closely the values expected for pure ErSi_2 and Pd_2Si . The 50-50 alloy does not segregate Er or Pd and this is reflected in the barrier height values which remain almost constant at around 0.55eV. Further annealing at 650°C produces a strong intermixing and the barrier height reaches a final value. The sum of barrier height values taken on n and p type silicon is very close to 1.1eV supporting the idea of an almost uniform coverage of the silicon surface. Moreover the data of 650°C on n-type silicon plotted as a function of Pd atomic concentration, Fig. 10, show a linear variation between the Pd_2Si and ErSi_2 values suggesting again the presence of

a layer having a uniform ternary composition. A nonuniform composition consisting of patches of ErSi_2 and Pd_2Si should behave similarly to the solid curve indicated for discrete parallel diodes.^{16,17}

E. Electrical Resistivity

Four-point probe measurements have been used on alloys deposited either on Si or on SiO_2 substrates to investigate the effect of the amorphous-crystalline transition on the silicon-alloy interaction. Two kinds of *in-situ* measurements have been performed: as a function of temperature at a constant rate of heating or as a function of time at fixed temperature. For alloys deposited on Si, to correct for the contribution from the silicon substrate, measurements have been performed at constant temperature as a function of time.

In Fig. 11 the resistivity annealing curves for the three alloys are shown; the substrate is SiO_2 in all cases. The samples were annealed at a constant rate of heating at about $3\text{-}4^\circ\text{C}/\text{min}$. The resistivity values have been normalized to the room temperature values of 200 to $300\ \mu\ \Omega\text{-cm}$. The resistivity of the sample $\text{Pd}_{45}\text{Er}_{55}$ shows a slight drop in the early stage of annealing. At temperatures around 220°C after a small increase the resistivity drops precipitously. The recrystallization phenomenon is responsible for the decrease in resistivity as indicated by x-ray diffraction. The alloy $\text{Pd}_{65}\text{Er}_{35}$ follows substantially the same path with the major difference being the recrystallization temperature ($\sim 410^\circ\text{C}$). The compound $\text{Pd}_{15}\text{Er}_{85}$ has two steps of recrystallization. The first decrease occurs at a very low temperature (100°C) where the resistivity drops to 0.6 of the room temperature value. Subsequently at a high temperature, $\sim 400^\circ\text{C}$, another decrease occurs. After the first drop in resistivity, the sample is no longer completely amorphous. After the second drop the x-ray diffraction pattern changes relative to the previous one suggesting that a new compound is formed. Silicide formation occurs around

300°C; consequently only the crystallization around 100°C can affect the kinetic path for Si-alloy interaction.

The resistivity values when the alloy is deposited on silicon and on SiO_2 are compared in Figure 12 with the values normalized to room temperature values. The annealing was carried out at constant temperature at 386°C and the variations in relative values are due mainly to recrystallization of the alloy. For the Pd rich alloy which has a recrystallization temperature around 400°C the presence of the silicon strongly enhances the crystallization process. The Er rich case, after the first drop in resistivity, follows the same path as for the Pd rich case. In Fig. 12 we show only the initial stages of the reaction. For long time anneals the resistivity values approach the same value on both Si and SiO_2 . This shows that the decrease in resistivity is due to the recrystallization and not to the formation of silicide. We attribute the difference between the behavior on Si and SiO_2 substrates to the depletion of Pd or Er from the amorphous layer. This depletion modifies the stability of the amorphous layer and lead to an early crystallization as measured by x-ray diffraction.

In Fig. 13, the resistivity changes as a function of annealing time at 386°C for the $\text{Pd}_{45}\text{Er}_{55}$ alloy on SiO_2 or on Si are presented. The $\text{Pd}_{45}\text{Er}_{55}$ alloy crystallizes at very low temperatures, so the depletion action with consequent instability of the amorphous layer does not take place.

IV. Discussion

Backscattering, x-ray diffraction and barrier height measurements give a consistent picture for the behavior of the Pd-Er alloys. The Er rich alloy forms ErSi_2 as the initial reaction at the silicon-alloy interface, the Pd rich alloy forms Pd_2Si at the silicon-alloy interface and the nearly 50/50 Er-Pd alloy reacts primarily to form the intermetallic PdEr. The PdEr intermetallic

is stable on silicon at temperatures around 400°C where silicides are formed from the Pd- and Er-rich alloys.

The *in situ* measurements of the resistivity show clearly the stages in the recrystallization behavior. For the alloys on SiO₂ the resistivity data obtained by increasing the annealing temperature at a constant rate show that the Pd₄₅Er₅₅ recrystallization starts at low temperature and is complete at 300°C. The other two alloys have a full recrystallization at higher temperatures. The recrystallization of the Pd₄₅Er₅₅ alloy is approximately the same for the alloy on silicon and on SiO₂ showing that the presence of silicon does not affect the recrystallization process. In contrast to this, for the Pd and Er rich alloys the samples on silicon substrates recrystallize faster than those on SiO₂ substrates. In Table II, we summarize the substrate effects on the crystallization temperature of amorphous Pd-Er alloys.

We propose that the explanation for the behavior is based upon the diagram shown in Fig. 14. The near 50/50 Pd-Er data are interpreted as crystallization of the intermetallic compound from an amorphous matrix with nearly the composition of the intermetallic phase. In other words, no phase separation is required in the crystallization. Once crystallized the intermetallic compound is very stable and relatively high temperatures are necessary to decompose it and to form silicides. The stability of the PdEr compound is also suggested by the Pd/Er bilayer experiment where the compound PdEr is formed after annealing at temperatures as low as 250°C.

In the Er and Pd rich cases the amorphous layer is more stable on SiO₂ than on Si. The recrystallization of these amorphous alloys proceeds by phase separation and the Si serves as a sink for the excess Er and Pd. Therefore, the presence of silicon causes the depletion of Er or Pd from the original alloy driving the alloy composition toward a stoichiometric compound. This process apparently decreases the crystallization temperature of the amorphous alloy.

A similar situation showing an enhanced crystallization of amorphous $\text{Pd}_{80}\text{Si}_{20}$ on Si has been observed.¹⁸ The effect of non-reactive vs. reactive substrates on the crystallization behavior of amorphous alloys is interesting. A more detailed study will be required in order to understand the driving force and kinetic processes involved.

We believe that reaction kinetics rather than free-energies determine phase formation in the Pd-Er system. By assuming that the free energy of formation of the various compounds are proportional to their melting point, we expect to find that ErPd_3 (1710°C) which is the most stable compound. However the compound ErPd_3 has never been found in this work. This point is clearly illustrated by the reaction between $\text{Pd}_{65}\text{Er}_{35}$ with Si. Energetically, it is more favorable to form ErSi_2 and ErPd_3 ; instead the reaction produces Pd_2Si and Pd_3Er_2 as shown in Fig. 1. Furthermore, in the bilayer case, ErPd rather than ErPd_3 is formed in the initial stages of the reaction. These results show again that the sequences in compound formation can be affected by the free energy of the various compounds but the controlling factor is the reaction kinetics. The same conclusion has been reached studying the sequence of formation in various binary couples.^{19,20}

V. Conclusion

In conclusion we have found that the segregation of Pd or Er silicide at the alloy-silicon interface depends upon the composition of the as-deposited alloy. This result, in which the identity of silicide depends upon the alloy composition, differs from that of the near noble-refractory alloys in which the near noble metal segregates irrespective of alloy composition. The Pd-Er results suggest that the controlling force for the alloy-Si interaction includes the metal-metal interaction as well as the metal-silicon reactions.

We believe that the same pattern will hold for other rare earth-near noble metal alloys. The codeposition of such alloys results in the formation of an amorphous layer. The kinetic competition between recrystallization of the alloy and the alloy-silicon interaction will depend on the alloy composition and annealing temperature.

Acknowledgments

We acknowledge the assistance of the IBM Central Scientific Services Laboratory (J. Cuomo) for sample preparation and S. Valeri (at Modena University) for the Auger Analysis. One of us (J.W. Mayer) acknowledges partial support by NSF through the National Research and Resource Facility for Submicron Structures at Cornell University, and S.S. Lau acknowledges partial support by DARPA (S. Roosild).

Table I.

Schottky barrier height of Pd-Er alloy on n-Si (ϕ_{Bn}) and on p-Si (ϕ_{Bp}) after anneals. (ϕ_{Bn} of Pd₂Si and ErSi₂ are 0.75 and 0.38eV, respectively).

	400°C		450°C		650°C	
	ϕ_{Bn}	ϕ_{Bp}	ϕ_{Bn}	ϕ_{Bp}	ϕ_{Bn}	ϕ_{Bp}
Pd ₆₅ Er ₃₅	0.65	0.50	0.70	0.40	0.60	0.50
Pd ₄₅ Er ₅₅	0.54	0.60	0.50	0.58	0.50	0.55
Pd ₁₅ Er ₈₅	0.40	0.70	0.40	0.65	0.40	0.70

TABLE II

Effect of Substrate on the Crystallization
Temperature of Pd-Er Alloys

alloy Substrate	Pd ₆₅ Er ₃₅	Pd ₅₅ Er ₄₅	Pd ₁₅ Er ₈₅
Si	<350°C	220°C	<350°C
SiO ₂	410°C	220°C	100°C, 400°C

References

1. K.N. Tu and J.W. Mayer in "Thin Films - Interdiffusion and Reactions", edited by J.M. Poate, K.N. Tu and J.W. Mayer, Wiley, New York, (1978) p. 359.
2. G. Ottaviani and J.W. Mayer, Chapter 2 in "Reliability and Degradation", edited by M.J. Howes, D.V. Morgan, John Wiley and Sons, New York (1981) p.105.
3. S.P. Murarka, *J. Vacuum Sci. Technol.* **17**, 775 (1980).
4. R.D. Thompson and K.N. Tu, "Thin Solid Films, **53**, 4372 (1982).
5. G. Ottaviani, K.N. Tu, J.W. Mayer and B.Y. Tsaur, *Appl. Phys. Lett.* **36**, 331 (1980).
6. K.N. Tu, *J. Vac. Sci. Technol.* **19**, 725, (1980).
7. K.N. Tu, W.N. Hammer and J.O. Olowolafe, *J. Appl. Phys.* **51**, 1663 (1980).
8. J.W. Mayer, S.S. Lau and K.N. Tu, *J. Appl. Phys.* **50**, 5855 (1979).
9. R. Thompson, M. Eizenberg and K.N. Tu, *J. Appl. Phys.* **52**, 6763 (1981).
10. K.N. Tu, R.D. Thompson and B.Y. Tsaur, *Appl. Phys. Letts.* **38**, 626 (1981).
11. J.E.E. Baglin, F.M. d'Heurle and C.S. Petersson, *J. Appl. Phys.* **52**, 2841 (1981).
12. O. Loebich, Jr. and E. Raub, *J. Less - Common Metals* **30**, 47 (1973).

13. W.G. Moffatt, "The Handbook of Binary Phase Diagrams", G.E. Company, Schenectady, N.Y. (1981).
14. X-ray Powder Data File, JCPDS card no. 31-503.
15. H. Norde, J. Appl. Phys. 50, 5052 (1979).
16. I. Ohdomari and K.N. Tu, J. Appl. Phys. 51, 3735 (1980).
17. R.D. Thompson and K.N. Tu, J. Appl. Phys. 53, 4285 (1982).
18. S. Kritzing and K.N. Tu, Proceedings of 7th European Congress on Electron Microscopy, Vol. 1, 356 (1980).
19. K.N. Tu, G. Ottaviani, R.D. Thompson and J.W. Mayer, J. Appl. Phys. 53, 4285 (1982).
20. G. Majni, C. Nobili, G. Ottaviani, M. Costato and E. Galli, J. Appl. Phys. 52, 4047 (1981).

Figure Captions

- Fig. 1. Schematic diagram showing the initial phases of the reaction between silicon and Pd-Er alloys. The alloys have three different compositions and as deposited are amorphous. The layer thickness is given in angstroms.
- Fig. 2. Backscattering spectra of the alloy $\text{Pd}_{65}\text{Er}_{35}$ film as deposited and after annealing at 350°C (a) and 450°C (b) for 1 hour. At 350°C Pd segregates from the alloy and forms Pd_2Si at the Si- $\text{Pd}_{65}\text{Er}_{35}$ interface.
- Fig. 3. Backscattering spectra of the alloy $\text{Pd}_{15}\text{Er}_{85}$ film on silicon as-deposited and after annealing at 350°C (a) and 450°C (b) for 1 hour. At 350°C Er segregates from the alloy and forms ErSi_2 compound at the original Si- $\text{Pd}_{15}\text{Er}_{85}$ interface.
- Fig. 4. Backscattering spectra of the alloy $\text{Pd}_{45}\text{Er}_{55}$ film on silicon as-deposited and after annealing at 450°C for 1 hour. Both Pd and Er are segregated from the original alloy and react with silicon forming silicides.
- Fig. 5. Backscattering spectra of the alloys $\text{Pd}_{65}\text{Er}_{35}$ (a) and $\text{Pd}_{15}\text{Er}_{85}$ (b) films on silicon as-deposited and after annealing at 650°C 1 hour. The high temperature annealing produces a uniform ternary silicide for the $\text{Pd}_{65}\text{Er}_{35}$ alloy film. In the other case two layers are formed.
- Fig. 6. X-ray diffraction spectra of the three alloys films as-deposited. The broad peaks reveal the amorphous nature of the deposited films.

- Fig. 7. X-ray diffraction spectra of the three alloy films deposited on silicon after annealing at 350°C for 1 hour.
- Fig. 8. X-ray diffraction of the alloy film $\text{Pd}_{65}\text{Er}_{35}$ after annealing at 650°C for 1 hour. Most of the peaks are identified as reflections of the Pd_2ErSi_2 ternary compound.
- Fig. 9. X-ray diffraction spectra obtained from a Pd-Er bilayer as deposited; (a) and after annealing at 250°C for 5 hours (b). The scale in (b) has been magnified in order to show the weak reflections.
- Fig. 10. Schottky barrier height measured on n-type silicon after annealing at 650°C for 1 hour as a function of the Pd concentration near the Si surface. The Pd concentration has been measured by the backscattering spectra. The continuous line is the apparent value of the Schottky barrier calculated using the model of discrete parallel diode (See Ref. 16). The Schottky barrier heights of Pd_2Si and ErSi_2 are 0.74eV and 0.38eV, respectively.
- Fig. 11. Resistivity values as a function of the temperature obtained by increasing the temperature at a constant rate of 3-5°C/min. The resistivity values has been normalized to their room temperature values. The three curves refer to the three alloys considered. The change in resistivity is due to the crystallization process.
- Fig. 12. Resistivity values as a function of time at 386°C obtained in the two alloys, $\text{Pd}_{65}\text{Er}_{35}$ and $\text{Pd}_{15}\text{Er}_{85}$, deposited on Si and on SiO_2 . The change in resistivity is due to the crystallization process.
- Fig. 13. Resistivity values as a function of time at 386°C in the $\text{Pd}_{45}\text{Er}_{55}$ alloy deposited on Si and on SiO_2 .

Fig. 14. Schematic diagram showing the kinetic path followed by the three Pd-Er alloys during their crystallization and silicide formation.

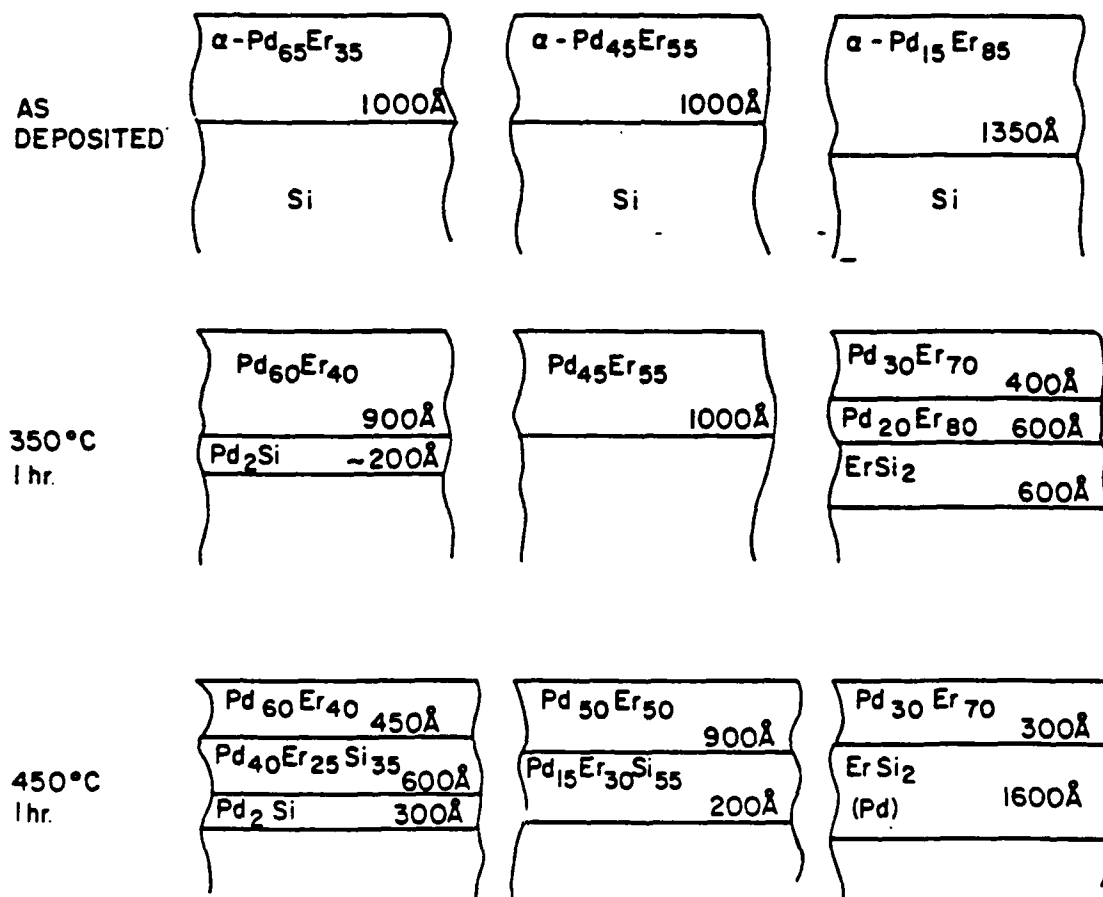
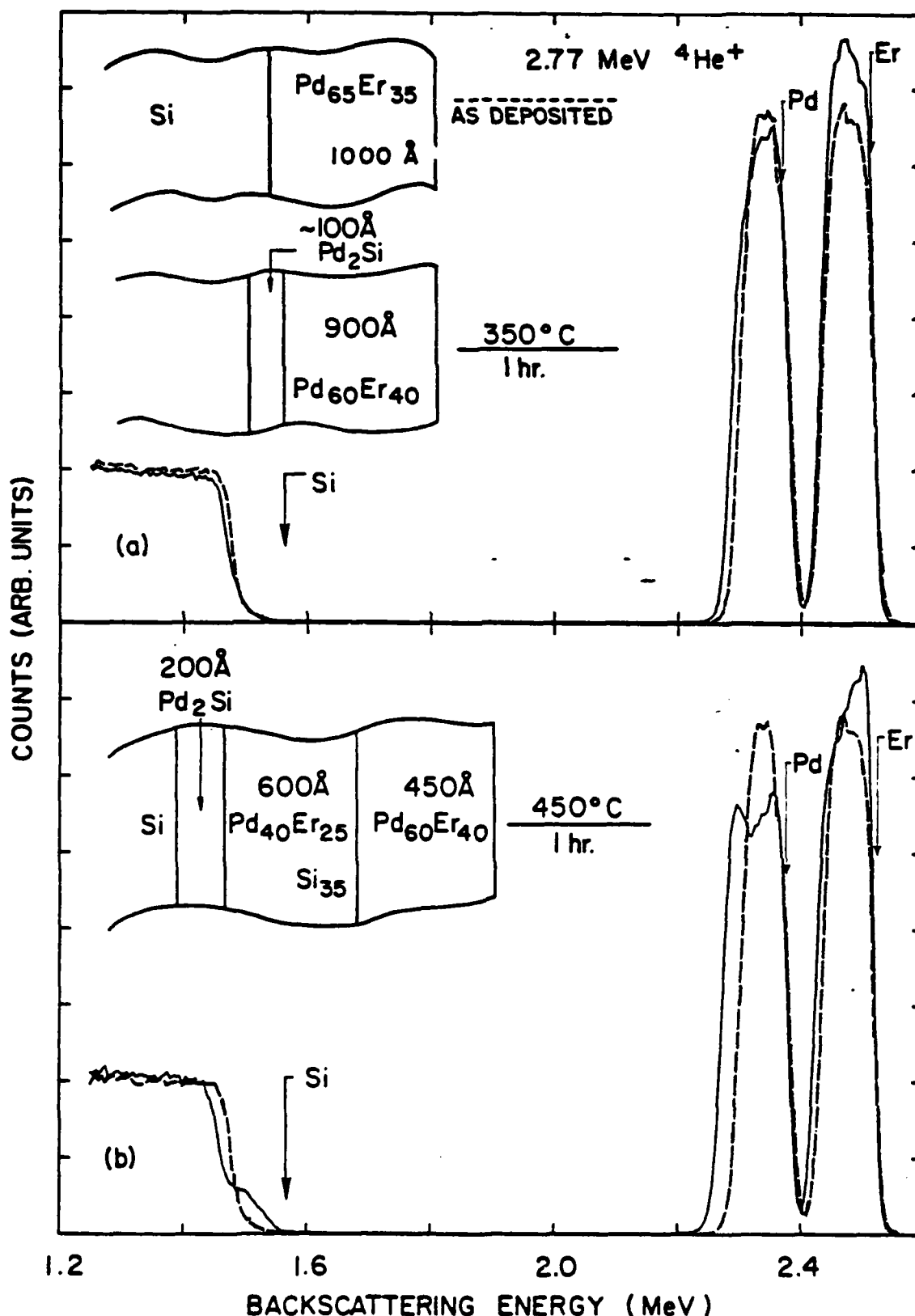
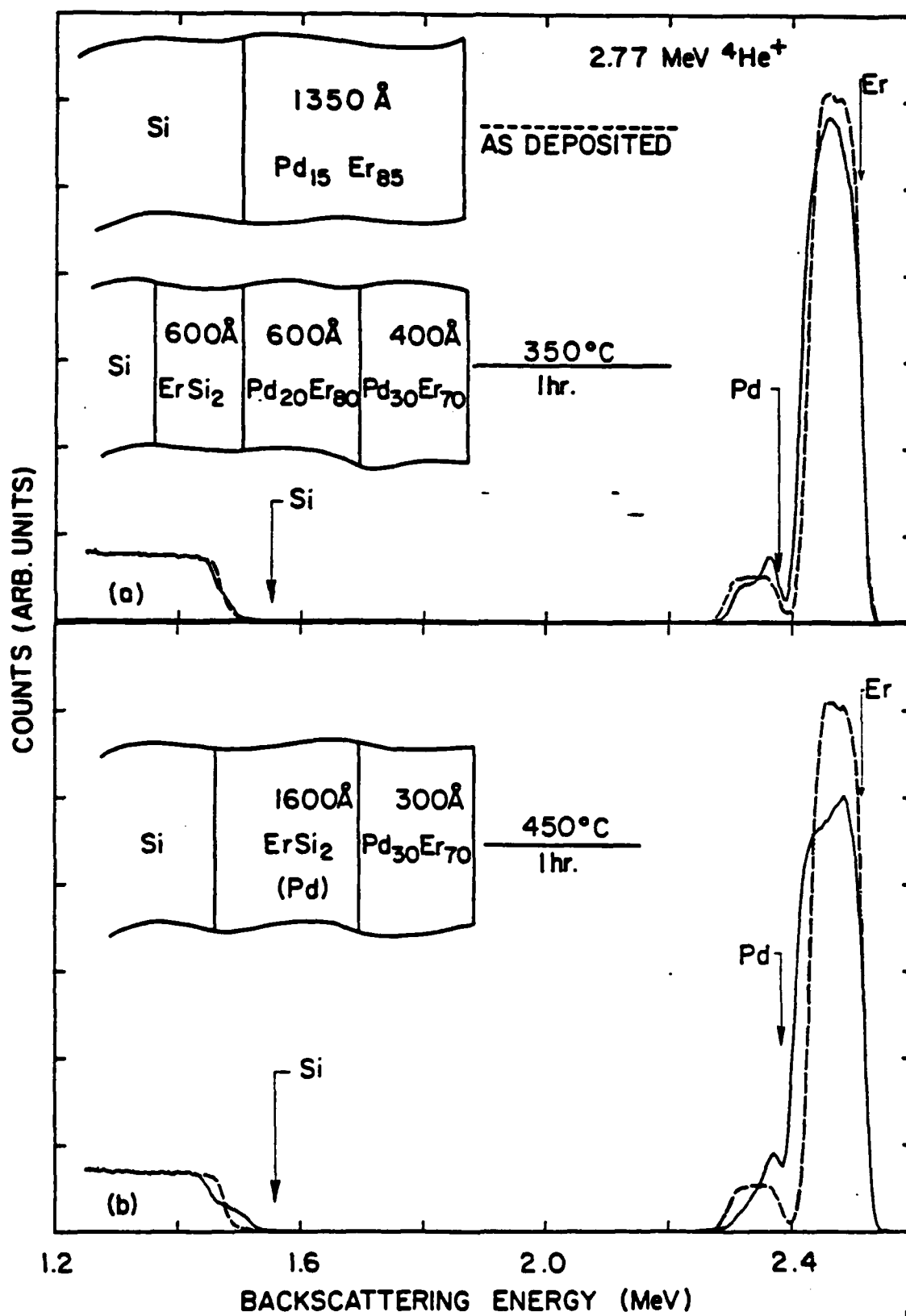


Fig. 1





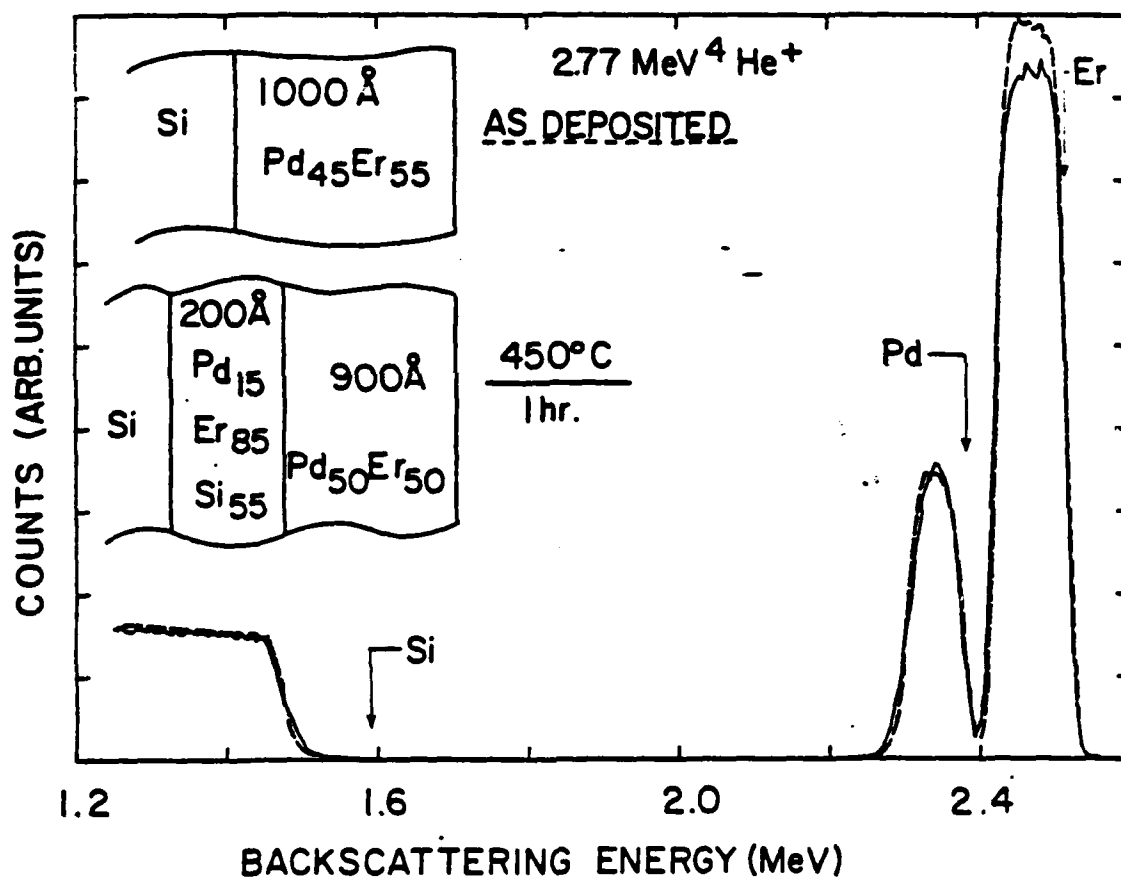
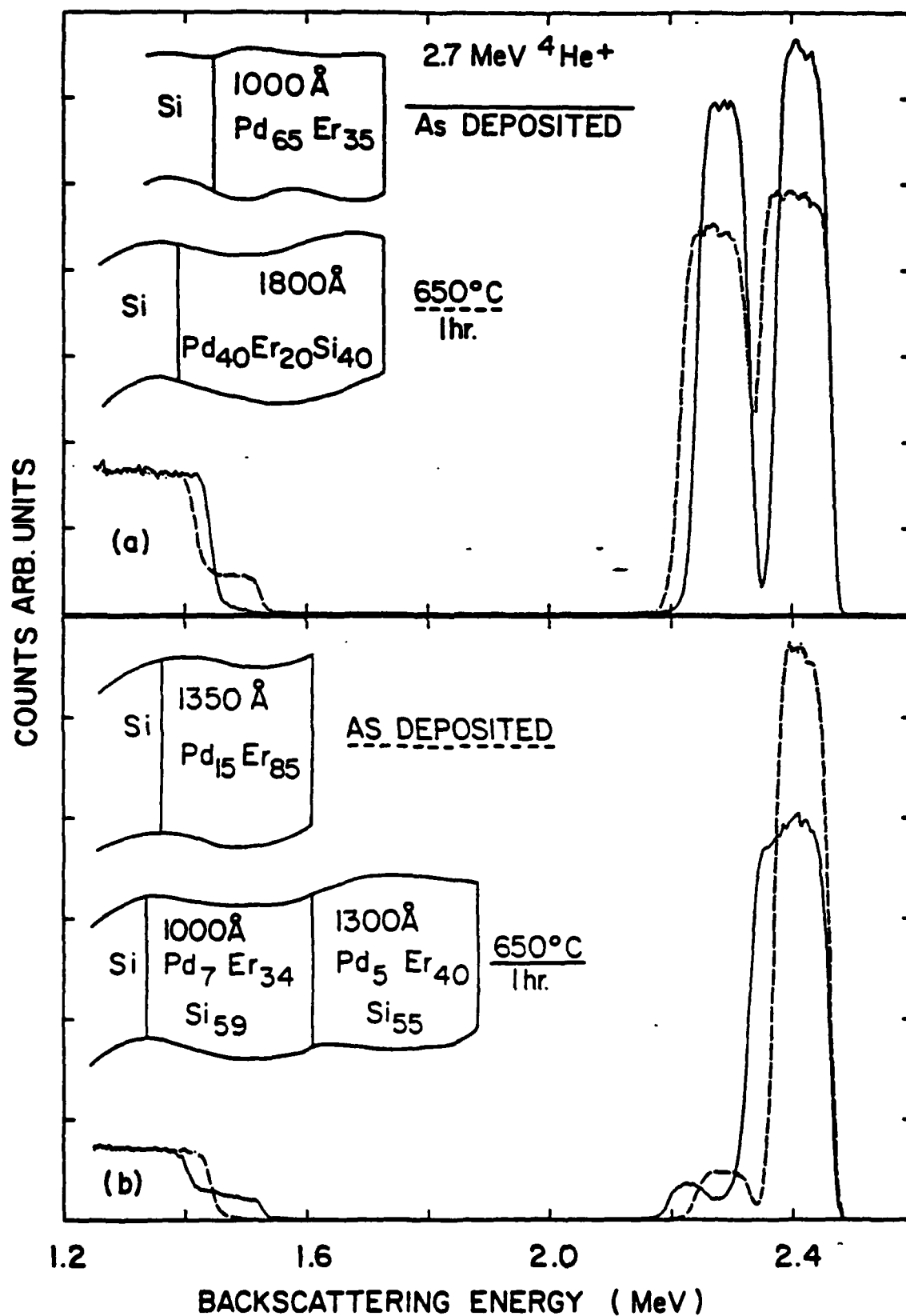
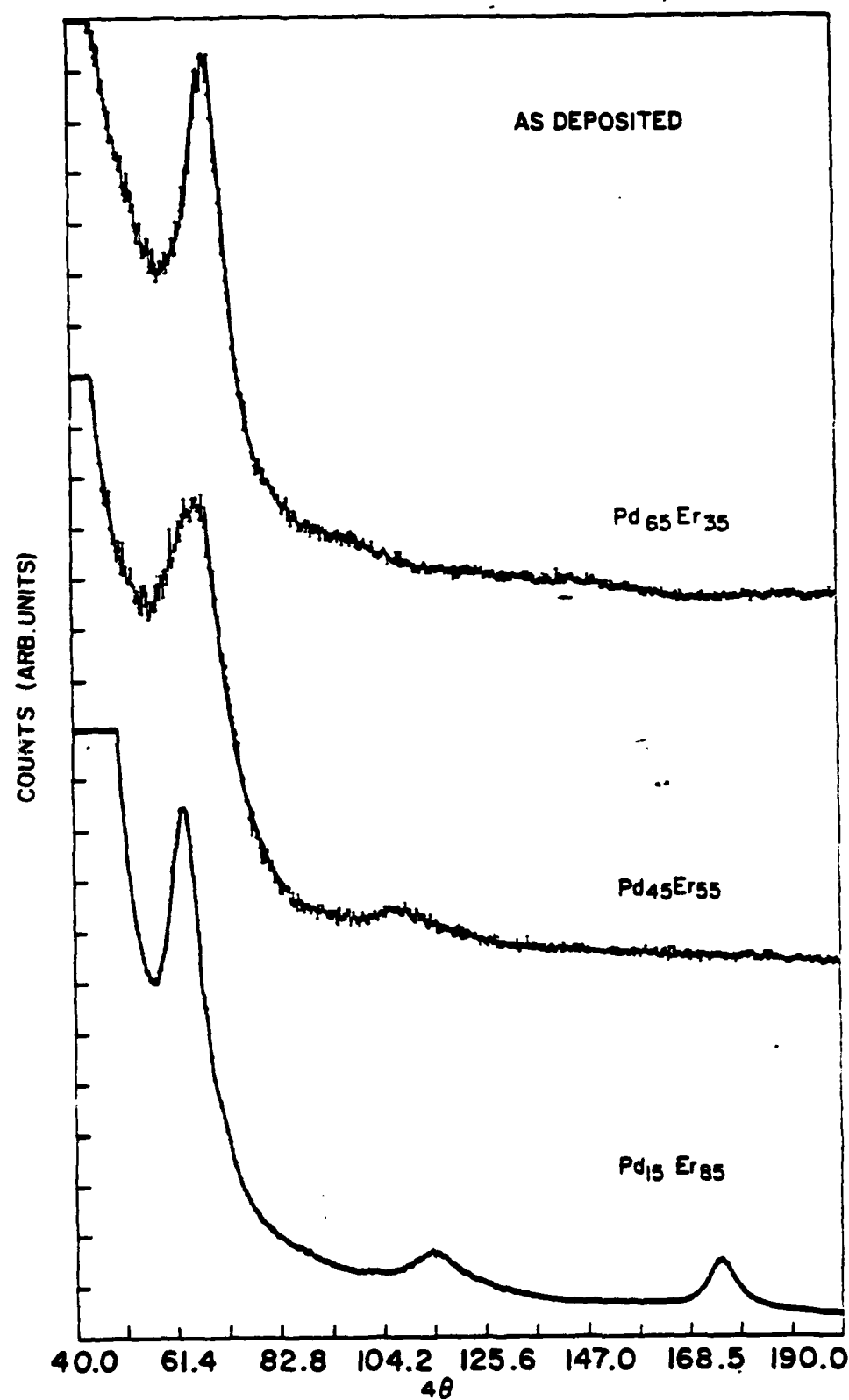
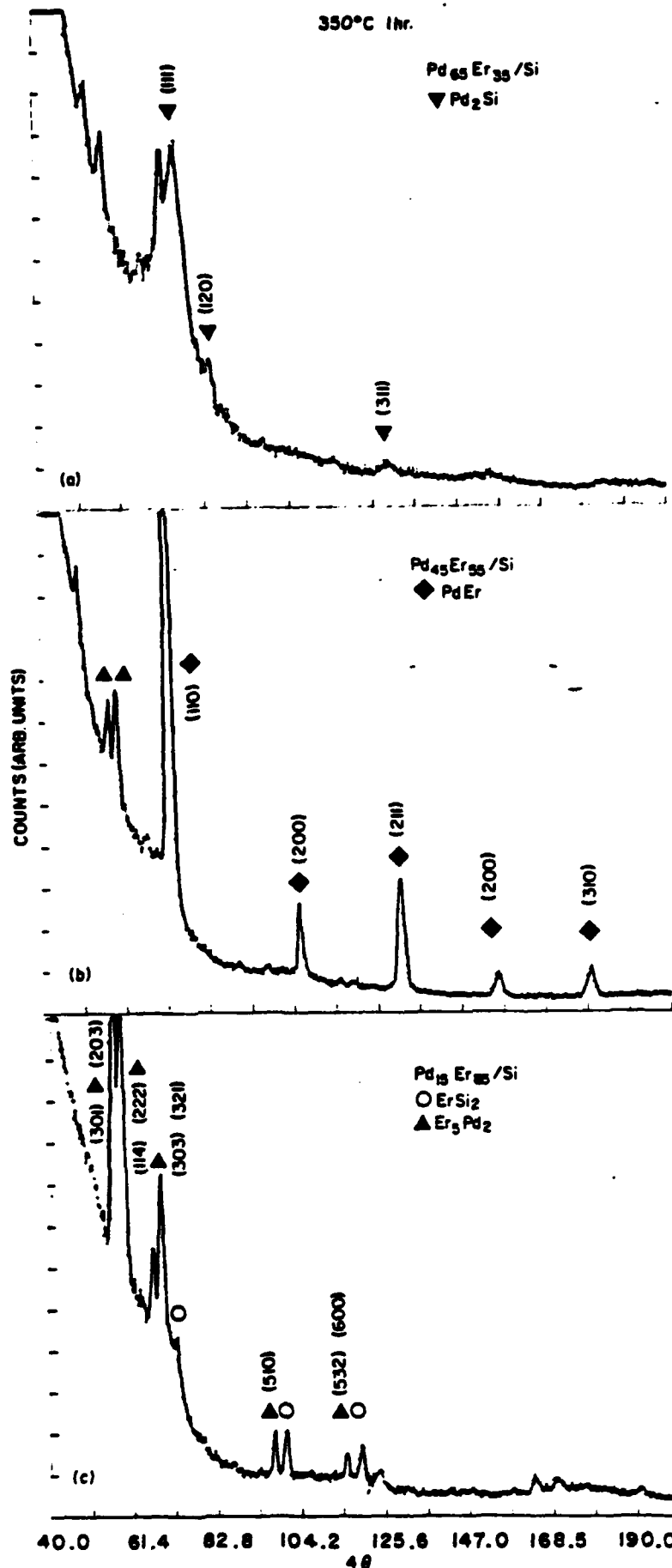
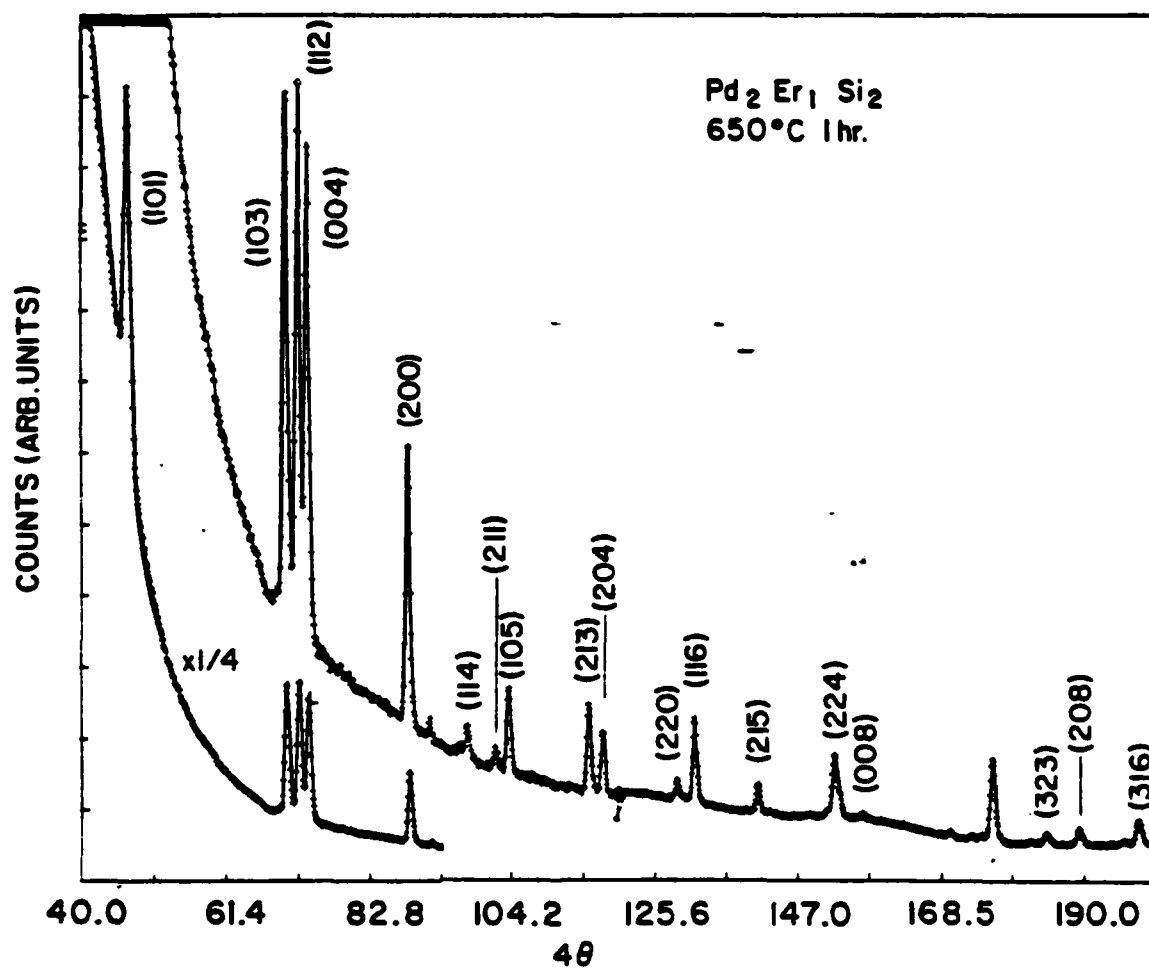


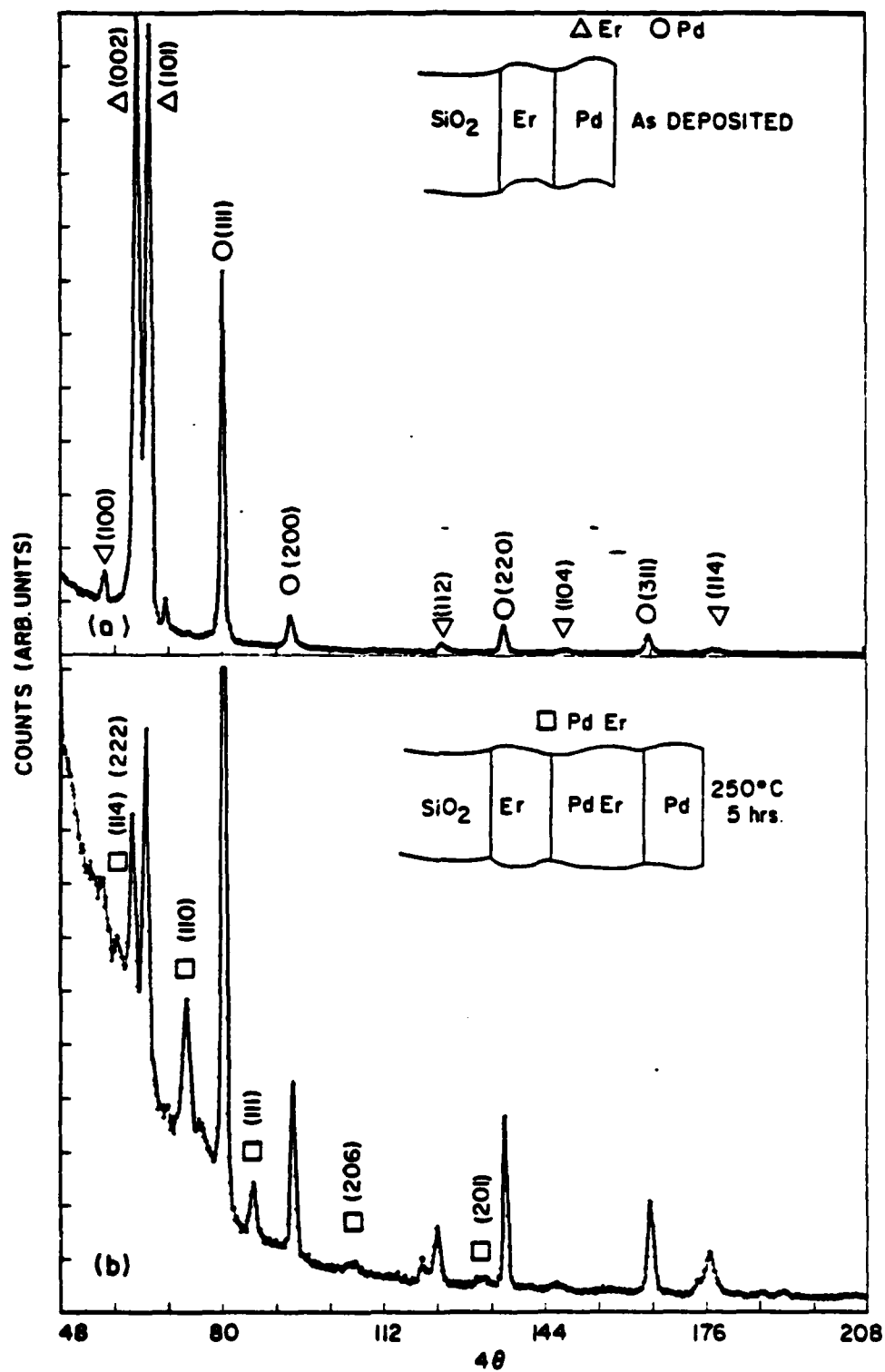
Fig. 4











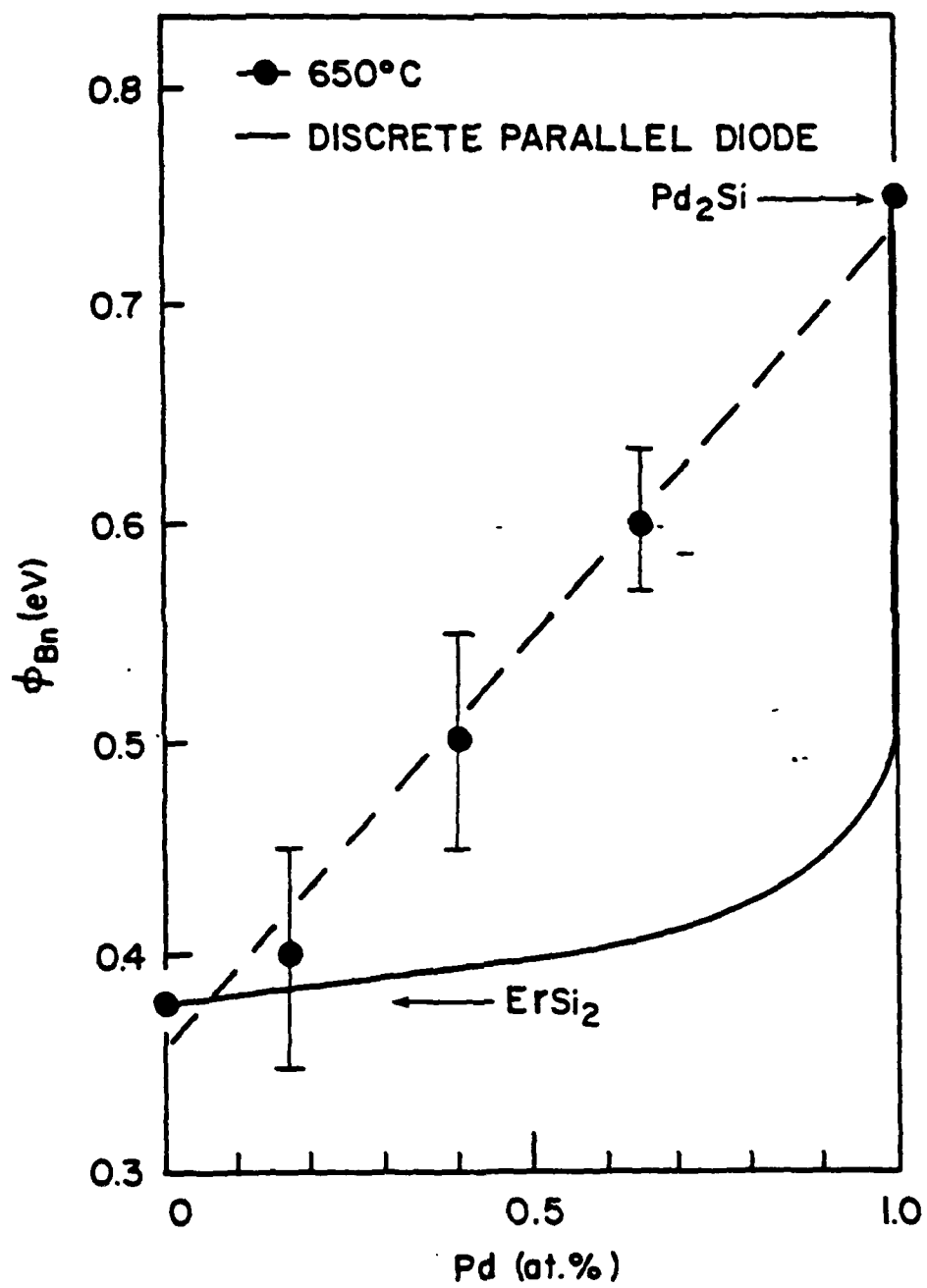


Fig. 10

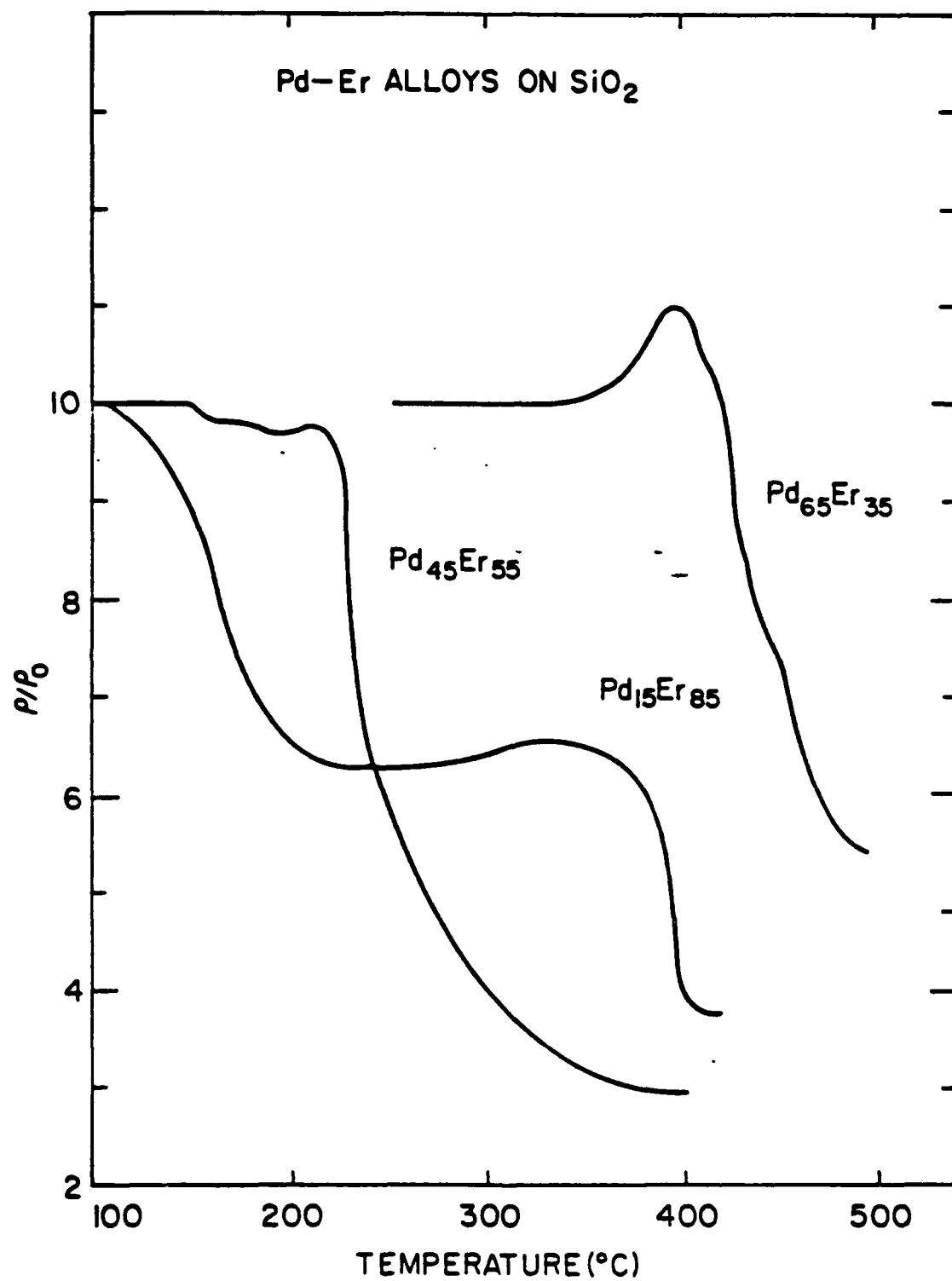


Fig. 11

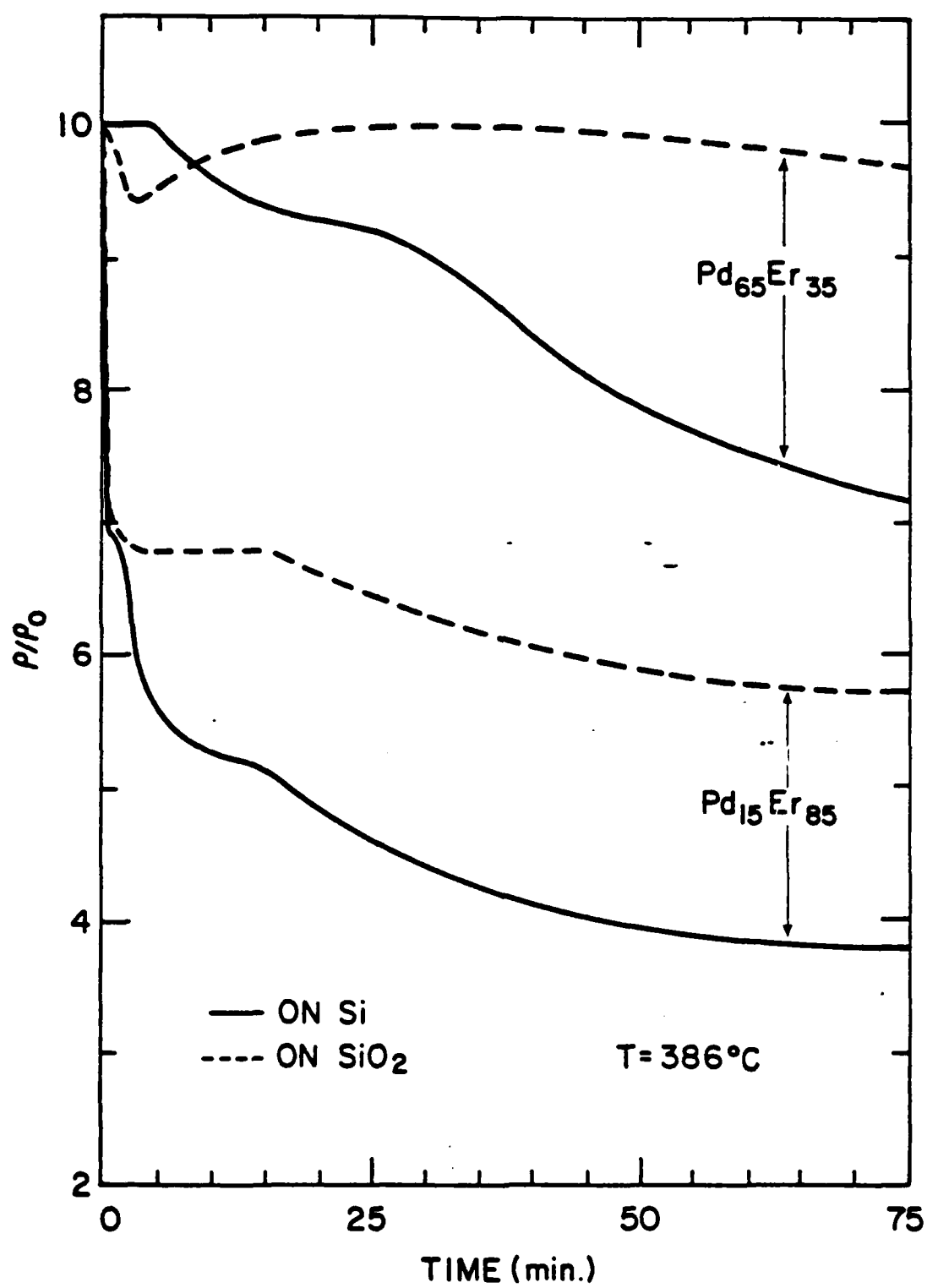


Fig. 12

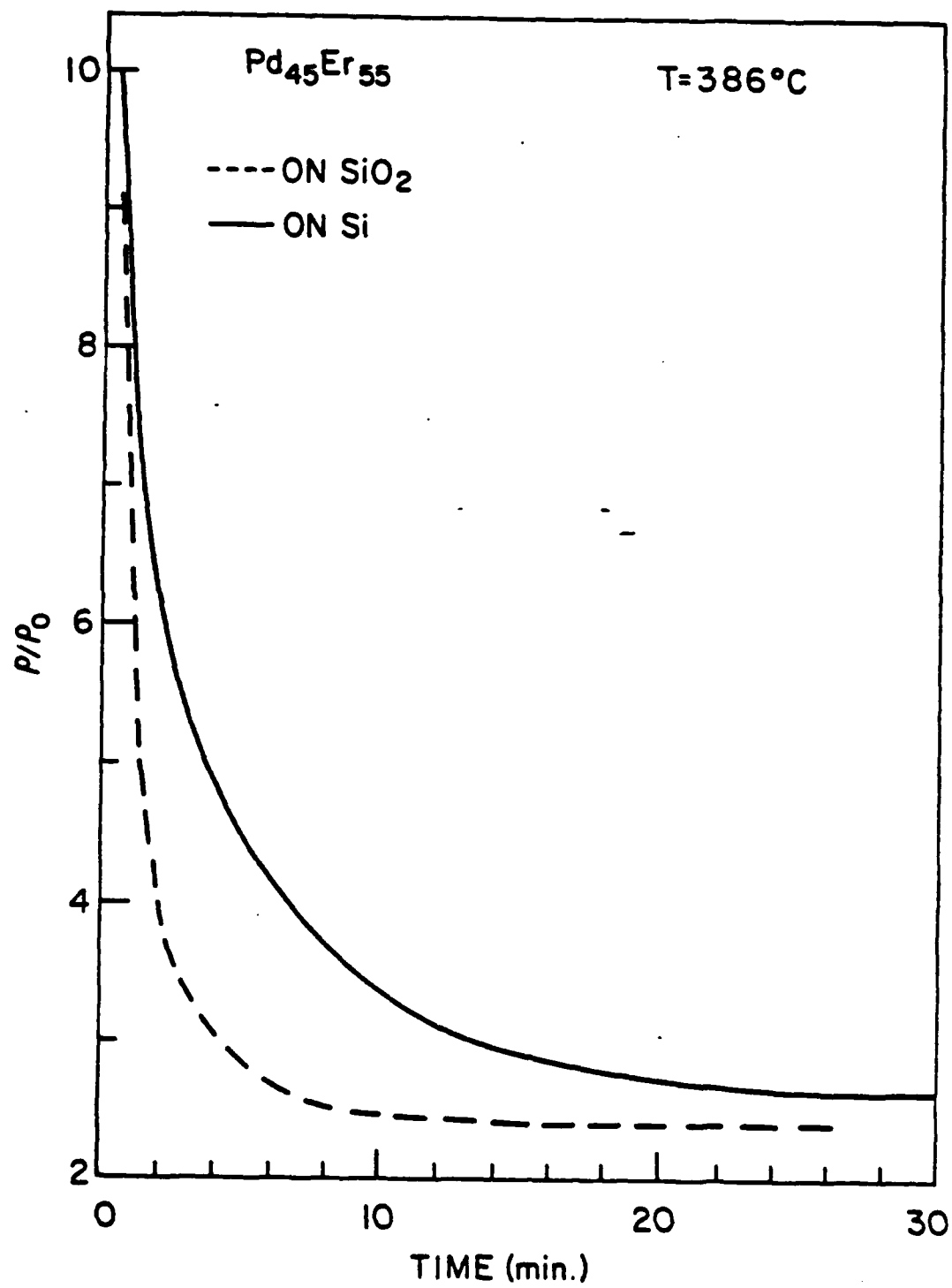


Fig. 13

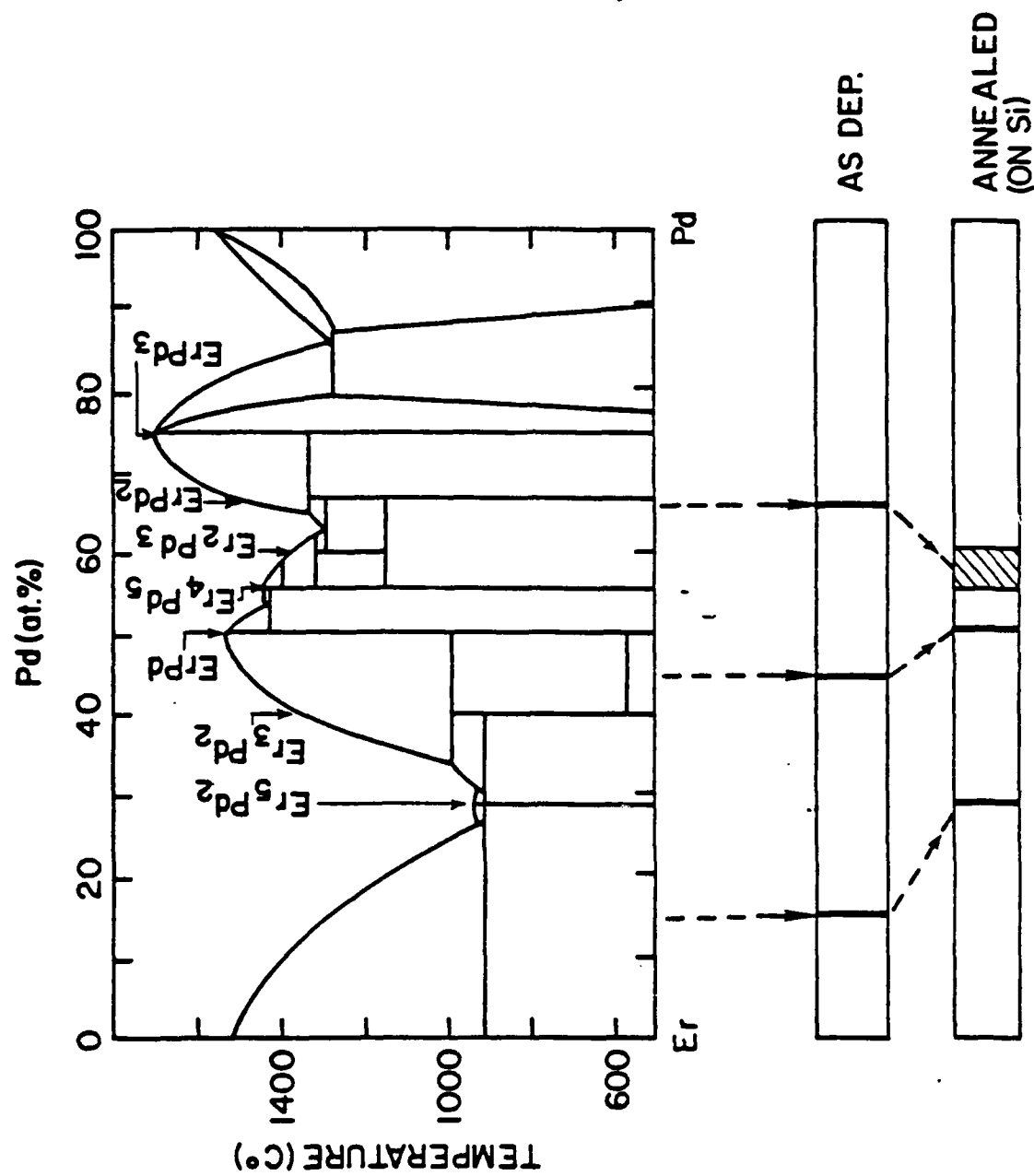


Fig. 14

APPENDIX 10

The Measurement of Silicide Schottky Barrier Heights By Use of Photovoltaic Techniques

T.F.Kuech

IBM Thomas J. Watson Research Center
P.O. Box 218, Yorktown Heights, New York, 10598

C.S.Wu and S.S.Lau

Dept. of Electrical Engineering and Computer Sciences
University of California, San Diego
La Jolla, California, 92093

Many Schottky barrier structures exhibit a marked deviation from ideal behavior on a logarithmic plot of current density, J , as a function of applied forward bias, V . Curvature in such a plot can make the determination of the actual Schottky barrier height from the current-voltage characteristic difficult if not impossible. In many cases, this deviation can be attributed to the influence of an appreciable series resistance on the diode characteristic. This is particularly evident when the device possesses either a low barrier height or when using a high resistivity substrate. Previous approaches to obtaining a reasonable value of the barrier height in such structures have employed either a mathematical model developed by Norde(1) or an electron beam technique described by Huang, et. al. (2). The former technique however requires assumptions not always met in many experimental situations (3), while the latter method utilizes high vacuum technology not always available.

In a recent study of rare earth silicides on Si, the present authors have successfully used an alternative technique. This technique is derived from conventional methods for obtaining barrier height and series resistance values in photovoltaic devices. The application of this simple technique, not necessarily requiring transparent metallizations, extends the linear region of the $\ln J$ versus V plot, allowing for an accurate determination of the saturation current. The Schottky barrier height can then be ascertained by the application of the usual thermionic emission theory. The measurement of both open circuit voltage and the short circuit current as a function of illumination intensity allows the junction characteristic to be determined free from series resistance effects. We have devised a simple scheme whereby this short circuit current may be easily acquired. A comparison will be made between the values of the barrier height derived from conventional I-V and photoresponse measurements, with photovoltaic measurements made on structures possessing either a semi-transparent or opaque metallization. The applicability of this technique to Schottky barriers formed on GaAs will also be discussed.

(1) H. Norde, J. Appl. Phys. 50, 5052 (1979).

(2) H.-C.W. Huang, C. F. Alliotto, and P. S. Ho, Appl. Phys. Lett. 41, 54 (1982).

(3) G. P. Schwartz and G. J. Gualtieri, Appl. Phys. Lett. 42, 265 (1983).